VTT Technical Research Centre of Finland

A Review of Aeronautical Fatigue Investigations in Finland May 2021 - April 2023

Viitanen, Tomi; Siljander, Aslak

Published: 21/06/2023

Document Version
Publisher's final version

A REVIEW OF AERONAUTICAL FATIGUE INVESTIGATIONS IN FINLAND MAY 2021 – APRIL 2023

Published at the 38th Conference of the
International Committee on Aeronautical Fatigue and
Structural Integrity (ICAF),
Delft, The Netherlands, 26-29 June 2023

Compiled by Tomi Viitanen, Aslak Siljander

Confidentiality Public

Preface

The Finnish Defence Forces Logistics Command, Joint System Centre (FDFLOGCOM JSC) initiated and supported this work. The editors are indebted to the following individuals who helped in the preparation of the review (organizations and individuals in alphabetical order):

Aalto	*Aalto University, School of Engineering, Department of Mechanical Engineering:* Olli Saarela, Iikka Virkkunen;
AFCOMFIN	*Air Force Command Finland:* Kalle Vaaraniemi (PoC);
ARCOMFIN	*Army Command Finland:* Ville Siiropää (PoC);
Arecap	*Arecap Ltd:* Eero Laitinen, Arto Mattila;
Elomatic	*Elomatic Consulting & Engineering Ltd:* Jarkko Aakkula, Juho Ilkko, Esa Salminen, Timo Siikonen;
Emmecon	*Emmecon Ltd:* Risto Hedman;
Eurofins ES	*Eurofins, Expert Services Ltd:* Juha Juntunen, Samuli Korkiakoski, Ari Lehtonen, Marko Ruotsalainen, Antti Sivonen, Kari Vähävaara;
FDFLOGCOM JSC	*Finnish Defence Forces Logistics Command, Joint Systems Centre:* Riku Lahtinen (PoC);
FINAFSAC ACC	*Satakunta Air Command, Air Combat Centre, Flight Test Section:* Pasi Greus (PoC);
Insta ILS	*Insta ILS Oy:* Kai Samposalo (PoC);
Patria	*Patria Aviation Oy, RTD & Aeronautical Engineering:* Patrick Dümig, Jarno Havusto, Jaakko Hoffren, Toivo Hukkanen, Heini Järvinen, Mika Keinonen, Jussi Kettunen, Yrjö Laatikainen, Miika Laulajainen, Sampo Lehtinen, Mirve Liius, Janne Linna, Simo Malmi, Matias Mattila, Antero Miettinen, Jaakko Mustonen, Risto-Pekka Niemi, Juho Niva, Mikko Orpana, Jorma Patronen, Jouni Pirtola, Tuomo Salonen, Jaakko Sotkasiira, Jarkko Tikka, Mika Vaskelainen, Kari Vertanen, Markus Wallin, Marko Ylitalo; *Patria Aviation Oy, Systems / Avionics:* Tini Mäkelä, Marika Vuori;
TAU	*Tampere University, Plastics and Elastomer Technology:* Mikko Kanerva, Jarno Jokinen, Olli Orell;
Trano	*Trano Ltd:* Harri Janhunen;
Trueflaw	*Trueflaw Ltd:* Tuomas Koskinen, Iikka Virkkunen;

VTT

VTT Technical Research Centre of Finland Ltd: Jouni Alhainen, Juha-Matti Autio, Samuli Eskola, Antti Forsström, Yasemin Inc, Oskari Jessen-Juhler, Jukka Koskela, Keijo Koski, Tuomas Koskinen, Juha Kuutti, Risto Laakso, Timo Lehti, Taru Lehtikuusi, Sebastian Lindqvist, Sauli Liukkonen, Jari Lydman, Jukka Maunumäki, Sakari Merinen, Jarkko Metsäjoki, Jukka Mäkinen, Aki Mäyrä, Vesa Nieminen, Arto Nyholm, Ahti Oinonen, Matti Okkonen, Pasi Puukko, Kalle Raunio, Joni Reijonen, Jarkko Saarinen, Mikko Savolainen, Aslak Siljander, Jussi Solin, Gonçalo Sorger, Carl Söderholm, Antti Tuhti, Antti Vaajoki, Aleks Vainionpää, Tomi Viitanen.

Espoo, 21 June 2023

Editors

Contents

1 Introduction

Aeronautical life cycle support research in Finland and its embodiment, the national research network, has over the decades been solely advocated and coordinated by the Finnish Air Force (FINAF). While the FINAF is concentrating to carry out its primary objective – to secure Finland's airspace on a 24/7 basis throughout the year, the national research network is helping the FINAF to optimize the use of their fleet in a cost-effective way. The assigned research activities by the FINAF are of two kinds. Routine tasks that are related to finding pragmatic solutions for every day's challenges with only a minor effort, and research tasks that feature a more scientific flavor, and thus require more time to mature. The FINAF has also found it advantageous that Finland belongs to the core of the international community of aeronautical fatigue research, being a member nation in the International Committee on Aeronautical Fatigue and Structural Integrity (ICAF). This commitment is manifested in the multiple ICAF National Reviews since 2001. [18], [19], [20], [21], [22], [23], [24], [25], [26], [27], [28]

The FINAF is one of the oldest independent air forces in the world. It all began in 1918 when the Swedish Count Eric von Rosen donated the Thulin typ D reconnaissance plane which is generally credited as the first aircraft of the FINAF. The aircraft arrived at Vaasa on 6 March 1918, and the date has since been celebrated as the founding date of the Finnish Air Force. [1]

Year 2021 symbolizes a historical event for Finland's future air defence capability. The service life of the Finnish F/A-18C/D Hornet fleet comes to an end by 2025–2030 as the aircraft will reach the end of their planned 30-year service life. In parallel, the replaced capabilities must be phased in and be fully operational in service in 2030. The HX programme replacing the Hornet capability was launched in 2015 including the following fighter aircraft systems: Boeing F/A-18 Super Hornet, Dassault Rafale, Eurofighter Typhoon, Lockheed Martin F-35, and Saab Gripen. After six years of intense efforts, on 10 December 2021, the Government of Finland authorized the Finnish Defence Forces Logistics Command to sign a procurement contract with the Government of the United States on Finland's next multi-role fighter. The fighter replacing the Hornet fleet's capability will be the Lockheed Martin F-35A Lightning II (**Figure 1**). The procurement contains 64 F-35A Block 4 multi-role fighters, substantial and versatile weaponry tailored for the operating circumstances, required training and sustainment solutions, other related systems as well as sustainment and maintenance services until the end of 2030. [2]

Figure 1: *The Finnish Air Force F/A-18C/Ds (HN-408/HN-466) conducting interoperability training with the United States Air Force F-35A Lightning II (20-5570) from the 48th Fighter Wing. Figure courtesy of the FINAF.*

The Finnish Defence Forces (FDF) has clearly set tasks to maintain a credible and preventive defence capability that secures Finland's territorial integrity. Responsibility for Finland's air defence and air operations is with the Air Force. The observance of active air policy mission aims to secure Finland's airspace and react to airspace violations, if necessary. It can be concluded that the primary objective of the FINAF has remained unchanged over the time, but the tools to implement the objective are somewhat more capable - and considerably more complicated systems - than back in the old days. The current fixed wing aircraft inventory of the FINAF is summarized in **Figure 2**.

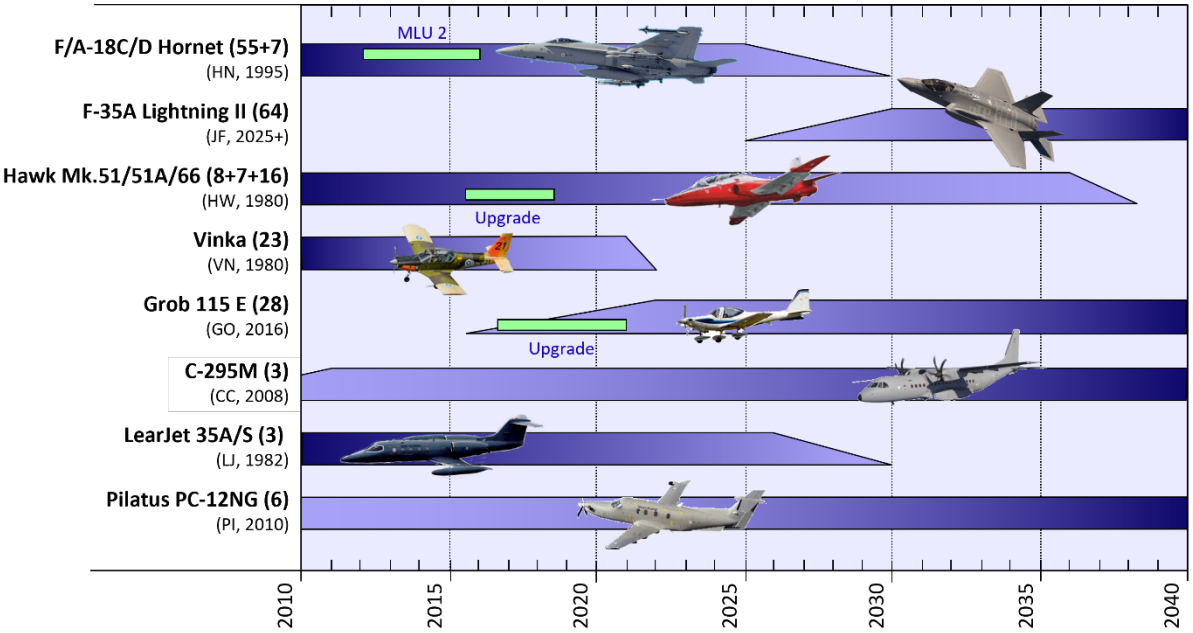

Figure 2: *An overview of the fixed wing aircraft inventory of the Finnish Air Force (FINAF). Figure courtesy of the Joint Systems Centre.*

The 20 TTH/SAR NH90 helicopters purchased earlier by the FDF were retrofitted (by Patria Aviation) and reached the Full Operational Condition (FOC) status. The retrofits (including the platform and various systems therein) started in 2014 and were completed in 2019. The assessment of NH90 maintenance system and tasks was finished during 2022. This will increase the fleet availability in the future.

Presently, the MD500 fleet is going through a cockpit modification project in which avionics will be upgraded. The result will increase the MD500s' operative performance, improve their interoperability with the other branches, and facilitate pilot transitions into the NH90 platform.

The current rotary wing aircraft inventory of the FDF is summarized in **Figure 3**.

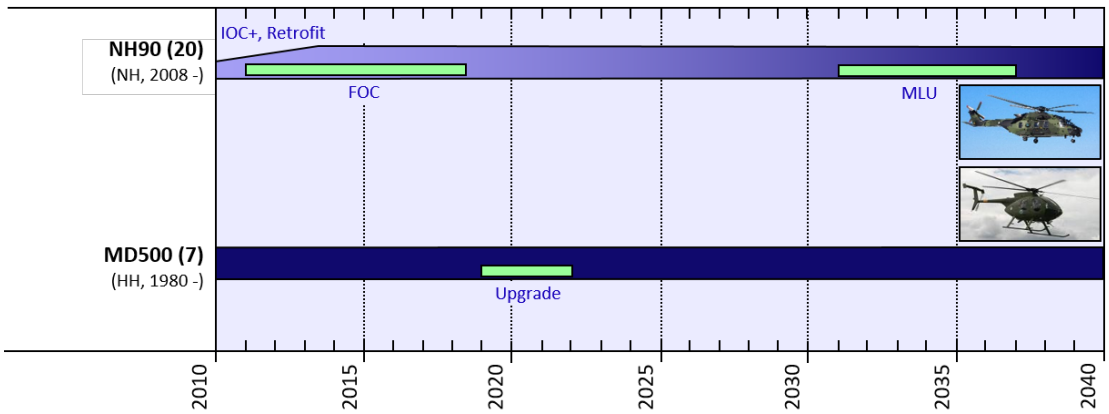

Figure 3: *An overview of the rotary wing aircraft inventory of the Finnish Defence Forces (FDF). Figure courtesy of the Joint Systems Centre.*

Before proceeding into the highlights of the structural integrity management activities, a brief update of the FINAF's fighter aircraft and associated pilot training aircraft is provided next.

1.1 Valmet L-70 Vinka

A remarkable era in the Finnish aviation history ended on the 31st of August 2022 after 194 276 flight hours as the Valmet L-70 Vinka (the FINAF military designation VN) had its last FINAF mission (**Figure 4**). Since 1980, the indigenous Vinka primary trainer served as a training platform on which military pilots flying fixed- and rotary wing aircraft of the FINAF and the Border Guard learned the basic skills of flying. Thereafter, the Grob G 115E has taken on the primary and basic training role (Chapter 1.2). [3]

Figure 4: *The last FINAF Vinka flight was flown in August 2022. Figure courtesy of the FINAF.*

The Valmet L-70 Vinka is a three-seat piston-engine aircraft of Finnish design and manufacture. Due to its 40-year service life, the Vinka fleet had undergone several minor structural reinforcements and other modifications. Between 2002-2004 a Life Extension Program (LEP) was carried out to the Vinka fleet. Its technical background was described in the ICAF 2001 report (Chapter 3 of Ref. [18]). During LEP each aircraft was equipped with a g counter. The structural life consumption and severity of the usage was monitored by Patria Aviation from the g counter data. Patria also issued recommendations on a yearly basis regarding the rotation of the Vinka fleet to obtain a more even rate of structural life expended.

Based on the g counter information, the severity of usage was more benign compared to the basis of the LEP analyses and tests, see **Figure 5**.

The first fleet leader was removed from operation in September 2015 after logging 7100 FH (it was given 100 FH extension to the official 7000 FH limit). After that, the plane was disassembled for structural inspections. Most of the inspections were done visually but the most critical locations were inspected using NDT. No cracks or loose rivets were found. Based on the inspection results, and the fact that originally three fleet leaders were selected as a precaution, it was decided that the two other fleet leaders do not any more need to log hours differently compared to the rest of the fleet. In late 2018 loose rivets were found from the lower surface of the wing of the fleet aircraft. This finding could not be predicted based on the fleet leader inspection.

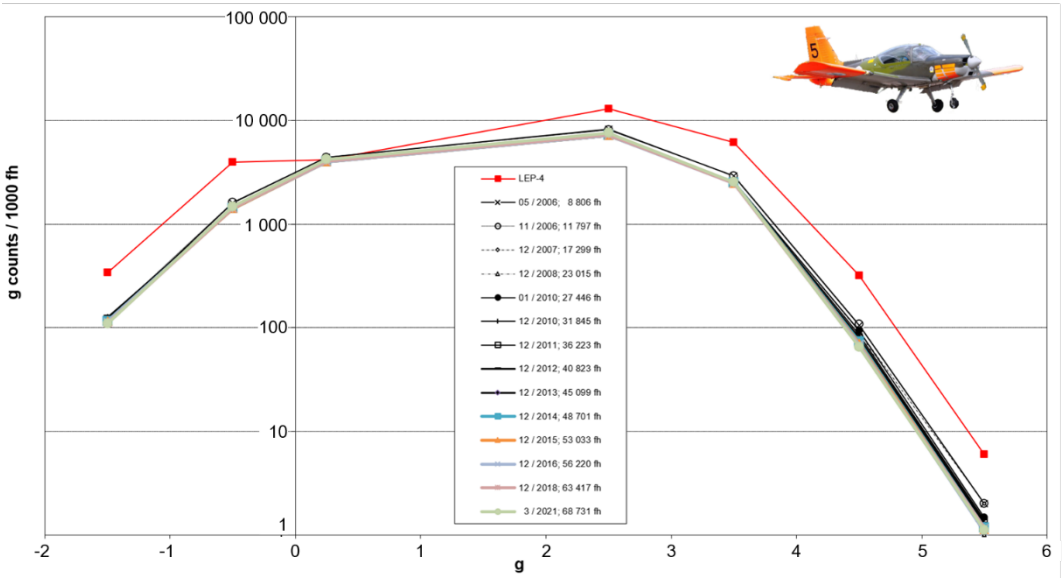

Figure 5: *The g counts per 1000 FH of the Valmet Vinka. From top to bottom: The spectrum representing the LEP design assumptions (LEP-4); the post LEP g counter spectrum as of May 2006; as of November 2006; as of December 2007; as of December 2008; as of January 2010; as of December 2010; as of December 2011; as of December 2012; as of December 2013; as of December 2014; as of December 2015; as of December 2016; as of December 2018; and the update from the previous review: as of March 2021 including a total of 68 731 FH. All curves (excluding the red LEP-4) represent the fleet average from all Vinkas, as ranked according to the aircraft center of gravity normal acceleration. Figure courtesy of Patria Aviation.*

1.2 Grob G 115E

The Grob G 115E is a small, lightweight, two-seat piston-engine aircraft built in Germany by Grob Aircraft. In October 2016, the FINAF procured 28 pre-owned Grob G 115Es for the Defence Forces to supersede retired Valmet L-70 Vinkas (Chapter 1.1) in primary and basic training roles. The aircraft were purchased from the Great Britain, Babcock Aerospace Limited, which had previously operated them as a training platform for the Royal Air Force. [4]

The Finnish Grobs are allocated GO-series military registrations and were delivered to Finland in 2016-2018. Before the start of flight training, the Grob fleet has went through a cockpit modernization project. Avionic and communication systems upgrade, and state-of-the-art multi-function displays were fitted to bring the cockpit layout compatible with the other aircraft operated by the Defence Forces and meet the requirements of the future military aviation.

On the contrary to its predecessor (Vinkas), the structure of Grob G 115E is manufactured of composite materials. It is constructed predominantly from carbon fibre reinforced composites, has a tapered low wing, a 180 hp engine with a 3-bladed variable-pitch propeller, a fixed tricycle undercarriage, fixed horizontal and vertical stabilizers and conventional flight control surfaces. The large glass canopy renders clear all-round visibility to the crew (**Figure 6**).

Figure 6: *Grob G 115E primary trainer aircraft (GO-27). Figure courtesy of the FINAF.*

National efforts related to the structure of the Grob G 115E aircraft are highlighted in Chapter 2.2.1.

1.3 Hawk Mk.51/51A and Mk.66

The BAE Systems Hawk is a British single-engine two-seat advanced jet trainer which is operated in Finland by the Air Force Academy, primarily in advanced and tactical training roles. The Finnish Air Force became the first export customer of the type, and the first fifty Hawks, Mk.51s, entered Finnish service in 1980-1985. In 1993, the FINAF ordered an additional batch of seven Hawk Mk.51As that contain minor improvements in structure and avionics compared with the Hawk Mk.51. Finland augmented its Hawk fleet in 2007 by sourcing 18 low-hour Hawk Mk.66s from Switzerland. Externally, the former Swiss Hawks stand out from the grey legacy Hawks owing to their red-and-white paint scheme (see **Figure 7**). Since 2021, the Mk.66 aircraft have received a grey livery like older model aircraft. The Hawk is also flown by the Air Force's official display team the Midnight Hawks. [5]

Figure 7: *BAE Systems Hawk advanced jet trainer variants in the FINAF fleet (from left to right): Hawk Mk.51, Hawk Mk.51A, and Hawk Mk.66. Figure courtesy of the FINAF.*

Due to increasing signs of metal fatigue, a major structural reinforcement program (SRP) was performed to extend the operational life of Finland's Hawks. The Hawk SRP was completed during the late 1990s for the Mk.51 and Mk.51A fleet and started for the Mk.66 fleet in 2020. Along with the Mk.66s, the Finnish Hawks underwent an extensive cockpit upgrade program carried out by Patria Aviation. The glass cockpit upgrade program included the replacement of analogue cockpit instruments with modern displays which narrows the gap between the instrument layout of the Hawk and F/A-18C/D Hornet (see Chapter 1.4). In the first phase, all Mk.66s, seven Mk.51As, and one Mk.51 received the cockpit modification and were delivered to the FINAF by January 2018. Later, eight additional Mk.51s were modernised in 2016-2020 based on the refined Hawk life cycle plans and to compensate the loss of two already modernized Mk.66 aircraft. Thus, the 2023 fleet consists of 31 upgraded Hawks[1]: 8 Mk.51s, 7 Mk.51As and 16 Mk.66s. They are expected to remain in service until 2040. The current flight service target will require extension to certified usage life by Finnish Military Aviation Authority (FMAA). Required investigations for re-certification will be completed during 2023.

The inherent fatigue tracking of each FINAF Hawk aircraft relies on counting g level exceedances and calculating a usage index i.e., Fatigue Index (FI) by the variant specific equations on a flight-by-flight basis. This method is adequate for monitoring the

[1] On 15 May 2023, a Mk.51 (HW-320) was crashed without fatalities. Based on started (on-going) air accident investigations it has become clear that the engine had already shut down in the air and was no longer running when the aircraft hit the ground. An interesting curiosity is that the HW-320 had been in an accident already in 1998 and repaired thereafter, so this is possibly the first case in the world when there had been four (4) ejections from the same aircraft in an emergency. [115]

structural locations mainly influenced by the aircraft normal acceleration (multiplied by weight). However, the current FI tracking does not consider buffet loading which is the main driver for the structural fatigue issues e.g., in the empennage of the Hawk aircraft. The Fatigue Index summary of the Finnish Hawk fleet is shown in **Figure 8**.

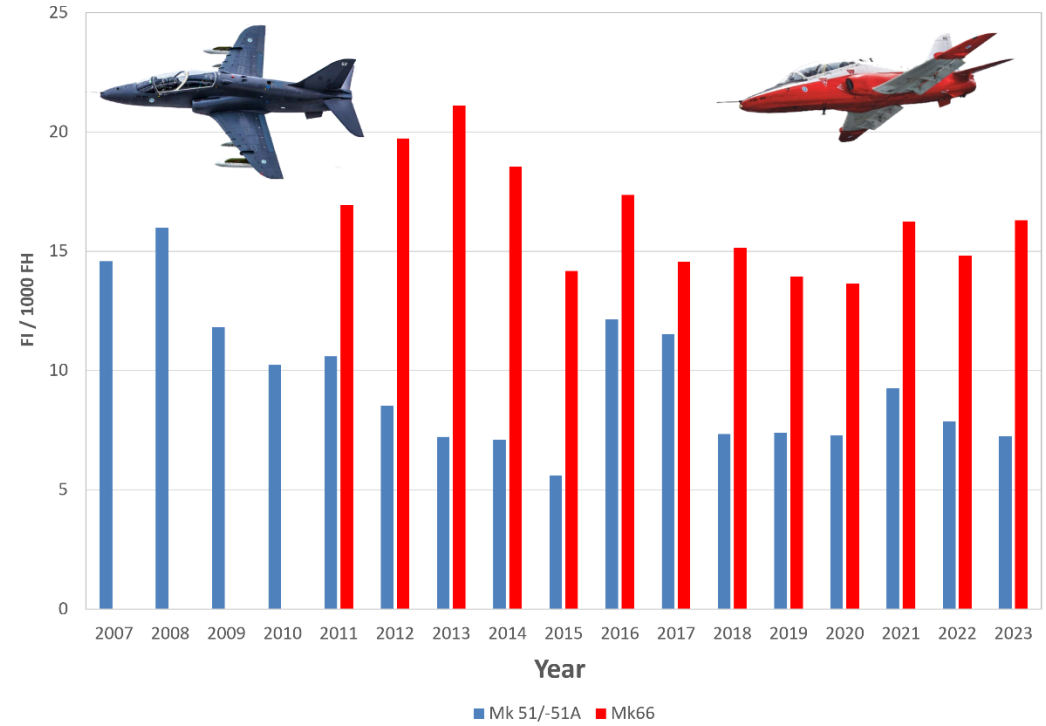

Figure 8: *Annual Fatigue Index (FI) accrual of the FINAF Hawk aircraft (Mk.51/51A in blue; Mk.66 in red). Figure courtesy of the FINAF.*

1.4 F/A-18C/D Hornet

The Boeing F/A-18C (single seat) and F/A-18D (two seat) Hornet are twin-engine, mid-wing, carrier-capable, multirole jet fighters, which form the nucleus of the Finnish air defence. In 1992, Finland selected the Hornet to replace its aging Saab J35 Draken and MiG-21bis interceptors. The late-production Lot 17 aircraft entered Finnish service in 1995-2000, bearing the military designation HN. The Finnish two-seaters were built in the United States by McDonnell Douglas which later merged with Boeing, while the single-seat aircraft were assembled at Patria Finavitec (nowadays Patria Aviation) facility in Finland. [6]

The FINAF Hornet fleet consists of 62 aircraft: 55 C-models (**Figure 9**), and 7 D-models (**Figure 10**). Most of the fleet is divided between two operational fighter wings: Lapland Air Command (Fighter Squadron 11) at Rovaniemi Air Base and Karelia Air Command (Fighter Squadron 31) at Kuopio Rissala Air Base.

Figure 9: *Boeing F/A-18C Hornet multirole jet fighter. Figure courtesy of the FINAF.*

Figure 10: *Boeing F/A-18D Hornet multirole jet fighter. Figure courtesy of the FINAF.*

It was recognized already in the planning stage of the Hornet program that technology of the 1990s would be obsolete way before the planned withdrawal date of the type, 2025–2030 time frame. Therefore, to keep the Hornet fleet at their highest level of performance, the fleet needs to be subjected to planned and systematic updates over its life span. On the heavier end of the spectrum have been the full-scale upgrades.

The Finnish F/A-18 fleet has undergone two extensive mid-life upgrades, designated as Mid-Life Update (MLU) together with the partners: Boeing, Naval Air Systems Command as an upgrade design organization and equipment supplier, and Patria Aviation as a life cycle support service provider for the aircraft.

The focal point in MLU 1 was to enhance the FINAF Hornets' Air-to-Air (A/A) capability. The upgrade involved the incorporation of a helmet-mounted sighting system mated with the state-of-the-art AIM-9X Sidewinder infrared guided missile for improved close-in air combat performance. MLU 1 also introduced features to better the pilot's situational awareness and joint operation capabilities. The MLU 1 was completed in 2006-2010. [7], [8]

The primary objective in MLU 2 was to enable the FINAF Hornets' air-to-ground (A/G) capability by integrating various types of weapons (the short-range guided bomb JDAM, medium-range glide bomb JSOW and the long-range JASSM standoff missile), and modern self-protection, communication, navigation, and information distributions systems which make the aircraft more interoperable in joint operations. Other examples of MLU 2 upgrades were the cockpit upgrades with new displays and the BOL countermeasures dispensers. The MLU 2 was completed in 2012-2016.

From structural point of view, the MLU 2 upgrade included structural strengthening and a purchase of Line Replaceable Units (LRU) and other spares to ensure the safe and reliable performance until the sundown of the aircraft type. All structural MLU 2 modifications were carried out by Patria Aviation, and the MLU 2 preparation work was done in cooperation with the Swiss Air Force.

There are special arrangements to manage the C and D model differences between the USN and the FINAF in the MLU 2 induced configurations: The software testing will be done in Finland by the FINAFSAC ACC (Satakunta Air Command, Air Combat Centre, Flight Test Section) and Patria Aviation's STIC laboratory (Software Test and Integration Centre). For the first time in the history of the Hornet, there is a foreign (Finnish) organization approved as a part of the approval process of the US software.

Along with the MLU 2 upgrade, the FINAF F/A-18C/D Hornet has finally reached its Full Operational Capability (FOC) that expands the operational envelope for a true multi-role aircraft. The Finnish pilots are now enabled to exercise the full potential of the Hornet in joint and combined operations with a wide range of air-to-air and air-to-ground capabilities. The new type of mission capability reflects on training programs and the use of the aircraft and thus, also the airframe stressing.

Fatigue tracking of the FINAF Hornet fleet is currently based on: 1. Flight Hours (FH), 2. Wing Root Fatigue Life Expended (WR FLE) -value, and 3. T*-value (time spent in a buffet-dominating Point In The Sky, PITS) for the Vertical Tail [66]. Summary of the WR FLE of the FINAF F/A-18C/D fleet is presented in **Figure 11**.

It is known that the WR FLE is primarily dependent on the aircraft normal acceleration, so it does not provide useful fatigue information about the structural locations prone to the buffeting. As the Vertical Tail of the F/A-18 aircraft is typically buffeting-strained structure, a more useful usage index, developed by the international F/A-18A/B/C/D Hornet user's community, has been put into practice in the FINAF. A T* (T star) value indicates time spent [h] in the PITS that contributes most of the fatigue damage for the Vertical Tail. Summary of the T*-values of the FINAF F/A-18C/D fleet is presented in **Figure 12**.

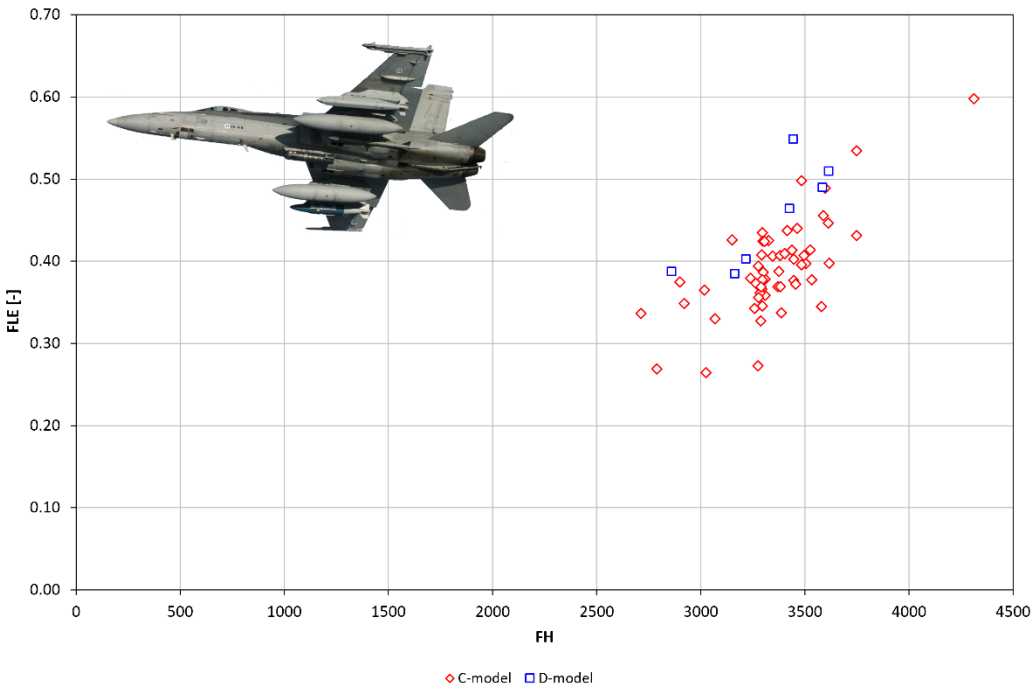

Figure 11: *Summary of the Wing Root Fatigue Life Expended (FLE) of the FINAF F/A-18C/D fleet. The data is from all 62 aircraft included [66]. Figure courtesy of the Joint Systems Centre.*

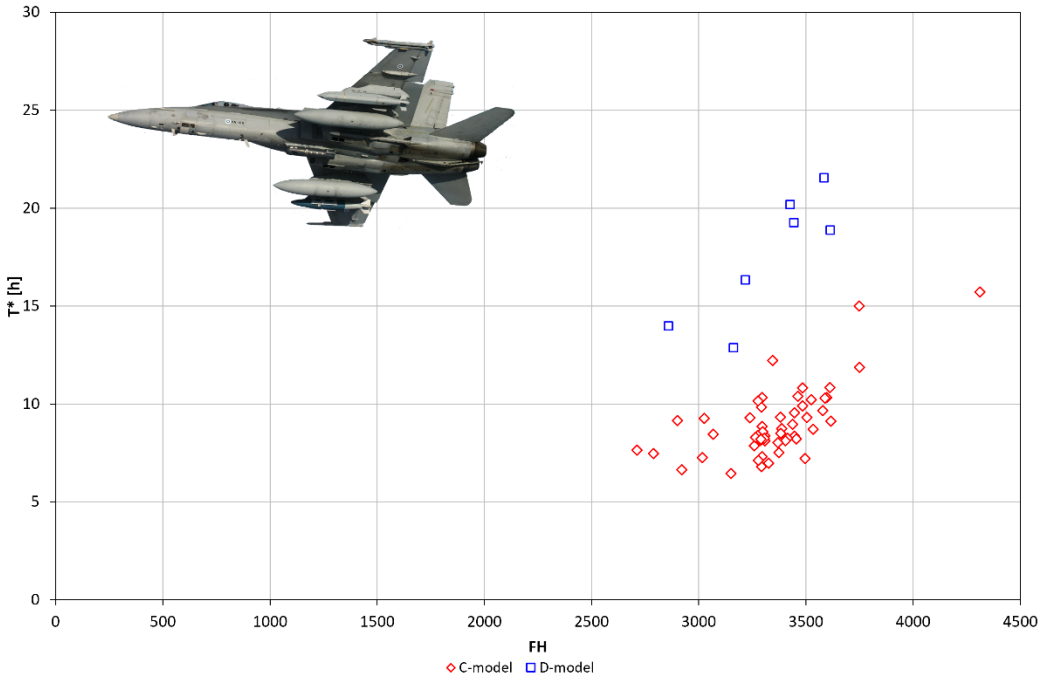

Figure 12: *Summary of the Vertical Tail fatigue tracking (T*-value) of the FINAF F/A-18C/D fleet. The data is from all 62 aircraft included [66]. Figure courtesy of the Joint Systems Centre.*

The Finnish F/A-18C/D fleet can accomplish its operations safely and reliably until the mid-2020s. The decommissioning of the Hornet fleet will start in 2025. Phasing out the aircraft becomes a reality when they are about to reach their structural flight hour limits between 2025 and 2030. Then the Lockheed Martin F-35A Lightning IIs will replace an obsolescent Hornet fleet (see Chapter 1.5).

1.5 The mystery of X resolved

The service life of the Finnish F/A-18C/D Hornet fleet comes to an end by 2025–2030 as the aircraft reach the end of their planned 30-year service life. In parallel, the replaced capabilities must be phased in and be fully operational in service in 2030. The major factors that limit the service life of the FINAF Hornet fleet are [9], [10]:

1. Structural fatigue,
2. Expiring system support, and
3. Weakening comparative capabilities.

Extending the lifespan of the FINAF Hornet fleet into the 2030s, contrary to the present plans, would increase expenses in life-cycle management and increase the cost risks of system support. The relative capabilities of the Hornet fleet will degrade in the 2020s and the most significant degradation falls on its interdiction capability: the next generation multi-role fighters in Finland's neighborhood will technologically surpass the Hornet's capabilities. Extending its structural life and implementing a new, sizeable midlife upgrade would make it possible to delay the decision to replace the Hornet capabilities by five years, at most. It is estimated that the capability would be fully available no earlier than eight years after the financial decision is taken. As a result, substantial additional costs would be incurred in case of the service life of the Hornet fleet would be extended. This is neither a cost-effective solution nor would it be sufficient in terms of Finland's defence.

Based on the preliminary assessment, it was recommended that the most cost-effective manner to Finland's state economy was to replace the nationwide air defence capability of the F/A-18C/D Hornet fleet with the solution based on a multi-role fighter system. The replacement programme was named as HX according to the Finnish Air Force tradition: the first letter comes from the platform to be replaced (here H stands for Hornet), and the X is used for its, yet unknown, successor i.e., the fighter aircraft candidate in the bidding competition.

The HX programme was launched in 2015 by the decision of the Minister of Defence and subsequent Request for Information (RFI) phase. The HX bidding competition began in 2018 with the initial Requests for Quotation (RFQ) sent to the governments (alphabetically) of France, Sweden, the United Kingdom, and the United States. The aim of the competitive bidding was to build with each tenderer a comprehensive solution fulfilling the requirements and producing the best possible capability to replace the Hornet fleet for the Finnish defence system in the operational environment of the 2030s as well as within the HX system's lifespan.

The offered solutions in the HX programme were set up around the following fighter aircraft systems: Boeing F/A-18 Super Hornet (the United States), Dassault Rafale (France), Eurofighter Typhoon (the United Kingdom), Lockheed Martin F-35 (the United States) and Saab Gripen (Sweden).

The Defence Forces Logistics Command received the final and binding offers from all five HX tenderers by the end of April 2021 deadline [11]. The offers were assessed in accordance with the HX Request for Quotation, decision-making model, and Evaluation Handbook to reach the procurement proposal.

The tendering was based on four decision-making areas: Military Capability, Security of Supply, Industrial Participation and Affordability. When a tenderer passed the Security of Supply, Industrial Participation and Affordability considerations, it proceeded to the final phase of the Military Capability evaluation in which the offered solutions were placed in order.

The Defence Forces evaluated the offered comprehensive solutions' capability in three phases based on performance demonstrated in testing events. In the final phase, the military capability effectiveness of each candidate's HX system was evaluated via a thorough and long-run war game supported by simulation. The Defence Forces' proposal for the system to be selected was based on the results of the war games and estimated future development potential.

In the HX bidding competition, the F-35 passed the security of supply, industrial participation, and affordability decision-making areas. The F-35 solution achieved the highest operational effectiveness and future growth potential in the capability assessment.

The Government of Finland authorized 10 December 2021 the Finnish Defence Forces Logistics Command to sign a procurement contract with the Government of the United States on Finland's next multi-role fighter. The fighter replacing the Hornet fleet's capability will be the Lockheed Martin F-35A Lightning II (**Figure 13**). The procurement contains 64 F-35A Block 4 multi-role fighters, substantial and versatile weaponry tailored for the operating circumstances, required training and sustainment solutions, other related systems as well as sustainment and maintenance services until the end of 2030. The F-35As will bear the military designation JF as per Joint Fighter, emphasizing its interoperability capabilities.

Figure 13: *The current and future backbone of the Finnish air defence. The F-35A Lightning II will replace the F/A-18C/D from 2025-2030. Figure courtesy of the FINAF.*

1.6 Scope of the review

This national review on aeronautical fatigue concentrates on the fixed wing aircraft of the FINAF related to fighter aircraft and associated pilot training aircraft. The FINAF inventory includes: 62 F/A-18C/D Hornet fighters, 8 Hawk Mk.51, 7 Mk.51A and 16 Mk.66 jet trainers, (23 Valmet L-70 Vinka primary trainers; last FINAF mission on the 31st of August 2022), and 28 Grob G 115E primary trainers. By now, approx. 213 000 FH have been flown with the Hornets, 280 000 FH with the Hawks, and 194 000 FH with the Vinkas.

No FINAF aircraft of these type designations have been lost due to structural issues.

The severity of the Finnish usage in view of structural fatigue with the aircraft of noteworthy maneuvering capability (**Figure 8** (Hawk) and **Figure 11**, **Figure 12** (Hornet)) clearly demonstrates the need to maintain, further develop and apply concrete and systematic efforts to cope with the structural deterioration effects.

In 2005, the International Committee on Aeronautical Fatigue and Structural Integrity (ICAF) formally welcomed Finland as a full member of the ICAF, making Finland the 13th member nation. The 10th national review as a full member about the aeronautical fatigue investigations in Finland May 2021 - April 2023 was compiled by Tomi Viitanen and Aslak Siljander (VTT).

The review comprises inputs from the organizations listed below (in alphabetical order):

Aalto	Aalto University, School of Engineering, Department of Mechanical Engineering, P. O. Box 14300, FI-00076 Aalto, Finland (http://appmech.aalto.fi/en/).
AFCOMFIN	Air Force Command Finland, Plans Division A5, Programmes Coordination Section, P. O. Box 30, FI-41161 Tikkakoski, Finland.
ARCOMFIN	Army Command Finland, Plans Division C2, P. O. Box 145, FI-50101 Mikkeli, Finland.
Arecap	Arecap Ltd, Toivolantie 4, FI-04800 Mäntsälä, Finland (https://arecap.fi/).
Elomatic	Elomatic Consulting & Engineering Ltd, Vaisalantie 2, FI-02130 Espoo, Finland (https://www.elomatic.com/en/).
Emmecon	Emmecon Ltd, Tammitie 12, FI-53810 Lappeenranta, Finland (https://www.emmecon.fi/).
Eurofins ES	Eurofins Expert Services Oy, P. O. Box 47, FI-02151 Espoo, Finland (https://www.eurofins.fi/expertservices/).
FDFLOGCOM JSC	Finnish Defence Forces Logistics Command, Joint Systems Centre, P. O. Box 69, FI-33541 Tampere, Finland (https://puolustusvoimat.fi/en/about-us/logistics-command).
Insta ILS	Insta ILS Oy, Sarankulmankatu 20 (P.O. Box 80), FI-33901 Tampere, Finland (https://www.insta.fi/en/en/).
Patria	Patria Aviation Oy, Lentokonetehtaantie 3, FI-35600 Halli, Finland (http://www.patria.fi/).
TAU	Tampere University, Plastics and Elastomer Technology, FI-33014 Tampere, Finland (https://www.tuni.fi/en).
Trano	Trano Oy, Vetikonkuja 13, FI-04300 Tuusula, Finland.
Trueflaw	Trueflaw Ltd, Tillinmäentie 3 Tila A113, FI-02330 Espoo, Finland (http://www.trueflaw.com/).
VTT	VTT Technical Research Centre of Finland Ltd. P. O. Box 1000, FI-02044 VTT, Finland (https://www.vttresearch.com/en).

2 Current activities: ASIMP 2021-2022 and ASMIP 2023

The Aircraft Structural Integrity Management Program (ASIMP) 2021-2022, as briefly outlined in [28], has been completed. After the previous two-year research period, the follow-on research, ASIMP 2023, with its yearly basis assignments has begun. An attempt is provided below to provide highlights of the ASIMP 2021-2022, and 2023 achievements.

2.1 Loads and stresses

2.1.1 Computational Fluid Dynamics at Elomatic Ltd.

Today the Computational Fluid Dynamics (CFD) research at Elomatic Ltd is based on the in-house flow solver FINFLO. In Finland, the F/A-18 related research is done in collaboration with Patria Aviation and VTT who also utilize FINFLO. Moreover, Elomatic and the Swiss companies CFSE and RUAG collaborate on projects to study the life span of the F/A-18 Hornet structures. Over the decades, Finland and Switzerland have done small-scale collaboration concerning the CFD. Collaboration between Switzerland and Finland has contained regular meetings of persons who work with the F/A-18C CFD models and develop the FINFLO and Navier Stokes Multi Block (NSMB) flow solvers [109]. In the year 2020 a large project concentrating on code validation as well as on developments in Fluid Structure Interaction (FSI) and Chimera-grid technique was started. A goal is to achieve a better understanding of the differences in the results predicted by the CFD codes and to investigate the effects of FSI in the simulations.

The FINFLO flow solver and the MSC Nastran structural code [69] are coupled using a code coupling software called MpCCI developed by SCAI Fraunhofer in Germany [70]. The MpCCI Coupling Environment has been developed to provide an application independent interface for the direct coupling of different simulation codes. The software allows the CFD and Finite Element Method (FEM) models to communicate with each other and exchange data in real-time. Running the codes parallel takes place by defining the coupling process via MpCCI GUI and then advancing the solution using the MpCCI server (see **Figure 14**). MpCCI visualizer is used to show how the wetted surfaces develop in both models during the iteration. In the simulations, an explicit coupling is used between the codes. The calculations are started from a well-converged steady-state solution without the FSI. In steady-state cases typically 5 to 10 coupling iterations are made between the structural model and the CFD solution to find the deformed shape of the aircraft under aerodynamic loads. In time-accurate cases, first a single physical time step with the previous geometry is run by the FINFLO flow solver. After the FINFLO run that typically requires of the order of 50 internal iterations within the time step, MSC Nastran is applied to create a new deformed geometry. In the next phase the updated geometry is read inside the FINFLO code, and the new physical time step is started on the CFD side.

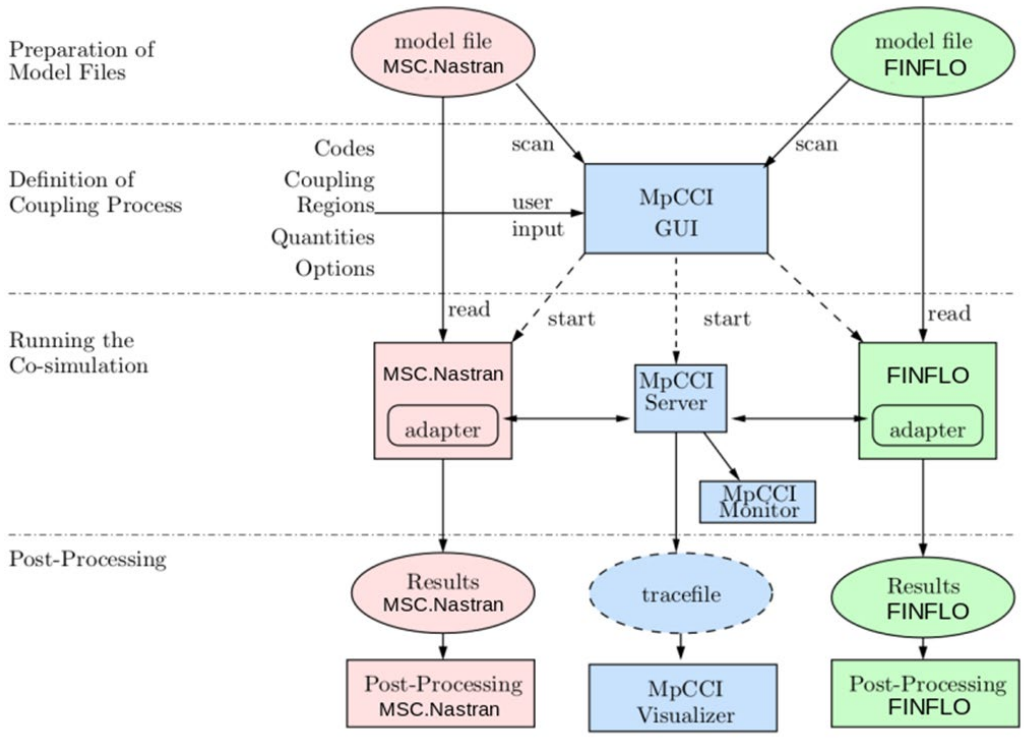

Figure 14: *Coupling between the MSC Nastran and FINFLO codes via the MpCCI software. Figure courtesy of Elomatic Ltd.*

The solution system is applied for the F/A-18C 7.5 g pull-up case at sea-level conditions with Ma = 0.849. The FE model consists of 1 658 546 degrees of freedom and 116 762 surface elements (see Figure 15). On the CFD side there are 50 915 328 cells with 125 536 surface elements. The height of the first cell in the CFD grid is nominally 5 μm and a low-Reynolds-number SST k-ω model is used. The main result from the simulations is the aerodynamic loading of different aircraft components on the deformed shape. The deformation history is typically visualized using animations. **Figure 16** shows just one frame from a geometry history and the aerodynamic load distributions integrated over the whole aircraft.

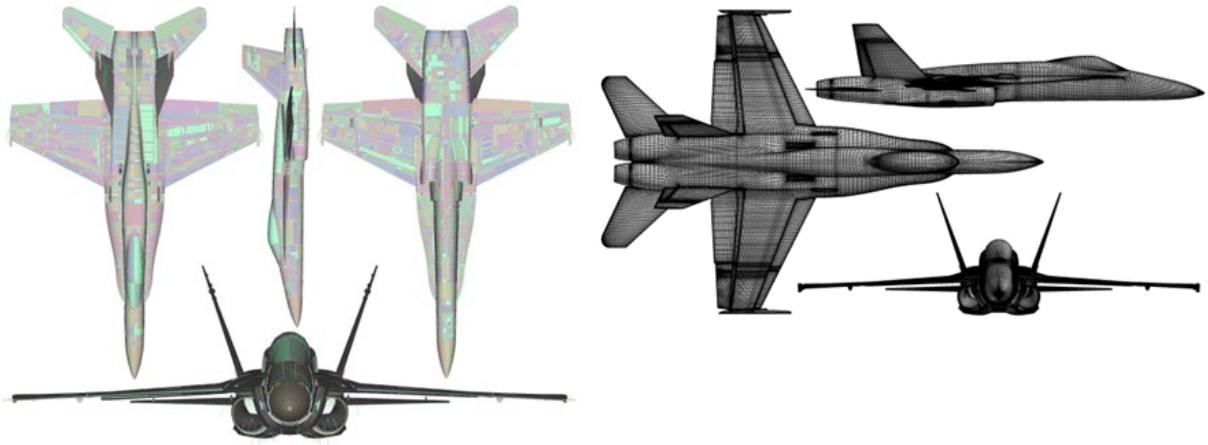

Figure 15: MSC Nastran model (left) and the surface grid for the FINFLO model (right). Figure courtesy of Elomatic Ltd.

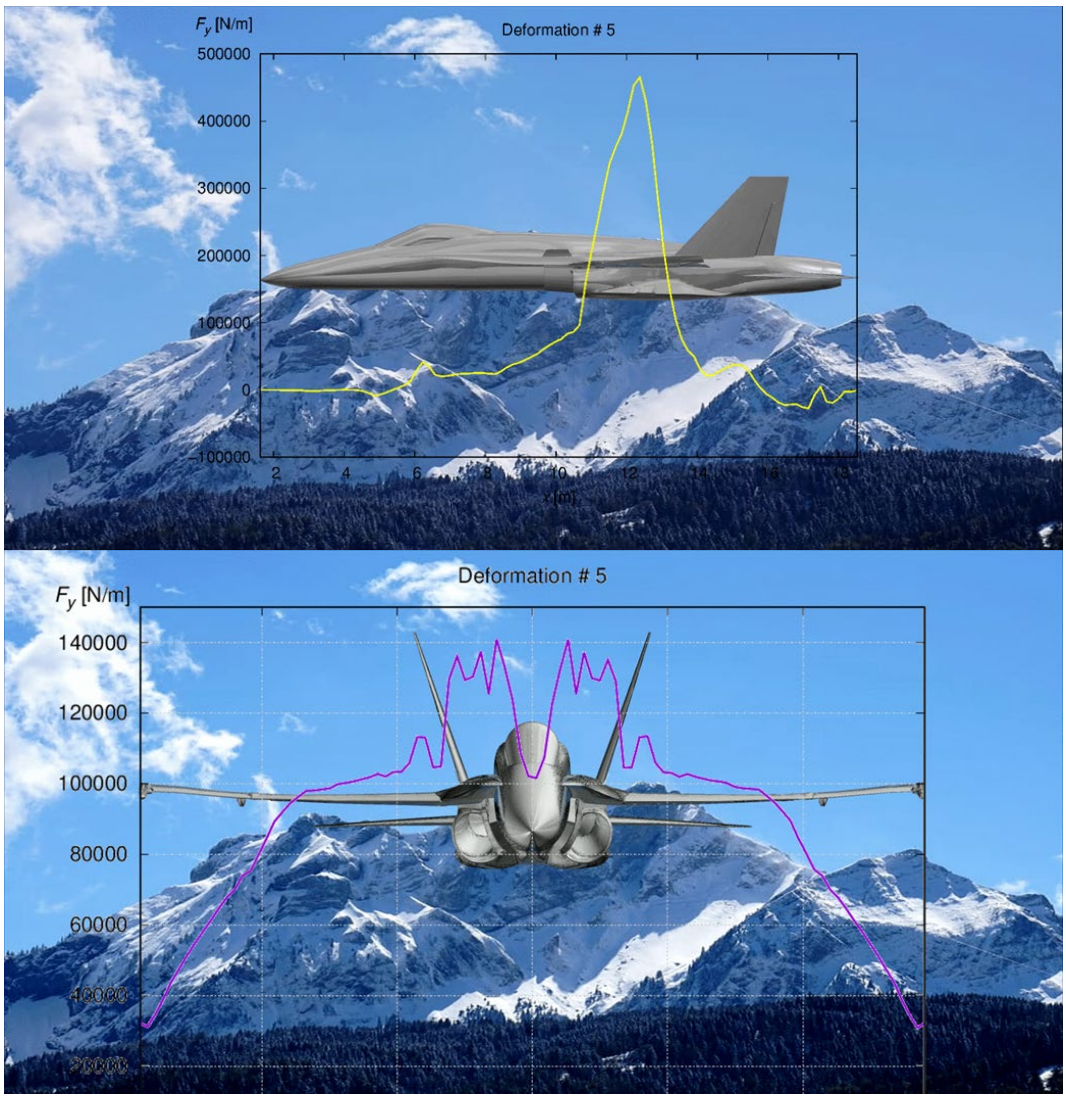

Figure 16: *Axial (upper figure) and span-wise (lower figure) vertical-force distributions for the deformed aircraft at 7.5 G pull-up at sea level, Ma = 0.849. Figure courtesy of Elomatic Ltd.*

2.1.2 Hornet FE modeling - update

In the ICAF 2021 report (Chapter 2.1.4 of Ref. [28]), previous development phases of the global and detailed Finite Element (FE) modeling of the FINAF F/A-18C Hornet were outlined. Since then, new detailed FE models, crack Initiation analyses based on the FINAF fleet usage representative FINAF BOS2 spectrum (Chapter 2.2.5 of Ref. [26]), Fail-Safe analyses have been prepared for the following structural locations: Inner Wing Front Spar Fasteners [49], FS233 Former [68], Vertical Tail Inner Structure [50], Dorsal Longeron (CEN/AFT Fuselage and FS557.7 Splice Plate), FS497 Former and Outer Wing Aileron Hinge [98] (**Figure 17**).

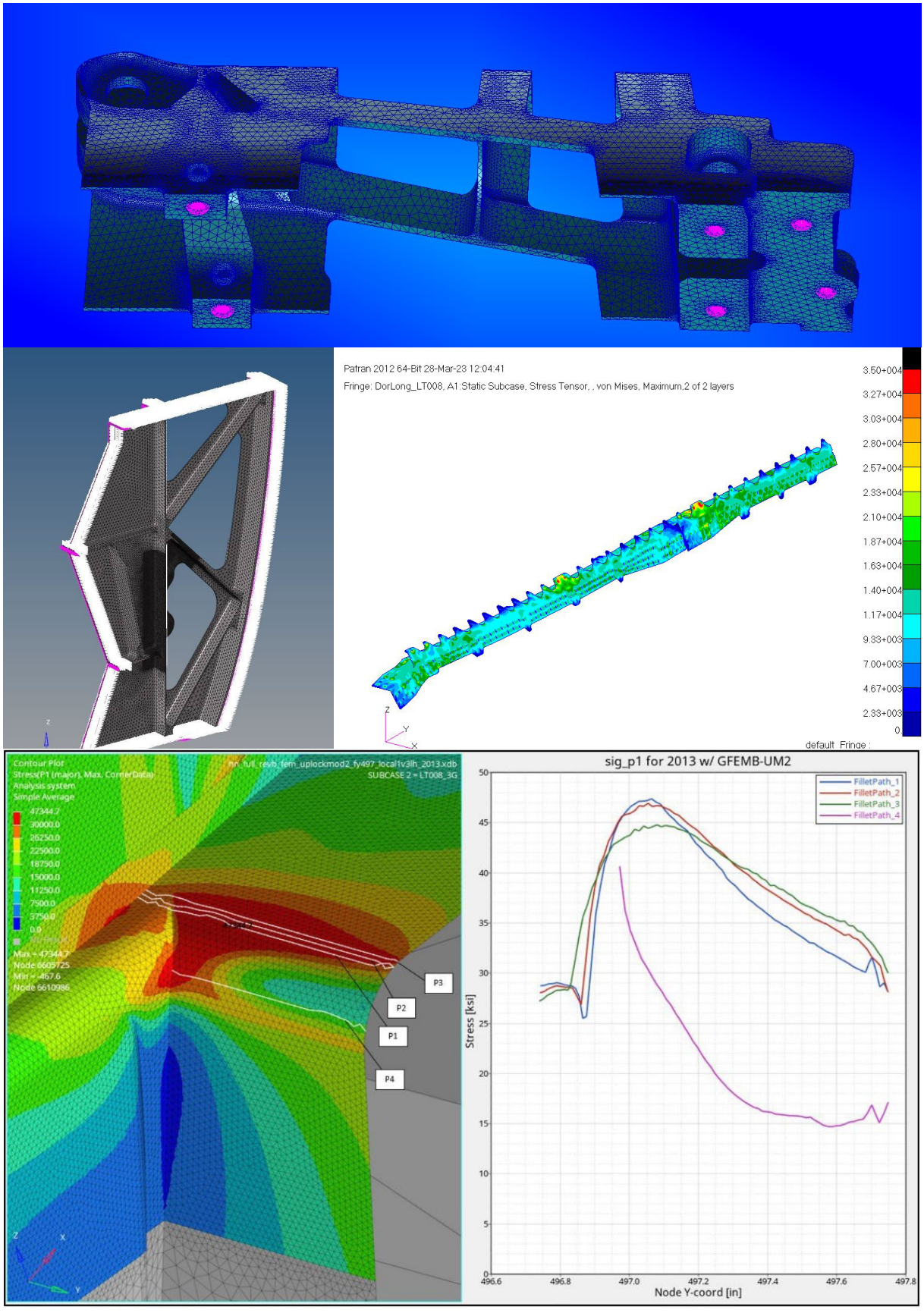

Figure 17: *Detailed FE models of Outer wing Aileron Hinge, FS233 Former, Dorsal Longeron (FS374-FS485) and FS497 Former. Figure courtesy of Patria Aviation.*

2.1.3 Vibration-induced fatigue life estimation of the Vertical Tail of the F/A-18 aircraft using virtual sensing

Unmeasured quantities and responses at selected locations in structural monitoring can be estimated by different virtual sensing techniques. Virtual sensing enables estimation of operational response of the structure at any location based on a limited set of measurements and the numerical model of the structure. This paper presents the study for expansion of sparse response data from the Vertical Tails (VT) of the FINAF F/A-18C HOLM aircraft (Chapter 2.2.2) by means of a component simulation model to enable fatigue analysis anywhere in the structural component or subassembly under question.

The virtual sensing applied in this study was based on bandpass filtering the measured acceleration data to get modal-specific responses for the primary VT modes. Component FE-model of the VT was then used to create modal-specific acceleration-to-strain conversion functions for the structural details of interest. For each mode individual virtual strain signal was generated at the chosen structural location. All the signals of the primary modes at the same location were combined by the superposition principle to achieve the total virtual strain, which then could be used as an input in the typical fatigue analyses.

To validate the FE model of the VT and its support structure and to evaluate model expansion capabilities for a single accelerometer data, vibration characteristics of the aircraft were identified experimentally. To identify vibration characteristics of the aircraft, lowest elastic natural modes of the VT, i.e., natural frequencies, modal damping factors and mode shapes were determined experimentally by modal testing [75], also Chapter 2.2.4 in Ref. [28].

Research focus of this study was applicability of the local/component FE models for the virtual sensing. Research question was to investigate the limitations of the method when applying only a local/component FE model and minimum number of sensors for the virtual sensing. The results demonstrated applicability of the local component FE model and only a single acceleration measurement for virtual sensing in cases where dominant modes were well separated. However, limitations of the component model should be checked, e.g., by Modal Assurance Criterion (MAC) correlation analysis for each dominant mode. [74]

2.2 Loads monitoring and fatigue tracking systems

2.2.1 Transition from Valmet L-70 Vinka to Grob G115E: Deepening the national technical understanding

It has been in the culture of the FINAF to be self-sustaining with their aircraft to a certain level. This for instance enables domestic life cycle support, modifications or repairs possible, if necessary. With this background the Finnish Defence Forces has funded a project in which Patria Aviation with its partners has built a basic technical understanding of the Grob G115E basic trainer fleet and developed a partial national maintenance, repair and overhaul (MRO) capability for the aircraft which fully replaced the Vinka in September 2022 (Chapters 1.1, 1.2).

The first step of the project, an aerodynamic model of the aircraft and initial computations with it, were described in the ICAF 2019 report (Chapter 2.1.4 of Ref. [27]). Applications and enhancements of the CFD model were further described in the ICAF 2021 report (Chapter 2.1.5 of Ref. [28]). It also contained preliminary information about the then ongoing flight test program mini-OLM i.e., a small-scale operational load measurement project (Chapter 2.2.7 of Ref. [28]). This work was carried out as a collaboration with the FINAF, Patria Aviation and VTT.

In the mini-OLM program two separate onboard data acquisition systems were used. The main system recorded data from 40 strain channels, 8 temperature sensors, pitot and static pressure sensors and an accelerometer. The strain channels were calibrated to indicate loads (**Figure 18**). The other system was a standalone gyro platform, which recorded for instance attitude, angular velocities, and accelerations, in addition of pitot and static pressures. [47], [53]

Figure 18: *Calibration of the wing strain channels of the instrumented Grob G115E aircraft. Figure courtesy of Patria Aviation.*

During the flight test phase, all the normal and acrobatic maneuvers of the aircraft were flown covering the whole flight envelope and varying the mass and center of gravity. A total of 22 flights were flown and 21 hours logged. [16]

From the flight test data, global loads were calculated using a neural network analysis and control surface loads were directly calculated using control system calibration results. Based on the temperature measurements it could be shown that the strains were not sensitive to ambient temperature changes [52]. The flight test data supported by the

CFD results have already been utilized when solving problems related to control surface attachments. [36]

The next step of the project was static ground tests to the following main components of the aircraft used in the mini-OLM program: wing, fuselage, horizontal stabilizer, aileron, flap, rudder, both elevators, engine mount and main landing gear leg. This work was carried out as a collaboration with Patria Aviation, VTT and Tampere University.

During the ground tests structural responses were measured from each component when loaded with a clearly defined load or load sets. Depending on the component, up to 35 load cases were used (**Figure 19**). The limit load levels for the tests were derived from either FAR Part 23 requirements or previously described flight tests. The actual used load levels during testing were kept low, as a fraction of the limit loads, as the aircraft will return to the FINAF operation.

Figure 19: *One of the load cases of the tested left wing. Figure courtesy of Patria Aviation.*

The purpose of the ground tests was to deepen understanding of the structures and to utilize the results in the future when building up FE models of the components. For these tests, the instrumentation was extended to a total of 260 strain channels supported by 6-8 displacement sensors depending on the article. In addition, 3D Digital Image Correlation (DIC) method was utilized in most of the measurements to get full-field deformation data from the main areas of interest of the tested components (**Figure 20**).

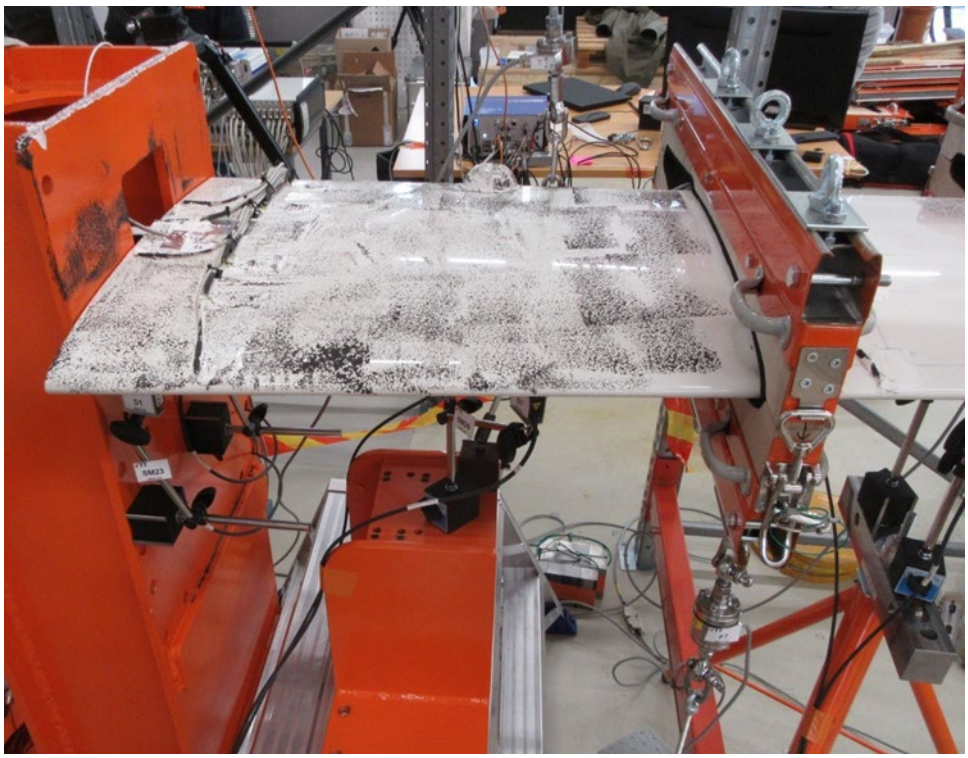

Figure 20: *Horizontal stabilizer test showing strain gages, displacement sensors and the speckle pattern for DIC measurements. Figure courtesy of Patria Aviation.*

Reporting of the tests have now been completed and the post processing of the results for validation of the FE-model is ongoing. [64], [54], [55], [56], [57], [58], [59], [60], [61], [62], [63], [81], [82], [83], [84], [85], [86], [87], [88], [89], [90]

The work done during the mini-OLM program and static ground tests is described in more detail in a paper presented in the ICAF 2023 [37].

2.2.2 The FINAF HOLM aircraft in routine squadron service

The FINAF has routinely been running the Hornet Operational Loads Measurement (HOLM) program since 2006 [21]. The goal in this program is to quantify the effects of operational loads on the structure of the F/A-18C/D Hornet aircraft and thus support the national aircraft structural integrity efforts. The HOLM program employs two Boeing F/A-18C Hornet aircraft (HN-416 and HN-432) with originally identical, but afterwards diverged onboard data acquisition systems (**Figure 21**) and instrumentation (Ref. [26] Chapters 2.2.2, 2.2.4). 44 strain sensors, in all, have been fitted on globally important locations as well as in the vicinity of structural locations addressed to be fatigue critical. In addition, four accelerometers have been installed in top section of the Vertical Tails. Concurrently the HOLM system monitors and records 250+ flight parameters from the MIL-STD-1553 data buses of the aircraft. The optimized sampling rates of the strains vary from 1280 Hz in the highly vibrating structural locations (e.g., Vertical Tail) to 640 Hz elsewhere. The sampling rate of the accelerometers is 2560 Hz.

Prior introducing the onboard HOLM system into service, the ground calibration tests (i.e. mechanical calibrations) for the system were performed, as highlighted in Chapter 13.5.1.3.3 of Ref. [21] and Chapter 2.2.4 of Ref. [26].

The onboard HOLM instrumentation has also been shunt calibrated on a regular basis by VTT in support of Patria Aviation. The annual electrical calibrations of HN-416 and HN-432 reveals if any changes in the measuring chain have occurred and/or if the calibration coefficients need to be adjusted. Based on the calibration results, the quality of the

system has remained outstanding: the quality of the strain signals is good, and all the recordable strain data has been captured (minimal missing data). This all forms a solid base for all the analyses that are made based on the HOLM data. [105], [106]

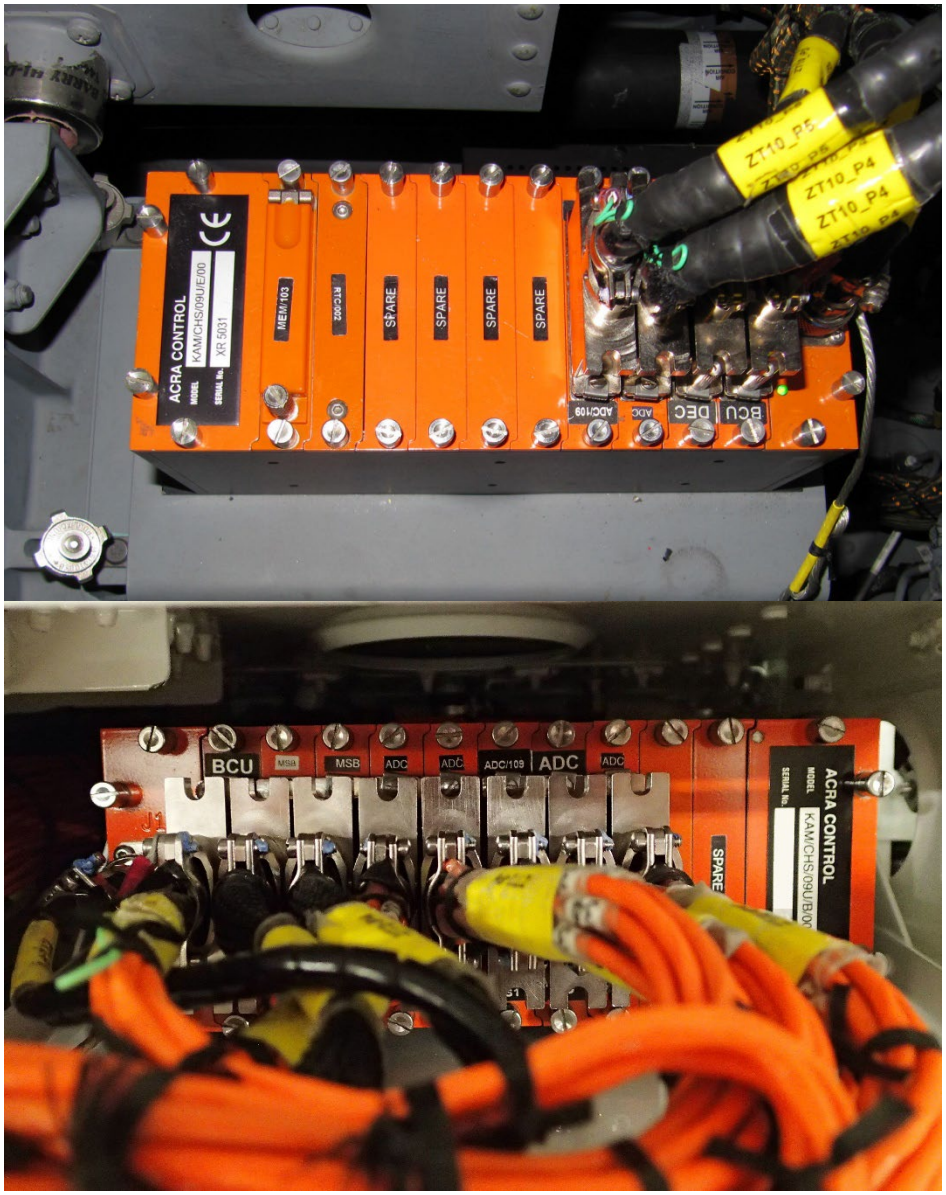

Figure 21: *HOLM DAU Master Unit (top), and Slave Unit (bottom). Figure courtesy of VTT.*

To date, VTT has analyzed in the HOLM ground analysis environment 4000+ flights from routine fleet operations and prepared several annual or semi-annual fatigue analysis reports. The reports summarize fatigue life estimates of the critical and the instrumented locations of the structure in a versatile way, such as from a syllabus, a sub-assembly, and from buffeting point of view. The ground analysis environment is based on the COTS software enhanced with the in-house codes (sequences and functions). The data flow is supported by the HOLM fatigue analysis database that combines seamlessly the data and information in the HOLM ground analysis environment. In addition to the fatigue analyses results, the database includes all the relevant information of the data analysis process. A remarkable advantage is the possibility to compare the results on a flight-by-flight basis in between various sources (SAFE and HOLM), and as recurring process, to track the trends of the analyses results.

After 17+ years of service in harsh environment, with a few exceptions, the hardware is still working great, and the quality of the recorded HOLM data has remained outstanding, that is, the HOLM data forms a good basis for all the subsequent analyses and data sets needed, like the FINAF F/A-18 Hornet Basic Operational Spectrum ver 2 “BOS2” (Chapter 2.2.5 in Ref. [26]) that was compiled on the basis of the HOLM and SAFE data in co-operation with VTT and Patria or for the parameter based fatigue life analysis (Chapter 2.2.3).

2.2.3 Parameter based fatigue life analysis

The parameter-based fatigue life analysis is an individual aircraft fatigue life monitoring system developed for the FINAF F/A-18 Hornet fleet by Patria Aviation. The analysis utilizes inherently recorded flight parameter (Memory Unit) data, by standard aircraft systems, and created artificial neural networks (ANN) to model strain histories, and further, from which to produce fatigue damage estimates of the fatigue critical structural locations on a flight-by-flight basis. The ANN has been trained with a various sets of flight parameter data (input data) and strain data from the two HOLM aircraft (desired target).

The ANN – on the basis of extensive HOLM data (Chapter 2.2.2) – enhances the nominal aircraft fatigue tracking and enables to evaluate the structural life consumption of the entire Hornet fleet with adequate reliability. The parameter-based approach enables the fleet to be sorted in fatigue index (FLE) order for scheduled inspections, repairs, and structural part replacements. The method is schematically illustrated in **Figure 22**. Technical background of the analysis is comprehensively explained in Refs. [101] and [102].

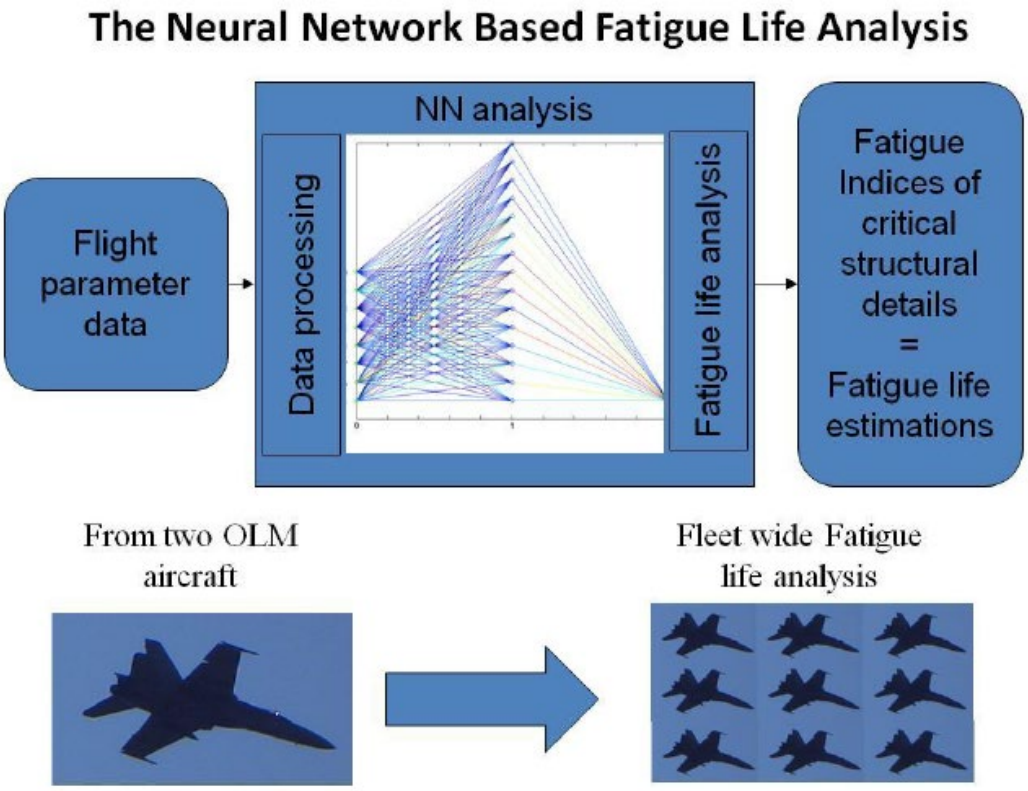

Figure 22: *Data flow in the parameter-based fatigue life analysis. Figure courtesy of Patria Aviation.*

2.2.4 Research efforts towards Hawk structural integrity management

The FINAF flight training syllabi changed significantly some years ago. For example, glass cockpit modification (see Chapter 1.3) enables practising some training flights with the Hawk aircraft which earlier were flown solely by the Hornet. These changes may reduce the life of some critical structural components or locations well known from the older FINAF Hawk Mk.51/51A fleet.

The inherent fatigue tracking system for each FINAF Hawk aircraft has been based on counting g level exceedances and calculating a usage index i.e., Fatigue Index (FI) by the variant specific equations. This method is adequate for monitoring the structural locations mainly influenced by aircraft normal acceleration (multiplied by weight). However, current FI tracking does not take buffet loading into account which is the main driver for the structural fatigue issues e.g., in the empennage of the Hawk aircraft.

2.2.4.1 Hawk Structural Health Monitoring (SHM) update

The Structural Health Monitoring (SHM) related Neural Network (NN) investigations for the FINAF Hawks were already explained to some extent in the previous ICAF 2019 (Chapter 2.2.3.2 of Ref. [27]) and ICAF 2021 reports (Chapter 2.2.6.1 of Ref. [28]). In summary, NN is an algorithm for calculating fatigue damage for critical structural parts by using the recorded flight parameter data as an input. Before NN can be used, it must be developed and trained by a separate data set to formulate the right correlations between the flight parameters and structural loadings.

After 2021, the FINAF Hawk NN was further developed with the training data from five SHM-instrumented aircraft on approx. 700 flights. The onboard instrumentation consisted of five strain sensors of which three were installed on the tailplane, one in the fin root, and one in the fuselage top longeron, left-hand side. The fuselage measurement point was highly influenced by the aircraft g-loads and was therefore used for synchronizing the strain sensor data with the flight parameter data. The data sets were acquired with Emmecon's Data Acquisition Unit (DAU, **Figure 23**). which measures and processes the strain signals as turning points and saves the result in a Rainflow matrix form in a flight-by-flight basis.

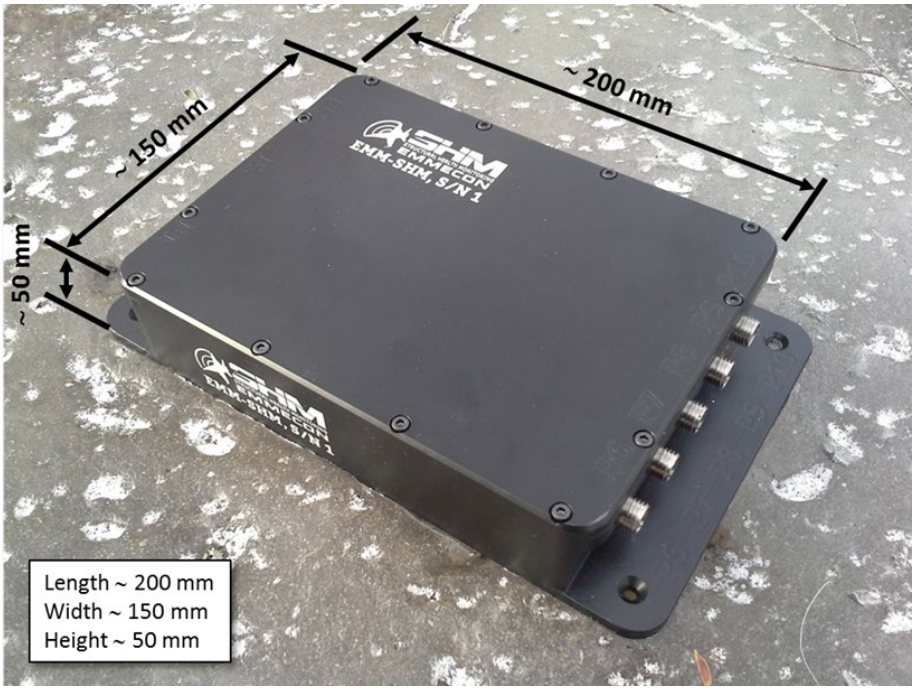

Figure 23: *Emmecon's onboard SHM system. Figure courtesy of Emmecon.*

However, flight parameter data was saved as time histories by the mission data recorder (MDR). That proved problematic to achieve precise synchronization between the DAU and MDR data, and finally new NN based SHM data became no more representative than the first version of the NN data based on the HW-368 mini-OLM flights (Chapter 2.2.6.1 of Ref. [28]). It became obvious for the next steps in the NN development that the SHM data recording should be based on the strain signal time histories.

Currently, further studies and development concerning the Neural Network for the FINAF Hawk aircraft are being considered. For example, feasibility of the NN for fatigue tracking in the centre fuselage is under consideration.

2.2.4.2 Creating an operational spectrum for the wing of the FINAF Hawk aircraft

Fatigue critical hot-spots and expected lifetime of the structure of the FINAF Hawk fleet are quite well known due to the long service history of the type. However, according to the current plans, the Hawk fleet service life extends to around 2035, and as the end of the planned withdrawal date approaches, it becomes increasingly important that the load spectrum which is used in the crack growth calculations and thus comprising a crucial part of the aircraft structural integrity, describes the use of the platform as representatively as possible. When the contents of the flight training syllabi and resulting effects on the structure changes, the operational (reference) spectrum must be updated. [65]

The aim of this study was to create an updated load spectrum for the wing of the FINAF Hawk aircraft. Firstly, the load spectra representing average flying were formed for three sub-assemblies of the aircraft: tail, fuselage, and wing. The flights representing the spectra were selected 1) based on the structure-specific relative fatigue values calculated at VTT from the flight measurement data of the instrumented Hawk aircraft (HW-368) flying in squadron use, and 2) based on the planned flight distribution of the FINAF's Hawk fleet. [39]

All the flight selections for the spectra were solely based on the Sortie Profile Code (SPC) of the target distribution. The impact of the training programmes was not specified, i.e., the flights selected for the flight tasks might have included flights flown in several different training programmes.

Fatigue analyses were based on the traditional OLM fitting factors and SN curves which had been used in the corresponding analyses for the FINAF's HW-319 and HW-348 aircraft. No assessment of the representativeness of the results for the HW-368 was made separately, as in this context the values represented only relative structural fatigue at the analysed structural locations. Thus, the damage results cannot be considered as values representative of actual fatigue damage.

Based on the generated AOA-Q matrices (classified combinations of angle of attack and kinetic pressure), Patria Aviation Ltd. checked the appropriateness of the flights selected for the spectra. This was to ensure that the selected flights corresponded to flying in accordance with the flight reports. After this, a final proposal could be formed for the spectra corresponding to the average flying of the FINAF Hawk fleet, and the load spectra could be made available to the national aircraft structures research community.

The plan was to select flights for the spectrum in such a way that it would cover maneuvering loads and high frequency buffeting loads of the tail. Most of the fatigue damage accrued in the empennage of the Hawk aircraft resulted from flying in the limited points in the sky (PITS). The calculated fatigue damage rates based on the tailplane strain sensor data were summed into the AOA-Q table which exposed a flight envelope that covered approx. 80 % of the fatigue damage accrued for the tailplane (**Figure 24**). The most severe AOA-Q combinations were representative for the average flying among the mini OLM flights (Chapter 2.2.3.1 of Ref. [27]).

		Q [hPa]																			
	Bin Damage / block																				
AOA [°]		0	2.434E-06	4.15913E-10	0	0	2.815E-11	3.01E-11	9.32E-08	1.78362E-10	0	0	0	0	0	0	0	0	0	0	0
		1.51188E-07	0.00011537	5.93326E-05	6.77604E-05	0	0	3.24E-08	1.17E-07	8.79905E-07	1.54929E-06	4.30723E-06	3.18254E-06	6.93556E-06	2.44796E-06	5.16068E-06	1.91956E-06	7.51633E-07	6.90484E-07	2.78831E-06	
		5.98943E-07	3.5047E-05	7.63349E-05	8.90889E-05	2.761E-06	0	1.53E-05	2E-05	7.41436E-05	4.74647E-05	1.29218E-06	2.16486E-05	2.27056E-05	7.85259E-06	1.27707E-05	2.30538E-06	1.01894E-07	0	0	
		2.32714E-06	1.1076E-05	5.81278E-05	2.35095E-05	3.283E-06	0.0086947	8.08E-05	0.000223	0.000718129	0.000999845	7.4565E-06	6.65388E-06	5.98733E-06	4.83461E-06	8.08788E-08	0	0	0	0	
		4.24095E-06	0	7.71101E-05	1.03947E-05	5.184E-05	0.000141	0.000526	0.003122	0.006513969	0.002508107	0.000175804	2.17667E-06	6.48231E-08	0	0	0	0	0	0	
		9.26368E-06	1.5263E-05	5.49803E-05	5.51655E-05	0.0001366	0.0012394	0.003713	0.015579	0.012952292	0.005601162	0.001346293	0	0	0	0	0	0	0	0	
		7.10523E-07	4.1694E-06	3.66568E-06	0.000181525	0.0009013	0.0099905	0.021427	0.077039	0.060026386	0.00926207	0	0	0	0	0	0	0	0	0	
		2.54437E-07	2.7114E-06	3.19482E-05	0.0011052	0.0112225	0.0576371	0.12353	0.121483	0	0	0	0	0	0	0	0	0	0	0	
		2.19544E-07	4.0053E-06	0.000471768	0.003380813	0.0198941	0.0201767	0	0	0	0	0	0	0	0	0	0	0	0	0	
		3.23647E-07	2.5168E-05	0.000303977	0.000286114	0	0	0	0	0	0	0	0	0	0	0	0	0	0	0	
		6.34449E-07	4.1216E-05	0.000112087	0	0	0	0	0	0	0	0	0	0	0	0	0	0	0	0	
		4.97746E-07	5.5759E-05	4.47465E-05	0	0	0	0	0	0	0	0	0	0	0	0	0	0	0	0	
		2.31234E-07	4.1718E-05	0	0	0	0	0	0	0	0	0	0	0	0	0	0	0	0	0	
		0	0.00013764	0	0	0	0	0	0	0	0	0	0	0	0	0	0	0	0	0	
		0	0.00026794	0	0	0	0	0	0	0	0	0	0	0	0	0	0	0	0	0	
		0	4.4516E-05	0	0	0	0	0	0	0	0	0	0	0	0	0	0	0	0	0	
		0	0	0	0	0	0	0	0	0	0	0	0	0	0	0	0	0	0	0	
		0	0	0	0	0	0	0	0	0	0	0	0	0	0	0	0	0	0	0	

Figure 24: *AOA-Q table (without class information) including fatigue damage rates of the tailplane. The most severe bins are highlighted in red. Figure courtesy of Patria Aviation.*

The generated load spectrum represents the average usage of the FINAF Hawk fleet in terms of Fatigue Index rate. The probability plot in **Figure 25** indicates that the data likely comes from a Weibull distribution.

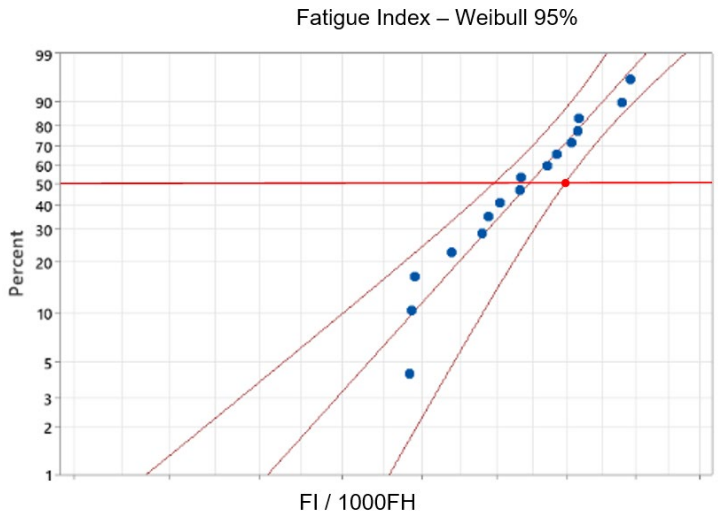

Figure 25: *Weibull probability plot with 95 % confidence intervals for the Fatigue Index rate (FI/1000 FH) of the Hawk Mk.66 aircraft. Figure courtesy of Patria Aviation.*

2.2.5 Fatigue and damage tolerance testing of Gripen E/F Rudder

Z. Kapidžić[1], J. E. Lindbäck[1], R. Laakso[2]

[1]Saab Aeronautics, Linköping, Sweden, [2]VTT Technical Research Centre of Finland Ltd, Espoo, Finland

This chapter highlights the international cooperation research activities between Saab Aeronautics (Sweden) and VTT (Finland).

A structural test of Gripen 39E/F rudder was performed to verify the safe-life and damage tolerance of the rudder structure, see **Figure 26**. The test was performed in 2021–2022 in Finland in collaboration with VTT Technical Research Centre of Finland Ltd and its partners Eurofins Expert Services Ltd and Arecap Ltd, and the results are presented in the paper in Ref. [51]. Two different design load sequences, one representing the operational profile of the 39E-version and the other for the 39F-version, with the latter being more severe, have been considered. Preliminary analyses have shown that a test using the more severe sequence 39F would likely not be able to verify the full service life. Therefore, a strategy was adopted to test the 39E sequence with upscaled loads during a part of the test campaign and thereby verify the 39E sequence, as well as part of the service life of the 39F. The test was successfully run to a number of simulated flight hours [32], [44] where the most critical crack had grown from an artificial defect to a predicted critical length [41]. A subsequent static test showed that the structure had sufficient residual strength. The paper [51] presents an analytical procedure, based on fatigue and crack growth calculations, to determine the corresponding percentage of the 39F service life that is considered to be verified by the performed test. This approach shows a cost-efficient way to utilize the test results as much as possible, without jeopardizing the primary goal of validating the configuration 39E of the aircraft.

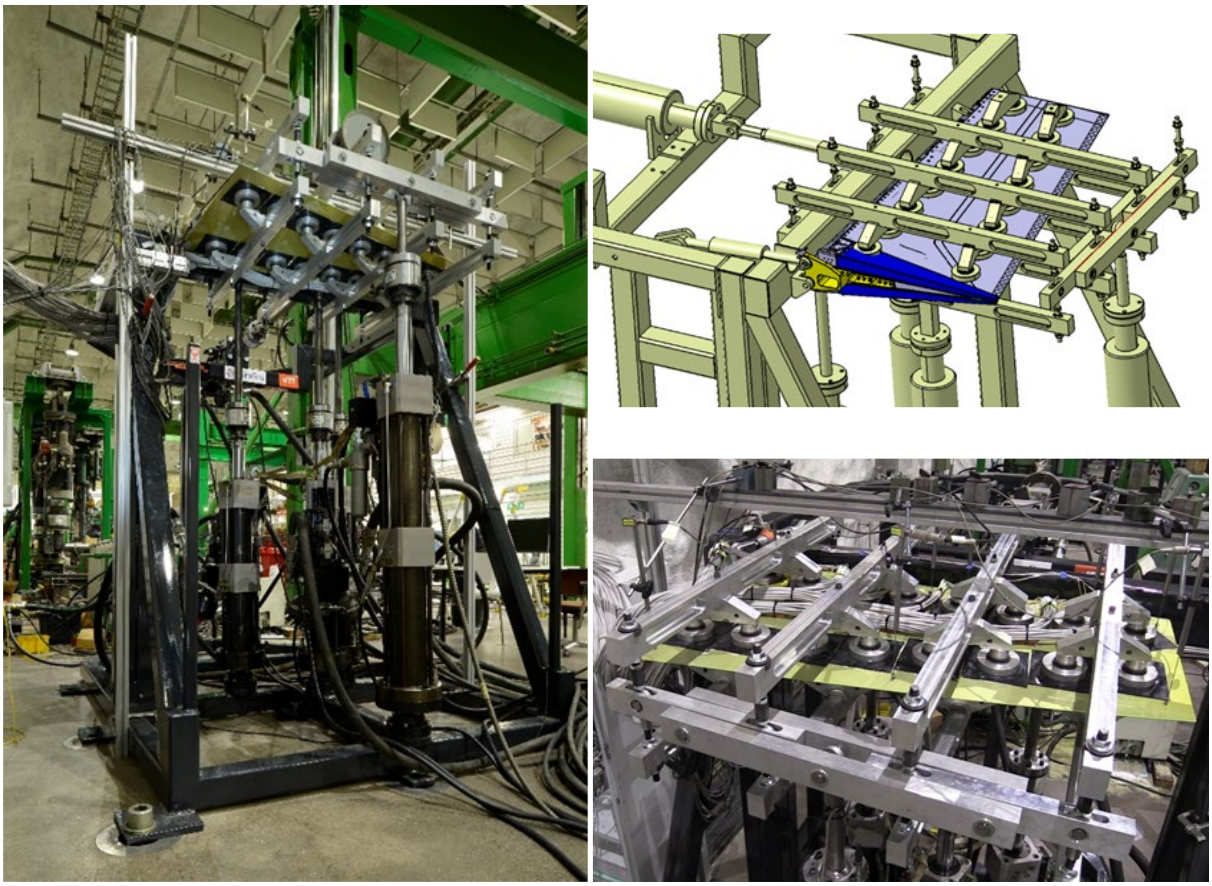

Figure 26: *Rudder fatigue and DT test object and test rig. Figure courtesy of Saab Aeronautics and VTT.*

2.2.6 Preliminary design of a full-scale component fatigue test

The need to promote national fatigue testing capabilities of larger-scale aircraft structures, i.e., verification of structural life of a component on an experimental basis has been recognized for a long time. It is especially relevant for the structures prone to high-frequency dynamic loadings (buffeting). The selected structure for the preliminary study of a component fatigue test was the F/A-18 Hornet's Bootstrap which is the primary load path for aerodynamic loads effecting on the horizontal stabilator and transmitted from the elevator actuator. In certain flight conditions, the stabilator is subjected to intense vibration loadings, which are transmitted to the Bootstrap, resulting fatigue damage. In addition, due to the substantial static loads experienced by the Bootstrap, an analyzed critical crack length of the component is relatively short (**Figure 27**). [17]

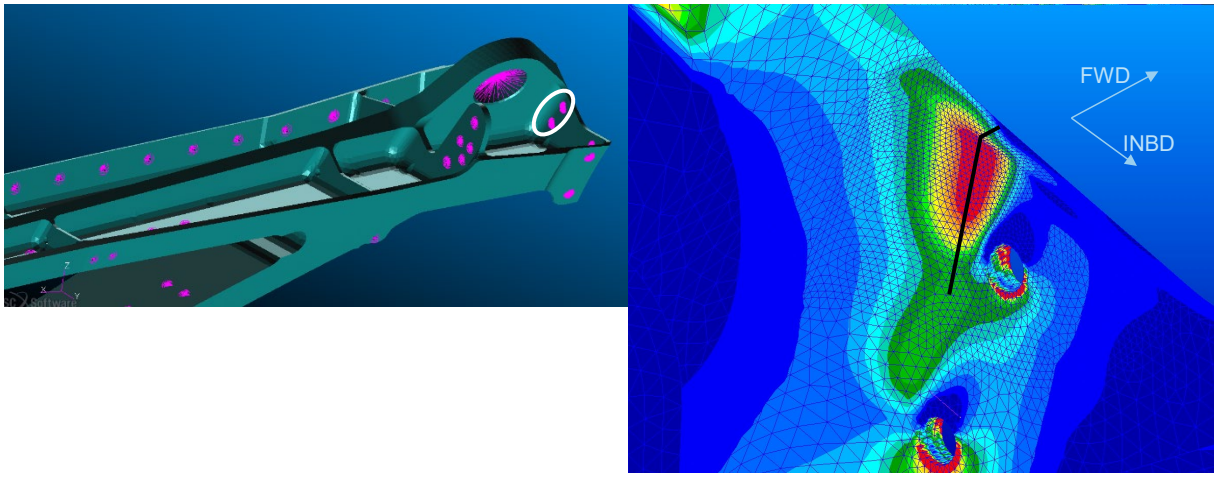

Figure 27: *Analyzed location of the Bootstrap. Figure courtesy of Patria Aviation.*

The designed test set-up included the essential load paths of the center and aft fuselage. The load introduction was designed to take place via the horizontal stabilator spindles, and the fuselage was supported by the wing attachment lugs. The preliminary fatigue test spectrum was either the BOS2 HTTOR torque spectrum of the stabilator or, alternatively generated BOS2 spectrum, also including the bending and shear load components from the stabilator. The representativeness of the load spectrum was planned to be verified by coupon tests before the actual fatigue testing.

The preliminary design of the fatigue test also included the study of the effect of spectral filtering level on the crack growth rate and test duration (**Figure 28**). However, the analytical effect of filtering on the representativeness of the spectrum must be verified with a test series before the actual fatigue test spectrum would be created and selected.

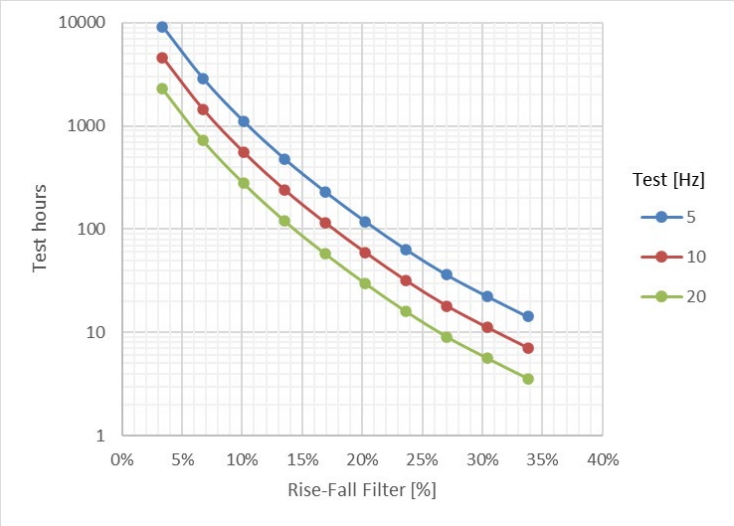

Figure 28: *The analytical effect of the spectral filtering level on the planned fatigue test duration. Figure courtesy of Patria Aviation.*

As far as the fatigue test equipment is concerned, a typical problem has been identified as producing a high load level associating a high loading frequency. Another strand of the project was to identify the necessary load equipment resources to enable demanding large-scale fatigue testing, including high-frequency loads, for the use of lifetime management of aircraft structures when testing full-scale assemblies and components. The end goal in the subsequent projects was to reproduce the stress states, experienced by the structures during flights, in laboratory conditions as realistically as possible.

The preference hypothesis was that the loads required for fatigue testing from more than one direction and point can still be implemented with conventional, good-quality servo hydraulic load actuators with life cycles of several decades. The rated actuator force should exceed the test requirements appropriately, and the stroke should be close to actual needs but as short as possible. This could be a difficult task, if the test specimen is e.g., a wing, rudder, or similar cantilever beam structure, whose loading requires large movements, i.e., long strokes. The most high-performance choice sometimes requires new investments, if any changes in load introduction structures is of no use. In any case, the mass of moving parts should always be minimized while maximizing the rigidity of the set-up.

The order in which the high-frequency performance is determined and the factors that directly limit the ability are 1) the load actuator, 2) the servo valve, 3) the minimization of moving masses, and 4) the rigidity of the test arrangement. Other factors affect test performance mainly indirectly. In a structural test arrangement, different factors each set their limits on the maximum possible load frequency, and the most limiting factor is typically the dynamics of the test arrangement itself. All these aspects are discussed in more detail in reference [33].

2.3 Structural integrity of metallic materials

2.3.1 Testing and analysis capability of small cracks

A small or short crack can be defined in several ways: (i) It can be a crack which is of length comparable to the scale of the microstructure (of the order of the grain size), or (ii) a crack which is of a length comparable to the scale of local plasticity (e.g. small crack embedded in the plastic zone of a notch or of a length comparable with their own crack tip plastic zone, or (iii) a crack which is simply physically small (e.g.~0.5-1 mm). [100]

Typically, small cracks grow faster than long cracks when subjected to the same Stress Intensity Factor (SIF) range ΔK, and they continue to grow below the long crack threshold (ΔK_{th}). The growth rate for small cracks may decelerate and then accelerate to merge with that of long cracks, or they may stop growing. These phenomena are commonly referred to as small crack effects, and they have practical engineering significance because the predictions based on Linear Elastic Fracture Mechanics (LEFM) methodology usually lead to non-conservative crack growth rate, inspection intervals or possibly critical crack size. The capability to analyze a small crack growth rate is of primary importance for highly-stressed aircraft structures because the critical crack length can be only a few millimeters. [15]

The growth of small cracks has previously been studied experimentally by fatigue tests which were introduced in Chapter 2.3.2 of Ref [27] and [28]. In this follow-on research, led by Patria Aviation Ltd., the goal is, via coupon testing, to define the small crack growth curves under spectrum loading and thus to get proper understanding on the effect of various test parameters, such as load transfer ratios, load levels and fittings/structural modifications on the behavior of small cracks propagating in aluminium materials. [111], [76]

First test parameter is the axial load transfer ratio (LT), i.e., the ratio between bearing and by-pass stresses. The test specimens are manufactured according to the ESDU low load transfer (LLT) and medium load transfer (MLT) geometry [13], [14]. Three different joint geometries were selected for the spectrum fatigue test: one LLT (LT<10 %) and two MLT (LT=10-30 %) type of joints. The number of test specimens will be approx. 100, and fracture surface analyses will be carried out for all the specimens to determine the small crack growth rates. The test specimens are made of Al 7075-T76 material, and their geometries are presented in **Figure 29**.

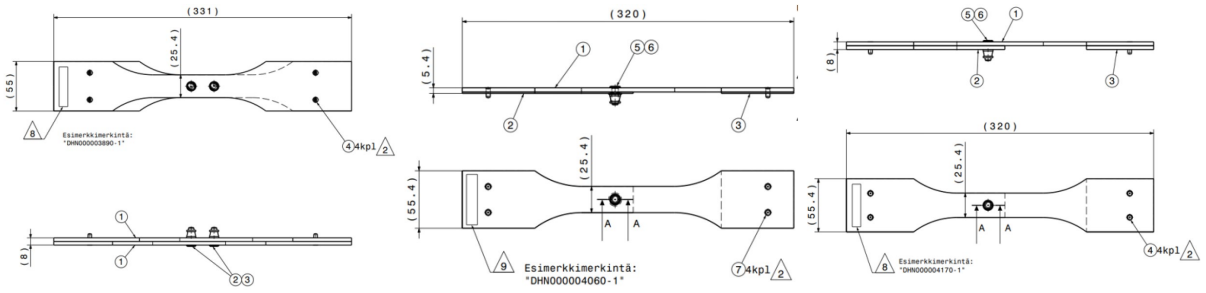

Figure 29: *ESDU test specimens in the small crack growth study. LLT specimen (left), MLT1 specimen (middle), MLT2 specimen (right). Figure courtesy of Patria Aviation.*

The second test parameter follows the preceding research being hole tolerances and preparation methods. Test coupons have Class 2 fit, interference fit (I/F), and cold

worked hole+Class 2 fit (CW+Class 2). Summary of the test specimens is presented in **Table 1**.

Table 1: *Test specimen summary. Table courtesy of Patria Aviation.*

Material	Joint Type	Load Level 1			Load Level 2			Total
		LLT	MLT 1	MLT 2	LLT	MLT 1	MLT 2	
7075-T76	Class 2	5	5	5	5	5	5	30
	I/F	5	5	5	5	5	5	30
	CW+CI2	5	5	5	5	5	5	30

Fatigue test spectrum is the BOS2 WRBM (Wing Root Bending Moment) spectrum which also includes compressive loads. These are clipped in various levels to prevent buckling of the test specimen. The buckling load level of the test specimen and the effective stress gradients used in the crack growth calculation were evaluated by means of FEM. Test spectrum block is presented in **Figure 30** and the FEA results of the test specimen in **Figure 31**.

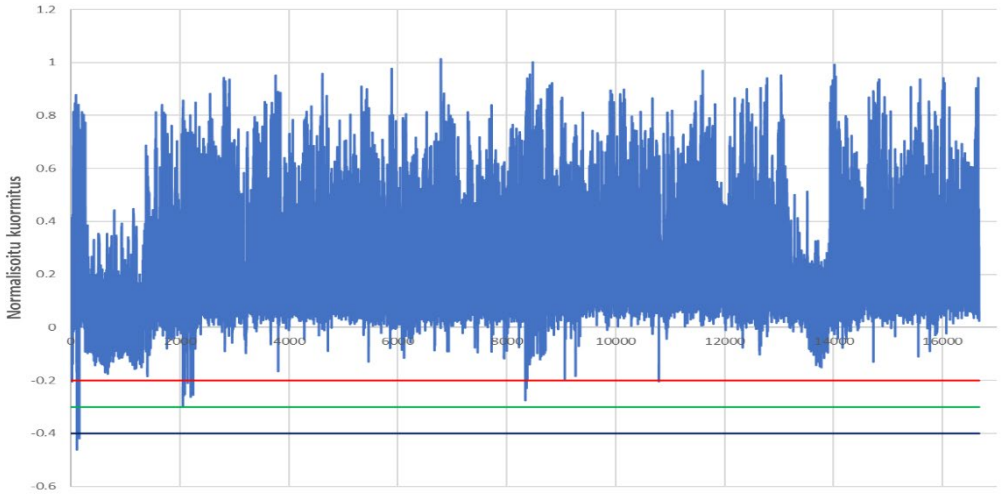

Figure 30: *The BOS2 WRBM fatigue spectrum. Horizontal lines represent different cut levels (red: 20 %, green: 30 %, black: 40 % of the maximum tensile load) for compressive loads. Figure courtesy of Patria Aviation.*

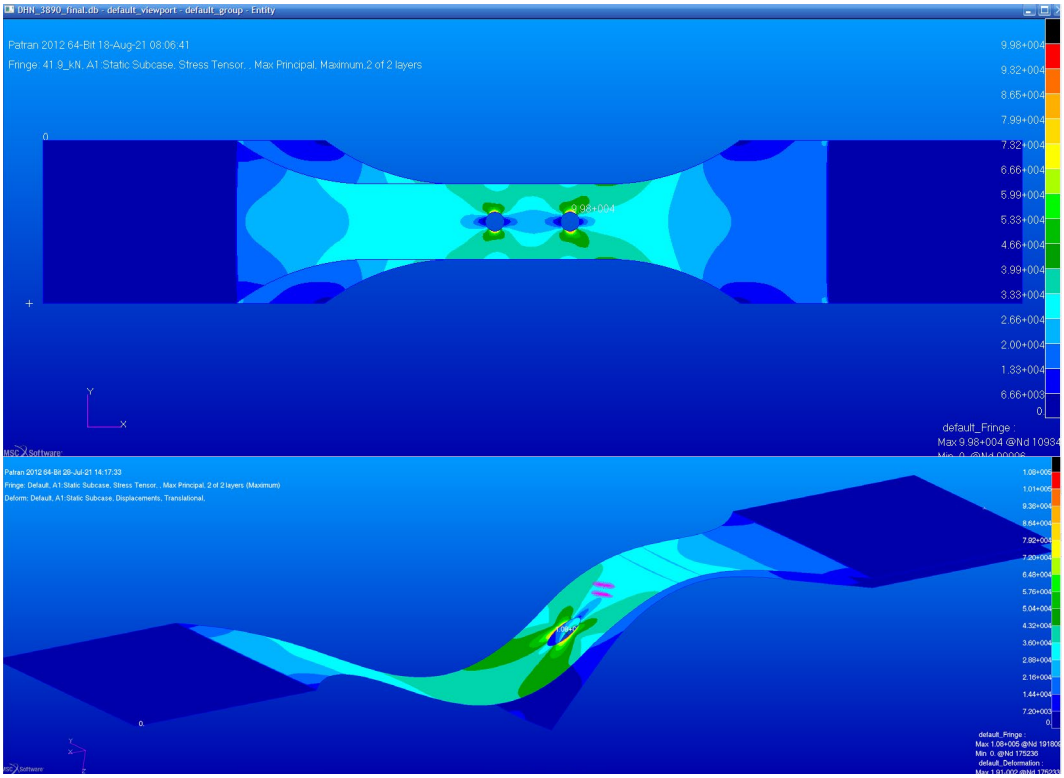

Figure 31: *The FEA of the ESDU test specimen (LLT: upper figure, MLT: lower figure). Figure courtesy of Patria Aviation.*

The estimated fatigue lives (crack initiation + crack growth) have been analyzed by the OEM's LifeWorks software [48]. The results with two different load levels per specimen are presented in **Table 2**.

Table 2: *Estimated fatigue lives (Total Life = Crack Initiation Life + Crack Growth Life) of the test specimen with two load levels. Table courtesy of Patria Aviation.*

Specimen, Load Level (LL)		**F_{ref}**	**S_{nom}**	**CI-Life**	**CG-Life**	**Total Life**
		[kN]	**[ksi]**	**[SFH]**	**[SFH]**	**[SFH]**
LLT	LL 1	39.6	30.0	1900	880	2780
	LL 2	32.9	25.0	3700	1680	5380
MLT 1	LL 1	26.5	38.0	2200	240	2440
	LL 2	22.4	32.0	4000	450	4450
MLT 2	LL 1	23.1	33.0	2000	230	2230
	LL 2	18.2	26.0	4300	560	4860

Since the main objective of the ability to analyze small cracks is to obtain crack growth curves based on physical evidence, the marker bands identified with quantitative fractography (QF) from the fracture surface must be combined with the load history.

The marker loading blocks were included in the BOS2 spectrum (**Figure 32**). Laboratory loading levels were adjusted in terms of fatigue lives of several types of small aluminium specimens. In addition, some natural parts of the spectrum that presumably leave visible and traceable markers were present (areas A and B).

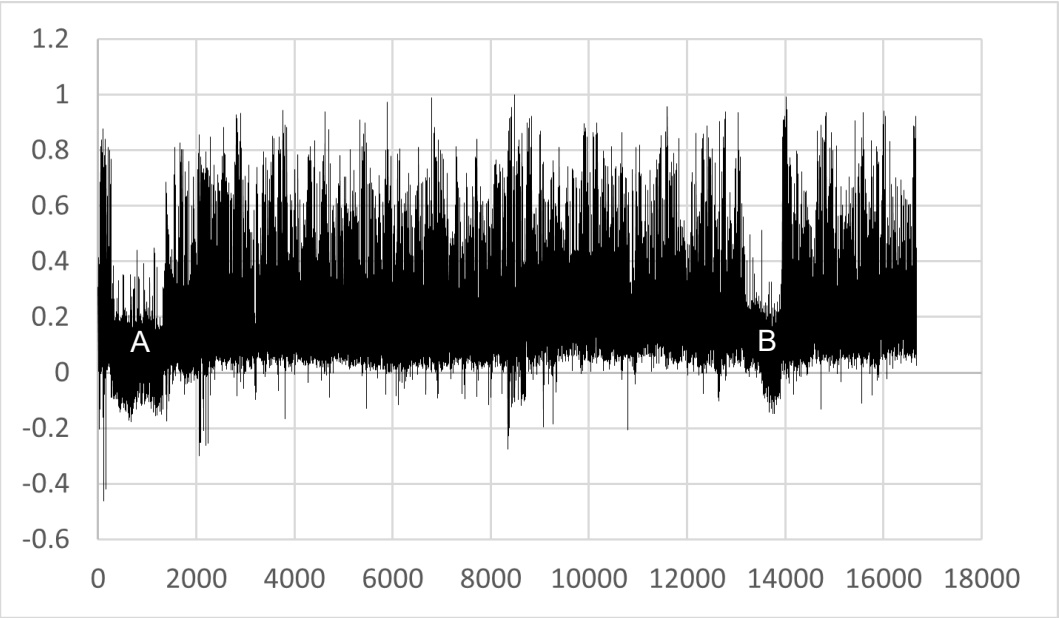

Figure 32: *The FINAF BOS2 spectrum. Horizontal axis: number of turning points; vertical axis: load level. Two weakly influencing parts, possible causing natural traceable markings, are visible at areas A and B. Figure courtesy of VTT.*

Marker loading block versions to be tested were selected based on the report "Study of Marker Loads" [45] including an extensive literature review and checked first with computational fracture mechanics. Changes in load ratios and constant amplitude loading blocks were chosen as marker load types to be further investigated. Several fatigue life and fracture surface studies were carried out, the purpose of which, in addition to investigate possible changes in fatigue lives and in test duration, was to ensure that the added marker loads – and natural marker-like parts of the spectrum – leave visible and traceable bands on the surfaces.

At first, only the scanning electron microscope (SEM) was used to assess the functionality of the marker loads. However, in the QF-marker tasks, the use of SEM was found to be too time-consuming. In this study, for a moment, and for the sake of comparison, both SEM and optical microscope (OM) were in use. In the end part of the study and from then onwards, the primary equipment is meant to be the optical microscope.

Different "barcoded" marker load block versions were tested, and the version shown in **Figure 33** was decided to be used as the added marker load type for the actual fatigue test series with approx. 100 specimens [38]. Within the fatigue tests, initial QF analyses were carried out to achieve crack growth curves and to have more feedback regarding the marker loads. In addition, more accurate estimates of required time for analysing fracture surfaces with an optical microscope were achieved and compared to the SEM analyses. The basics of defining, pre-design, and adding the marker loads, as well as related computational fatigue life estimates and fatigue testing, resulting in QF, are discussed in more detail in Ref. [46].

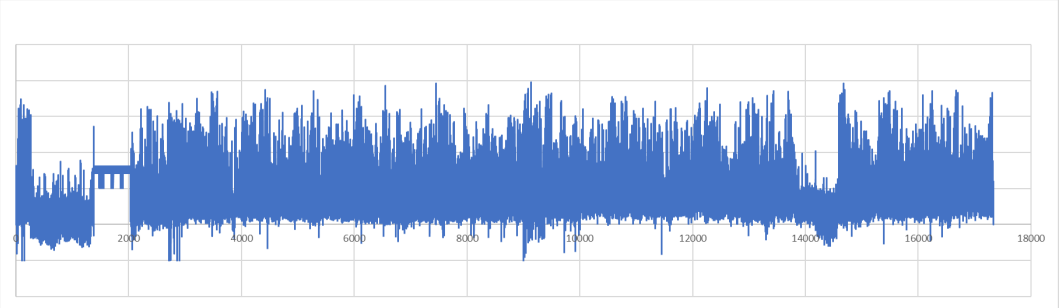

Figure 33: *"Barcoded" BOS2 test load spectrum which was introduced in actual fatigue test series [45]. Figure courtesy of VTT.*

For tracing crack growth rates particularly at small crack sizes, the use of an optical microscope alone without SEM analyses was found to be adequate but highly dependent on the fracture surface itself. An example of clearly distinguishable crack progression marks at low crack depth is presented in **Figure 34**. Based on the fracture surfaces that were analyzed also with SEM, there was no significant added benefit with SEM while tracing the crack progression. However, higher resolution was helpful for the initial identification of marker bands.

The preliminary results indicated that in terms of BOS2 marker bands optical microscope is appropriate, and SEM could be ignored for the upcoming QF analyses. Initial expectations are roughly 25–50 % reduction in working times compared to the SEM analysis, but even 80 % reduction can be achieved if the person performing the analysis is familiar with the marker bands.

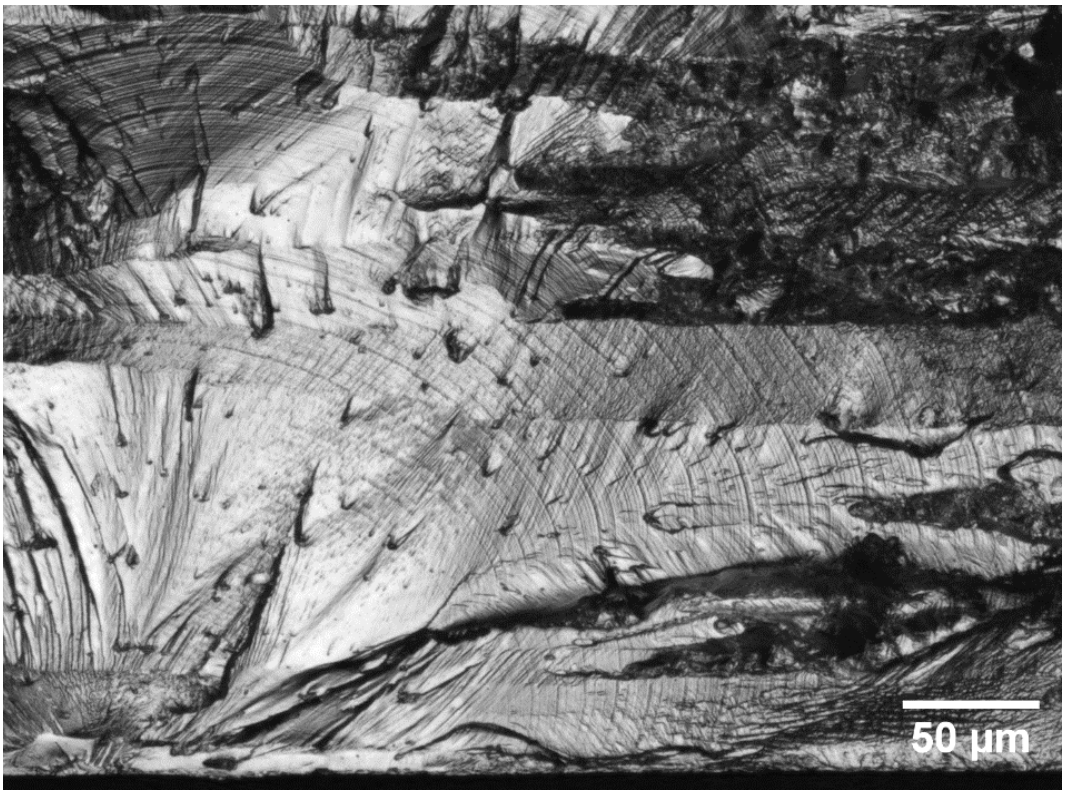

Figure 34: *Clearly distinguishable crack progression marks at low crack depth. Figure courtesy of VTT.*

2.3.2 Additive manufacturing process qualification activities

Metal Additive Manufacturing (AM) has risen as a manufacturing method to complement traditional technologies especially enabling geometrical freedom and lighter yet strong structures. The lightness in combination with the needed strength is a clear benefit in aviation applications and both the military and civil aviation industries have been pioneering in pushing the technology forward. In addition to manufacturing end-products, another interesting area of application are digital spare parts that are additively manufactured based on a digital model when needed, typically close to the end user. [99]

There are several benefits using metal AM, but there are also challenges of which quality control and assurance are of key importance. In AM, the product and the material are generated during the manufacturing phase and the process parameters are affecting the structure of the material. In contrast to e.g., casting, in additive manufacturing the practises, design principles and process control are not yet as stabilised to ensure quality products. Metal AM products are typically closer to machined than cast parts in a sense of custom components with a higher unit price instead of low-cost series products and are also target for higher quality demands. To achieve in the end fully qualified products, one needs to have all the process steps in place and the first stage in that chain is process qualification (**Figure 35**) that aims to secure that the manufacturing process is controlled, repeatable and able to produce items that meet the requirements set for them. The process qualification is a necessary step towards part and product level qualification. The AM process in target of this study was Laser-Beam Powder Bed Fusion (LB-PBF) and the used material Ti6Al4V.

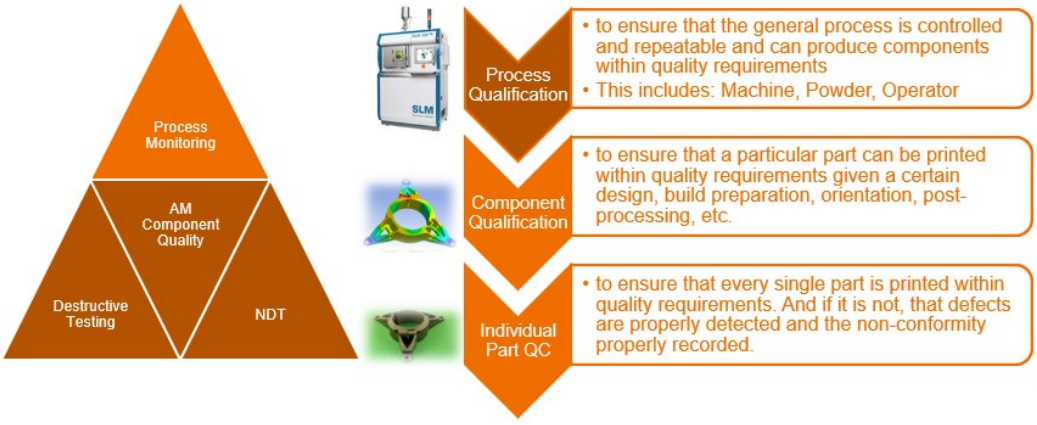

Figure 35: *Stages of additive manufacturing quality assurance and control and supporting methods for these. Figure courtesy of VTT.*

The study of process qualification was carried out in three tasks. The first task was to prepare guidance documents for additive manufacturing process qualification and to create test layouts for the following tasks. The second task was focusing on the investigation of AM process stability and the third on AM process repeatability.

First task was describing the process steps and prepared guidance on things to take into account during the additive manufacturing process based on existing documentation such as standards on material, general AM, aerospace, testing and other guidance documents. Based on the material, a detailed documentation was created including items on the qualification methodology (process, personnel, powder), product qualification (prototype, witness specimens), manufacturing procedure specification (general requirements, pre-, during and post-build operations, preliminary additive manufacturing process specification pAMPS, key performance values), test specification (visual, tensile, fatigue, porosity, metallography, chemical composition), AM process qualification records AMPQR and AM procedure specification AMPS. [95]

In addition, a test setup for the next tasks was defined which contained additively manufactured test specimens for tensile and fatigue testing, micrography and powder packing analysis in various locations of the build plate. Tensile test specimens contained specimens planned to be machined and to be tested in the as-built condition (designed together with Patria Aviation Oy). Test geometry for the tensile specimens is shown in **Figure 36**.

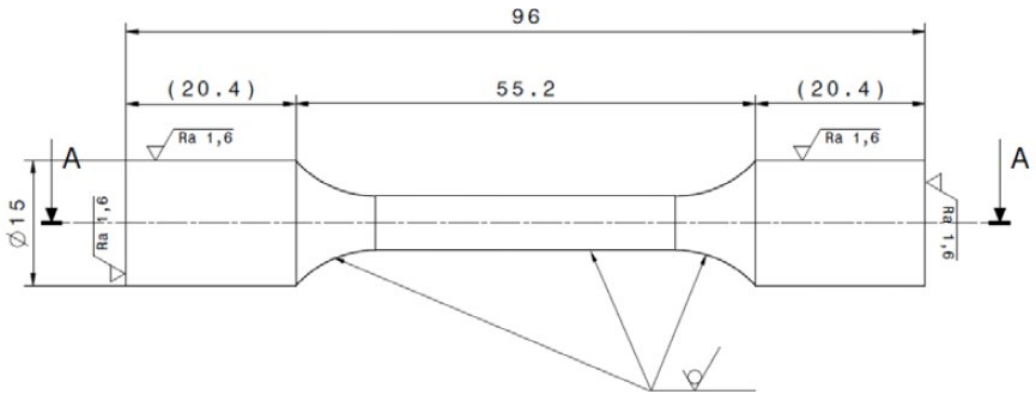

***Figure 36**: Geometry for the tensile test specimens. Figure courtesy of Patria Aviation.*

The tests of the AM process stability in the second task showed variations based on the location of the specimens on the build plate. For the specific LB-PBF machine utilized in the study, one of the build plate locations was observed to provide deteriorated results than e.g., the specimens in the middle of the build area [104]. In such scenarios, the identified area on the build plate could be considered a no-build zone for high critical components. Based on the results, two locations on the build plate were selected for the third task to analyse the process repeatability with three build jobs. The specimens of the repeatability build tests showed similar type of behaviour than in the stability build specimens resulting in the other area providing poorer results. Also, it was observed that the differences in the properties between the build locations in a single build was higher than for the same location between consecutive build jobs [96]. The results of the stability and repeatability builds are planned to be elaborated in more detail in an upcoming scientific publication.

It was acknowledged that manufacturing test specimens in the same process as the actual part is important to verify that the desired material properties are achieved. As the determination of the allowables is done using generally accepted statistical methods for aircraft materials, it is possible to start building a data bank of material properties at an early stage. However, due to the maturity of the manufacturing method and the layered texture of the material, it is recommended to run separate test series for different geometries, especially when manufacturing secondary/primary parts. [34], [35].

2.3.3 Risk-based Aircraft Structural Integrity Management

The Basic Operational Spectrum (BOS) representing the relevant flight load effects on the structure is a primary reference for generating fatigue life estimates for a structural detail of an individual aircraft of the fleet. However, the actual loading of an individual aircraft within the fleet can deviate from the BOS. In the load-time history this scatter in loading originates from deviations in the amplitudes and sequence of the turning points (Peaks and Valleys). These have an impact on the crack growth rate and could, in worst case, result in unconservative fleet-wise fatigue life estimates. It is imperative to statistically consider all the factors that influence the life estimates when determining the risk levels of various damage scenarios. This research was focused on modeling the scatter in the life estimates based on deviation in the selected load spectrum and was divided into two subtasks. [12], [112]

The first step was to fit a statistical distribution for the BOS2 Wing Root load spectrum (Chapter 2.2.5 of Ref. [26]). It was decided to utilize a kernel distribution in Matlab which provides a good fit for various data sets. The kernel density estimator is the estimated probability density function (pdf) of a random variable. For any real values of x, the kernel density estimate is given by Eq.(1)

$$\hat{f}_h(x) = \frac{1}{nh}\sum_{i=1}^{n} K\left(\frac{x - x_i}{h}\right) \tag{1}$$

where x_1, x_2, …, x_n are random samples from an unknown distribution, n is the sample size, $K(\cdot)$ is the kernel function, and h is the bandwidth, i.e., smoothing parameter [67].

The Peak-Valley table for the selected and normalized load spectrum is presented in **Figure 37**, and its Peak-value distribution together with the smoothing effect of various bandwidths on the kernel distribution fit is presented in **Figure 38**.

Occurrence		PEAK																																
		-0.24	-0.2	-0.16	-0.12	-0.08	-0.04	0	0.04	0.08	0.12	0.16	0.2	0.24	0.28	0.32	0.36	0.4	0.44	0.48	0.52	0.56	0.6	0.64	0.68	0.72	0.76	0.8	0.84	0.88	0.92	0.96	1
VALLEY	-0.48	0	0	0	0	0	0	0	0	0	1	0	0	0	0	0	0	0	0	0	0	0	0	0	0	0	0	0	0	0	0	0	0	0
	-0.44	0	0	0	0	0	0	0	0	0	0	0	0	0	0	0	0	0	0	0	0	0	0	0	0	0	0	0	0	0	0	0	0	0
	-0.4	0	0	0	0	0	0	0	1	0	0	0	0	0	0	0	0	0	0	0	0	0	0	0	0	0	0	0	0	0	0	0	0	0
	-0.36	0	0	0	0	0	0	0	0	0	0	0	0	0	0	0	0	0	0	0	0	0	0	0	0	0	0	0	0	0	0	0	0	0
	-0.32	0	0	0	0	0	0	0	0	0	0	0	0	0	0	0	0	0	0	0	0	0	0	0	0	0	0	0	0	0	0	0	0	0
	-0.28	7	6	0	0	0	0	0	0	1	0	0	1	0	0	0	0	0	0	0	0	0	0	0	0	0	0	0	0	0	0	0	0	0
	-0.24	0	5	4	0	0	0	0	0	0	0	1	1	0	1	0	0	0	1	0	0	0	0	0	0	0	0	0	0	0	0	0	0	0
	-0.2	0	0	4	0	0	0	0	1	1	0	0	0	0	2	0	0	1	0	0	1	0	0	0	0	0	1	0	0	0	0	0	0	0
	-0.16	0	0	0	1	0	2	1	0	10	6	0	1	1	0	0	0	0	0	0	0	1	0	0	0	0	0	0	0	0	0	0	0	0
	-0.12	0	0	0	0	6	6	9	15	30	26	9	4	0	0	0	1	0	0	0	3	1	1	0	0	0	0	0	1	0	0	0	0	0
	-0.08	0	0	0	0	1	27	48	71	122	94	23	15	4	0	2	2	1	4	0	0	1	0	2	1	0	1	0	2	0	0	0	0	0
	-0.04	0	0	0	0	0	3	185	292	407	220	126	53	17	7	7	8	7	6	4	6	6	0	1	0	2	0	0	1	0	0	0	0	0
	0	0	0	0	0	0	0	5	1227	1971	901	300	104	69	34	31	28	20	28	24	19	19	10	6	11	5	3	3	1	1	0	0	0	0
	0.04	0	0	0	0	0	0	0	147	5173	3730	1180	433	228	156	146	102	89	87	82	63	50	37	26	24	15	8	5	1	1	1	0	0	0
	0.08	0	0	0	0	0	0	0	0	316	9259	5116	1317	540	344	267	199	182	112	114	68	57	42	32	22	22	17	6	1	0	0	0	0	0
	0.12	0	0	0	0	0	0	0	0	0	561	11214	4295	899	552	402	201	172	124	90	64	44	20	22	14	6	8	1	0	0	0	0	0	0
	0.16	0	0	0	0	0	0	0	0	0	0	431	5837	2022	440	260	161	95	89	47	34	24	26	10	10	6	3	6	0	0	0	0	0	0
	0.2	0	0	0	0	0	0	0	0	0	0	0	268	4169	1441	238	111	93	72	37	29	29	11	9	7	4	3	2	0	0	0	0	0	0
	0.24	0	0	0	0	0	0	0	0	0	0	0	0	219	3958	1204	203	83	69	50	24	24	14	13	3	3	2	0	0	0	0	0	0	0
	0.28	0	0	0	0	0	0	0	0	0	0	0	0	0	182	2970	836	148	79	28	15	19	14	6	10	1	4	2	1	0	0	0	0	0
	0.32	0	0	0	0	0	0	0	0	0	0	0	0	0	0	166	2483	769	112	45	30	14	16	8	9	4	4	2	0	0	0	0	0	0
	0.36	0	0	0	0	0	0	0	0	0	0	0	0	0	0	0	131	2069	673	110	46	23	7	10	8	2	1	0	0	2	0	0	0	0
	0.4	0	0	0	0	0	0	0	0	0	0	0	0	0	0	0	0	98	1844	611	104	40	18	10	4	4	1	0	0	2	0	0	0	0
	0.44	0	0	0	0	0	0	0	0	0	0	0	0	0	0	0	0	0	100	1574	668	106	20	10	4	4	1	0	0	0	0	0	0	0
	0.48	0	0	0	0	0	0	0	0	0	0	0	0	0	0	0	0	0	0	91	1523	578	80	17	12	4	0	1	0	0	0	0	0	0
	0.52	0	0	0	0	0	0	0	0	0	0	0	0	0	0	0	0	0	0	0	87	1415	575	70	20	4	4	3	0	0	0	0	0	0
	0.56	0	0	0	0	0	0	0	0	0	0	0	0	0	0	0	0	0	0	0	0	67	1330	526	52	19	8	1	0	0	0	0	0	0
	0.6	0	0	0	0	0	0	0	0	0	0	0	0	0	0	0	0	0	0	0	0	0	65	1059	502	59	5	4	0	0	0	0	0	0
	0.64	0	0	0	0	0	0	0	0	0	0	0	0	0	0	0	0	0	0	0	0	0	0	43	876	451	55	5	3	1	0	0	0	0
	0.68	0	0	0	0	0	0	0	0	0	0	0	0	0	0	0	0	0	0	0	0	0	0	0	47	828	451	48	3	2	0	0	0	0
	0.72	0	0	0	0	0	0	0	0	0	0	0	0	0	0	0	0	0	0	0	0	0	0	0	0	48	718	386	48	2	0	0	0	0
	0.76	0	0	0	0	0	0	0	0	0	0	0	0	0	0	0	0	0	0	0	0	0	0	0	0	0	23	528	323	27	5	0	1	0
	0.8	0	0	0	0	0	0	0	0	0	0	0	0	0	0	0	0	0	0	0	0	0	0	0	0	0	0	21	444	186	21	1	0	0
	0.84	0	0	0	0	0	0	0	0	0	0	0	0	0	0	0	0	0	0	0	0	0	0	0	0	0	0	0	9	169	89	2	0	0
	0.88	0	0	0	0	0	0	0	0	0	0	0	0	0	0	0	0	0	0	0	0	0	0	0	0	0	0	0	0	1	94	31	1	0
	0.92	0	0	0	0	0	0	0	0	0	0	0	0	0	0	0	0	0	0	0	0	0	0	0	0	0	0	0	0	0	1	31	9	1
SUM		7	11	8	1	7	38	248	1752	8031	14800	18400	12348	8169	7115	5695	4465	3829	3397	2907	2785	2517	2288	1879	1635	1492	1320	1026	836	394	211	65	11

Figure 37: *Peak-Valley (PV) table of the example load spectrum. Figure courtesy of Patria Aviation.*

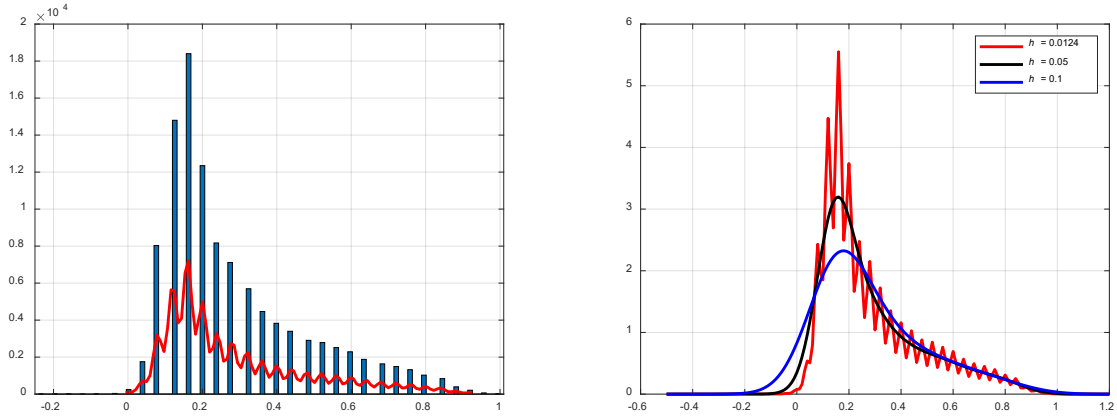

Figure 38: *Peak-value distribution of the load spectrum (left) and the smoothing effect of various bandwidths (h) on the kernel distribution fit (right). Figure courtesy of Patria Aviation.*

Similar distributions were defined for the Valley-values corresponding to the Peak-values. Then, a simulated load-time history was generated by randomly picking values from the created Peak and Valley distributions. The original and simulated load-time histories are presented in **Figure 39**, and their Peak-Valley exceedances in **Figure 40**.

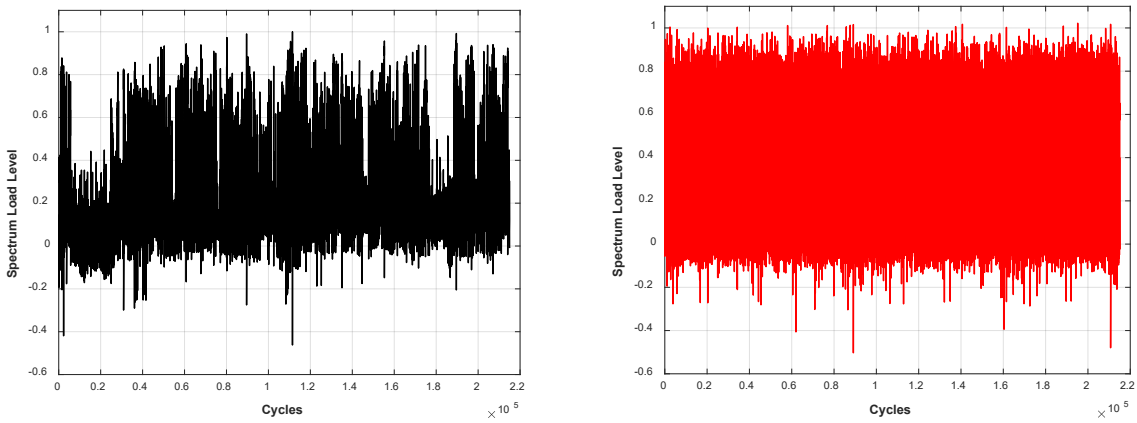

Figure 39: *Original load spectrum (left), and simulated load spectrum (right). Figure courtesy of Patria Aviation.*

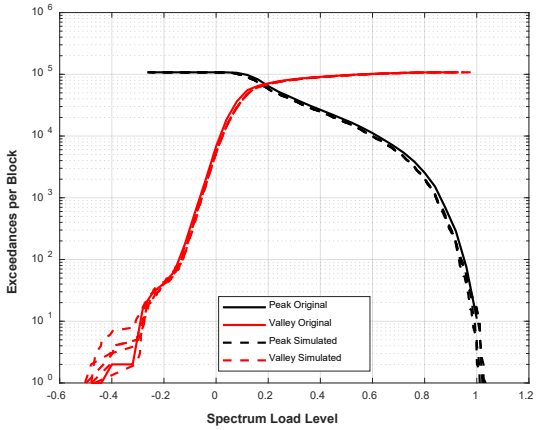

Figure 40: *Peak-Valley exceedances of the original (solid line) and simulated spectrum (dashed line). Figure courtesy of Patria Aviation.*

The second step was to evaluate the effects of deviation of the simulated load spectrum on the crack growth rate. Crack growth calculations were based on the NASGRO equation [73]. Instead of pairing Peaks and Valleys, a Range-Mean table of the original load spectrum was created as a starting point. A distribution fit was applied as before by generating distributions of the Mean and corresponding Range values. Finally, crack growth analyses were run based on the simulated spectra. The results are depicted in **Figure 41**.

Future research could include other parameters in the evaluation, like scatter in the initial crack lengths and deviation in the material properties. This would enable to evaluate the total cumulative risk over the life of the component.

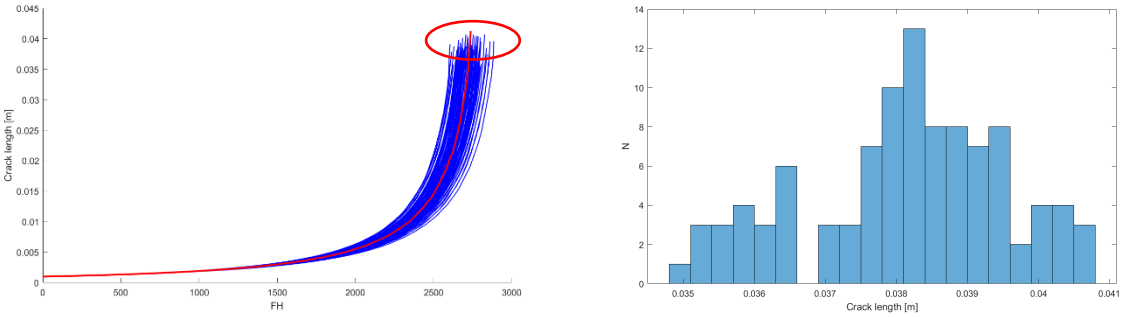

Figure 41: *Scatter of the crack growth rates and critical crack lengths in the simulated load spectra (left), and the final crack length histogram (right). Figure courtesy of Patria Aviation.*

2.4 Structural integrity of composite materials

2.4.1 Structural integrity of composite structures and adhesively bonded joints

Tampere University has continued the work with composite structures and adhesively bonded joints in the season 2021-2023. The ICAF 2019 review presented the development of the test setup for fatigue testing with fracture mode II (Chapter 2.4.1 of Ref. [27]). The target was to develop a new test rig, which allows using a negative load ratio (R < 0) during testing. A fitting test setup was created based on the End Notched Flexure (ENF) test specimen that is used in the quasi-static fracture testing of mode II crack tip loading [30]. To allow the loading direction change within a test, additional supports were added to the rig structure (**Figure 42**). The applicability of the developed test rig was analysed using Digital Image Correlation (DIC) and Finite Element (FE) analysis. In details, small gaps were left between the supports and test specimen to prevent any restraining of the specimen deformation. During a test, the specimen should not experience uncontrolled horizontal movement when the load removal related phase of load cycle takes place. The DIC measurements revealed the horizontal movement related to successful testing, and the absolute value was below the thresholds. [79]

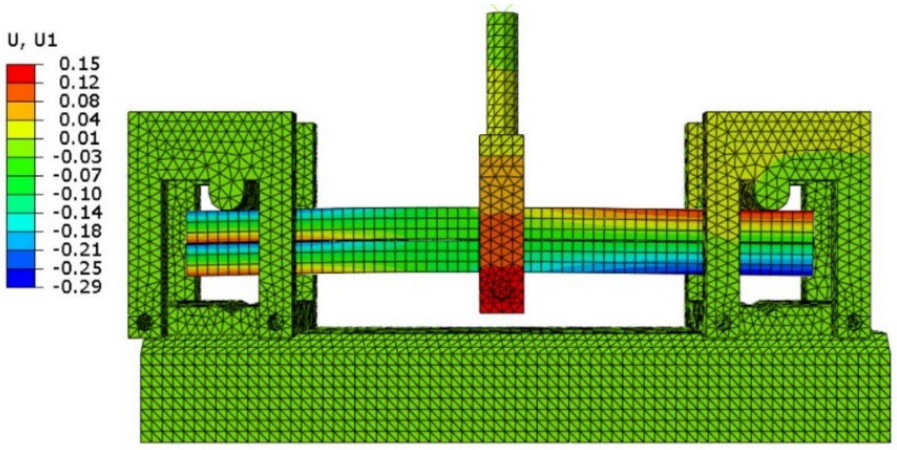

***Figure 42**: The FE model of the new test setup and rig with the ENF specimen in place. The horizontal displacement (U1) is shown in mm and the load level of the simulation is 60 % of the loading at the maximum static load derived from experiments [79]. Figure courtesy of Tampere University.*

The tests of the new rig were first run, and results compared to the results gained using a traditional ENF test setup ('old') at R > 0. When applying the test setup, the loading phases in both vertical directions were performed and results compared. These directional comparisons were performed using the load ratio of 0.1 (i.e., the total load removal did not exist). The comparison of the rig behaviour is shown in **Figure 43**. The developed test setup was shown to provide comparable crack propagation for both loading directions. The testing with a negative load ratio was performed with R = -1. These tests were shown to produce significantly faster crack propagation compared to the crack propagation with R = 0.1. This outcome emphasizes the importance of testing with negative load ratio for investigations of structural applications with similar loading (load change from positive to negative) [79].

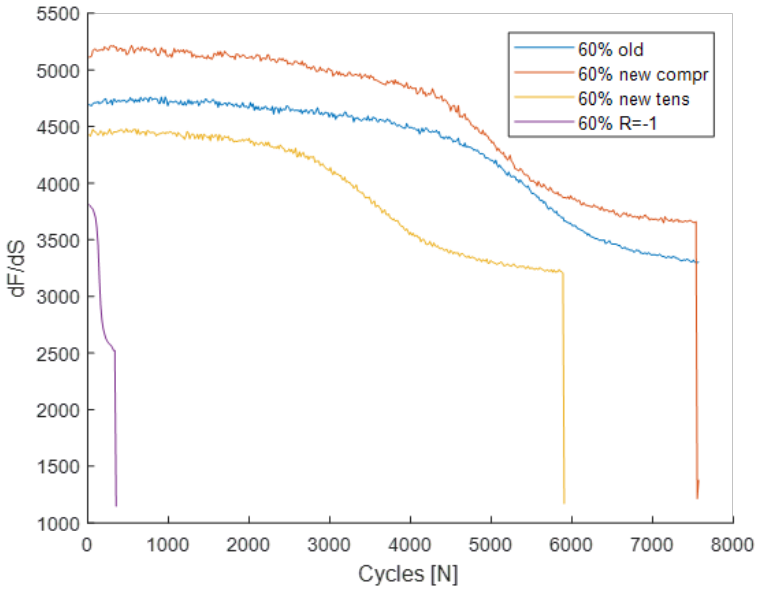

Figure 43: *The comparison of the slope of force-displacement data when using a traditional ENF method and when using the new test setup capable of negative load ratio (comparison at a ratio 0.1) [79]. Figure courtesy of Tampere University.*

The second work entity related to the fatigue experimentation with fracture mode II was focused on the usage of DIC for characterizing the crack (tip) propagation. In this task, fatigue testing was performed using the ENF method and the testing was monitored by DIC. In the procedure with DIC, the DIC data was used to follow two lines of measurement points placed on different sides of the bond line (**Figure 44**). These lines' displacements were post-processed further. The opening separation of the ENF adherends, in addition to the shear separation, was observed, in details, between the adherends adjacent to the crack tip. Naturally, the opening separation was not expected to occur in the theoretically pure fracture mode II method. The developed script to determine the opening separation was found valid and the observed opening was assumed to be caused by plastically deformed adhesive (at and adjacent the crack tip). Threshold values were defined for following the opening and shear; the definition was based on the deformation at the beginning of a test (no crack growth yet). The shear separation was revealed to be more sensitive to the exact threshold value than the opening separation. The crack propagation, provided by the opening and shear separations script, was compared to the results by visual observations as well as Compliance-Based Beam Method (CBBM) (**Figure 45**). The DIC-based scripts were shown to provide longer crack lengths than a length determined by the CBBM. This was explained by the 'microcracking' and plastic deformation that occurred adjacent to the fully open crack tip. Studies were also made using penetration liquid. [80]

In another work of adhesion testing by Tampere University, DIC measurements-analysis were used for analyzing adhesion testing of polymer coating for conditions where substrate and coating have severe plastic deformation [78]. The currently on-going work related to adhesion (testing) in structural bonds is focused on the surface treatment qualification by using the contact angle measurements and water as probe liquid [40].

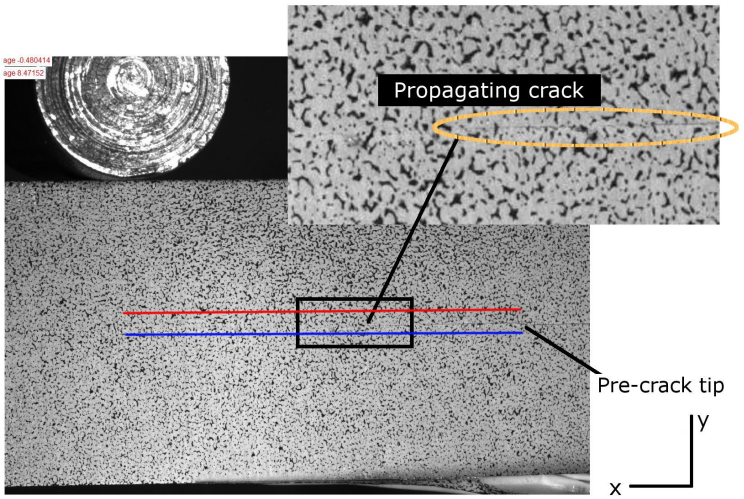

Figure 44: *The ENF specimen prepared for DIC application on the edge (free surface) and the two lines of measurement points emphasized [80]. Figure courtesy of Tampere University.*

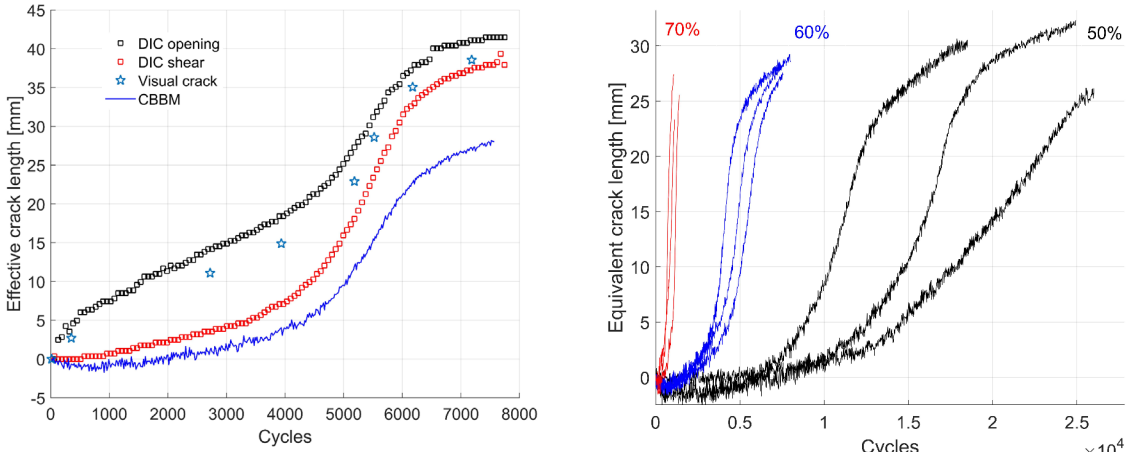

Figure 45: *The comparison of fatigue crack propagation using DIC-based data analysis methods, visual observation, and the Compliance-Based Beam Method (CBBM). The load (peak) in the indicated results is 60 % of the ultimate quasi-static strength (left). The determined fatigue crack propagation based on the CBBM method for tests performed at 50 %, 60 %, and 70 % of the ultimate quasi-static strength (right). [80] Figure courtesy of Tampere University.*

In addition to the focus area of fatigue testing development for adhesives, another essential research focus area during this season has been the research of simulation methods for impact damage in composite laminates. The impact damage in Carbon Fibre Reinforced Plastic (CFRP) and Flax Fibre Reinforced Plastic (FFRP) laminates was studied mainly for a 15 J impact energy via a drop-weight impact tower. The laminates were monitored, in addition to high-speed DIC, with high-speed infrared (IR) (emission) camera. The results for a of laminate in terms of the high-speed measurement of (converted) real surface temperature is shown in **Figure 46**. The measured surface temperature is due to released heat within the localized damage process in the laminates. The FFRP laminate experiences delamination and intralaminar cracking depending on the treatments of flax fibres during manufacture. Compared to CFRP, FFRP laminates indicate heat release for the earlier phases of the impact process. The CFRP laminate experience very fast heat release at the end of the impact process, which is

presumed mainly as a consequence of fibre breakage. The damage initiation in the CFRP and FFRP laminates was predicted using different failure criteria and FE software. The FE analysis was found as a valuable tool for understanding the localization and type of failure in the early phases of impact damage, i.e., onset. Two damage criterions, namely Puck and Hashin, were used in FE the 3D analysis of the laminates. An example of the visualization of the failure value, provided by these criteria, is shown in **Figure 47**. [97]

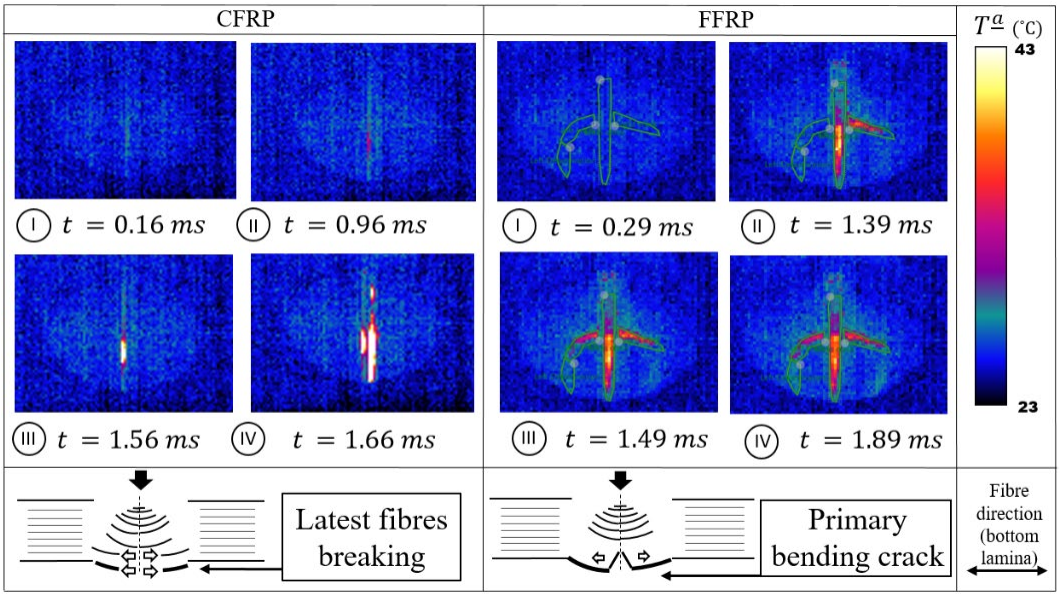

Figure 46: *Bottom surface temperatures of CFRP and FFRP laminates at the different phase of the impact [97]. Figure courtesy of Tampere University.*

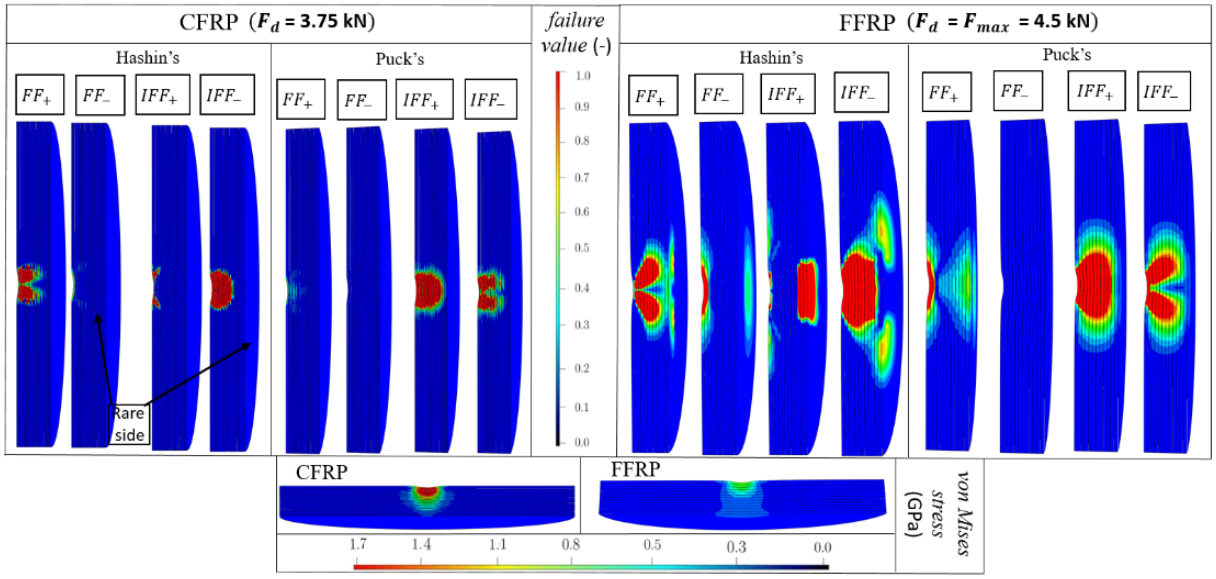

Figure 47: *The predicted damage initiation via an FE analysis in CFRP and FFRP laminates due to low velocity impact. Two different failure criteria are compared. [97] Figure courtesy of Tampere University.*

The investigation of the failure initiation, its prediction, were further worked on by using a lower, of 5 J, impact. This work was performed as a collaboration between Tampere University and University at Buffalo (NY, USA). The collaboration was established to perform a wider scale comparison of impact damage predictions. Two different FE software, Abaqus and LS Dyna, were used as comparative tools of numerical analysis. For the numerical work, experimental data of laminates' quasi-static indentation was used for the models' calibrations. The simulations for dynamic analysis revealed results where both FE software and the applied methods (models) of damage successfully predicted the damage onset with various distinguishable mechanisms – with an agreement to the experiments of impact. Selected results of the work with Abaqus and different stress criterion values are shown in **Figure 48**. In Abaqus, the modelling of delamination led to estimates where the damage onset occurred earlier than the predictions solved using the LS Dyna tool – the difference was found to be due different delamination modelling approach. [93], [94]

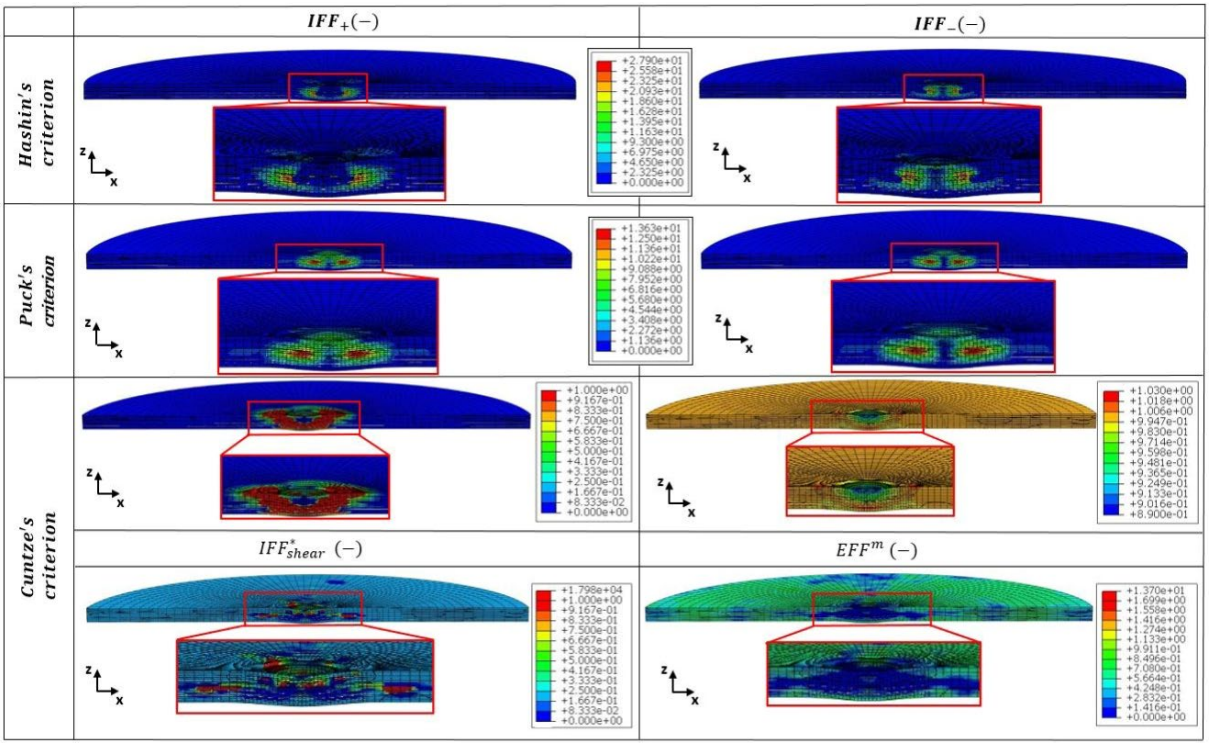

Figure 48: *Selected results of impact damage predictions via Abaqus. Results are shown for different criteria and over a laminate cross-section. [94] Figure courtesy of Tampere University.*

Over the course of impact investigations, it was found important to study the strain-rate sensitivity in more details. Overall, the experiments with Hopkinson split pressure bar (HSB) and corresponding dynamic numerical analysis were carried out for glass fibre reinforced pultruded (pull-wound) composite [91] and CFRP. The high strain-rate testing via HSB was monitored simultaneously using high-speed DIC and high-speed IR at Tampere University by the IMPACT research group. Finally, it was found crucial to understand what happens inside CFRP laminate in-situ. Collaborative research was carried out at the European Synchrotron Radiation Facility (ESRF) (Grenoble, France). Operando ultra-fast synchrotron X-ray phase contrast imaging (XPCI) was used for this research activity. XPCI was performed in-situ with HSB to adjust the strain-rate of specimen loading. The damage initiation and propagation during in-plane loading of a 28-ply CFRP laminate specimen is shown in **Figure 49**. The XPCI analysis also revealed failure modes in 45° angle orientation in other specimen loading directions. [92]

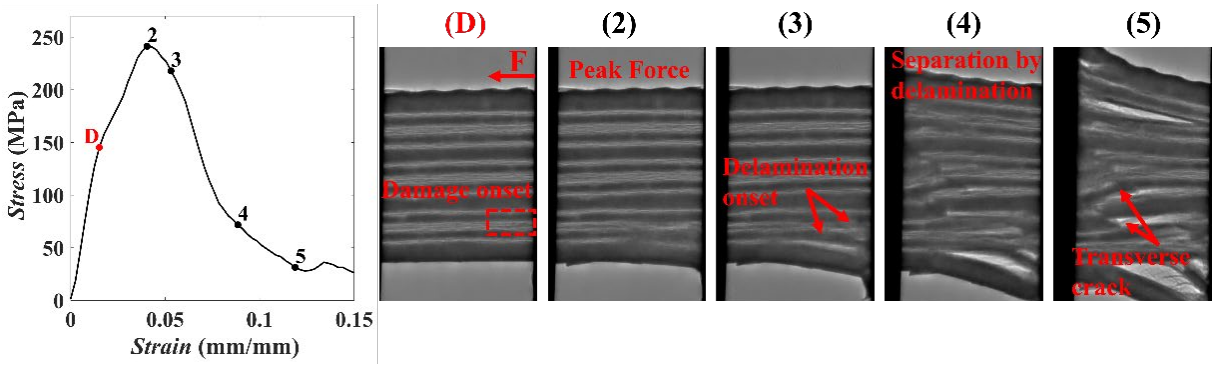

Figure 49: *High-strain rate Hopkinson split pressure bar testing of CFRP and internal in-situ damage observation via XPCI (at ESRF, France). Damage onset point (D) shown in the stress-strain graph with different phases of damage progress. Figure courtesy of Tampere University.*

A survey of new research themes was made during the season and work was made to analyse mechanical fastening in composite laminates. CFRP and FFRP laminates studied in form a numerical work. In this task, the damage initiation in the joint was analysed using a model with single fastener through a symmetric (minimized secondary bending) joint configuration (see **Figure 50**). The damage initiation due to load transfer through the fastener was studied by using two failure criteria, Puck and Hashin criteria. The results indicated that the damage onset pattern was sensitive to the finite element mesh. The distribution of predicted damage onset was found more even (less localized) in the CFRP laminate joints compared to the joint with the FFRP laminates. The Puck criterion provided higher values of failure (criterion) than the Hashin criterion in these investigations. The work was concluded by a finding that the Puck criterion's constants should be defined specifically for the FFRP laminate. [31]

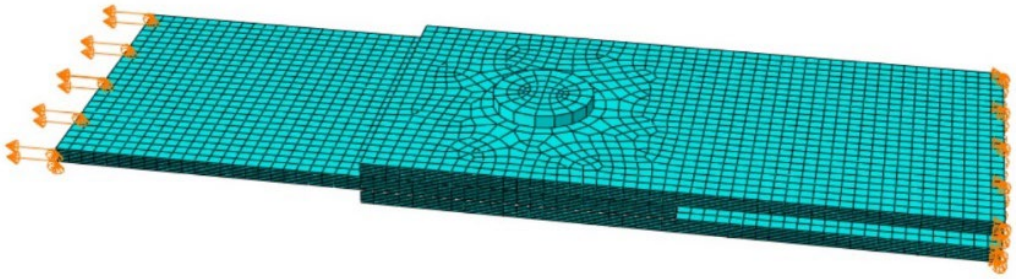

Figure 50: *The CFRP FE model of a joint with single fastener [31]. Figure courtesy of Tampere University.*

2.4.2 Development of interaction model for multiple delaminations

When analyzing the effect of multiple delaminations in laminated composite structures, the adjacent smaller delaminations have traditionally been modeled as a single continuous delamination area or the interaction between the delaminations has been estimated by the stress concentration factors of the isotropic materials. This simplified approach, however, leads in many cases to overconservative results, thus increasing the structural inspection workload.

Patria Aviation together with Tampere University had the project for analyzing multiple delaminations' interaction. The objective of the work was to gain a proper understanding about the interaction mechanisms of multiple delaminations and to create numerical tools to analyze such cases. Two delaminations were assumed to exist in a laminated composite plate of uniform thickness. Circular delaminations' diameter, delamination interface and their distance from each other were varied. Delaminations were located in line, overlapping and parallel to the load. The plate was subjected separately to tension, compression, and shear loadings. The studied cases are presented in **Figure 51**.

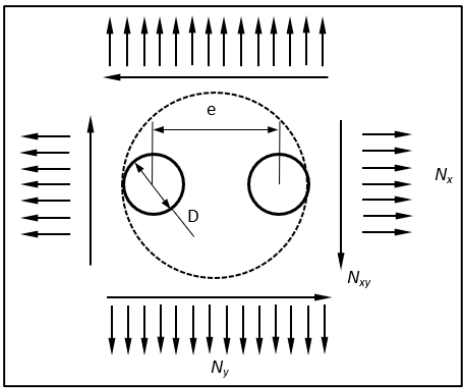

Figure 51: *The analyzed cases for studying multiple delaminations' interaction. Figure courtesy of Tampere University.*

Based on the specifications [110], Tampere University generated a Finite Element Analysis routine for analyzing the multiple delamination cases automatically. The results enabled to evaluate the type, size, and location of the delaminations correlation to the failure criteria maximum. This allowed to assess the criticality of each parameter for the structure under question. An example is given in **Figure 52**.

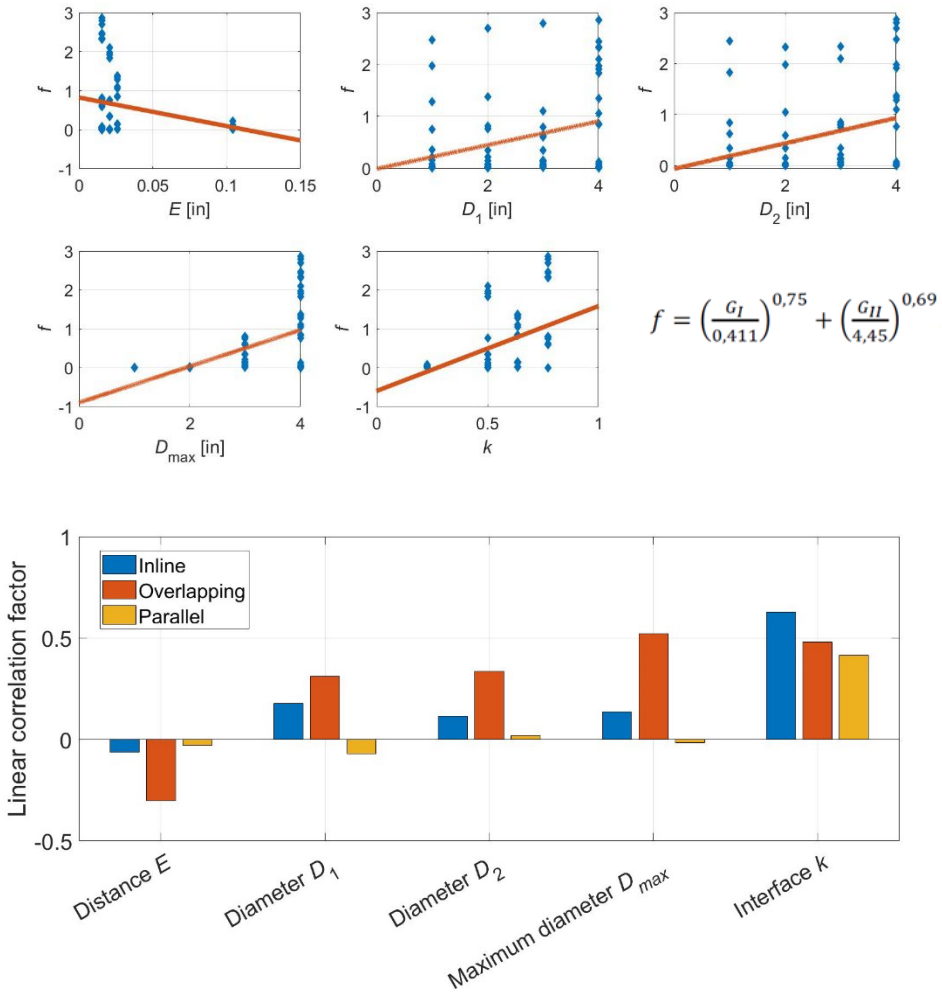

Figure 52: *An example of the analyzed multidelamination cases and the effect of distance (E), diameter (D), and location (k) of the delaminations for the failure criteria (f) maximum in terms of linear correlation [29]. Figure courtesy of Tampere University.*

The next steps will be to further develop the numerical model and to evaluate the grid size effects on the results in the tension loading case. The future analyses will also cover combined tension and shear – commonly existing loading case in the aircraft structures.

2.5 Repair technologies

2.5.1 EDA Patchbond II project

The four-year "Certification of adhesive bonded repairs for Primary Aerospace composite structures" (PATCHBOND II, PB II) project began in 06/2020 under the framework of the European Defence Agency (EDA) R&T Category B projects. The PATCHBOND II project is a follow-on project to the PATCHBOND I, see Chapter 3.1 in Ref. [26]. The project focuses on the development of certification methods for adhesively bonded repairs of aircraft composite primary structures, having the NH90 helicopter as a demonstrator platform.

The work concentrates on repair processes and repair strategies to enable beyond the Bonding Repair Size Limit (BRSL) repairs. The key element in overcoming current repair size limits and to ensure damage tolerance for bonded repairs is to understand the damage propagation in composite structures - and especially in the bondline. From manufacturing point of view co-bonding and secondary bonding (hard patch) methods together with proper material systems are in question. Adhesive bonding joint geometries include strap joints and scarfed joints.

Despite of limited number of material systems in question in the project, the EDA PATCHBOND II project includes substantial amount of experimental testing of various scale under different environments, also out-of-laboratory testing. Experiments and analysis have been concentrated on initial bondline defects and barely visible impact damages (BVIDs) to fulfil "analysis supported by test evidence" principle. The primary interest is in no growth (threshold) condition in the bondline. The secondary interest is in the stable/unstable damage propagation. The relevant loading types include both static, fatigue and impact.

The work will be performed by an international consortium consisting of 15 industrial and scientific partners from six European countries enabled to participate in EDA's projects, countries alphabetically: **Czech Republic**: Czech Aerospace Research Centre (VZLU); **Finland**: Tampere University (TUNI), Patria Aviation, VTT Technical Research Centre of Finland (VTT); **Germany**: Bundeswehr Research Institute for Materials, Fuels and Lubricants (WIWeB), Airbus Defence and Space (ADS), University of Stuttgart (USTUTT); **Italy**: Politecnico di Milano (POLIMI); **the Netherlands**: Netherlands Aerospace Centre (NLR), Fokker Services, KVE Composites Repair; **Norway**: Norwegian Defence Materiel Agency (NDMA), Norwegian Defence Research Establishment (FFI), FiReCo, Light Structures. Project Lead Contractor is NLR (the Netherlands). Tampere University is the national coordinator of the project (see also Chapter 2.5.1.1) and the Finnish Defence Forces Logistics Command (FDFLOGCOM) is the national bill paying authority of the project.

The EDA PATCHBOND II project structure has been divided into five Work Packages:

- WP 100: Management (lead by NLR)
- WP 200: Materials & Processes (lead by NLR)
- WP 300: Design & Analysis (lead by TUNI)
- WP 400: Tests (lead by VZLU)
- WP 500: SHM (lead by FFI)

2.5.1.1 EDA PATCHBOND II activities in Finland

The activities of the Finnish partners supported the certified repair process involving in analytical and numerical analyses, experimental testing, Non-Destructive Inspections (NDI) and Structural Health Monitoring (SHM) based on Acoustic Emission (AE).

The focus of the work by Tampere University in the project is related to the damage tolerance of bonded joints. Tampere University is mainly working in the WP 300 in which the target is to develop analysis methods for damage assessment and to predict crack propagation.

The experimental basis for the work was created based on tests of the basic fracture coupons: Double Cantilever Beam (DCB), End Notched Flexure (ENF) and Cracked Lap Shear (CLS) coupon. The fracture coupon specimens were used for determining the adhesive film's (FM 300-2) fracture properties. The test specimens were manufactured using the CFRP laminate made of AS4/3501-6 prepreg. One series of DCB specimens was manufactured and tested using titanium alloy (Ti-6Al-4V) adherends. In the previous projects, the tests of fracture mode I, II, and I+II (mixed mode) has been realized using aluminium adherends. Therefore, the DCB test results were compared with three adherend materials (CFRP, titanium, and the previously formed results with aluminium). The fracture energy was noticed to be at a similar range for the series, while the CFRP series provided lower values because of the mixed crack tip loading mode and failure mode with delamination. Moreover, ENF testing indicated cohesive failure mode (in adhesive) at the beginning of the test loading, and this data led to comparable fracture energies than the tests carried out before in earlier projects. All the specimens were monitored using DIC for detailed data of deformation – an example with an ENF specimen is shown in **Figure 53**.

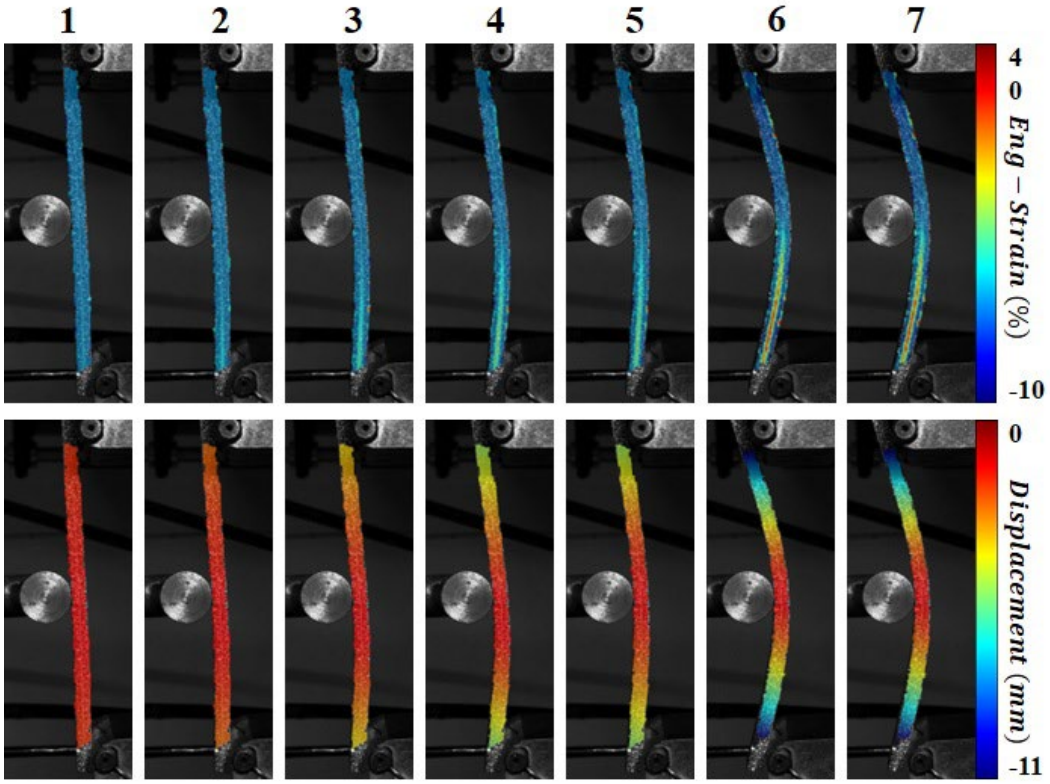

Figure 53: *The adhesively bonded CFRP ENF specimen and its displacement and strain fields determined using DIC. Figure courtesy of Tampere University.*

After performing the test programme with basic fracture coupons, the project has taken steps towards bonded coupons presenting an external patch repair. The Double Strap Joint (DSJ) method and specimen with an artificial crack (see **Figure 54**) has been tested under tensile and compressive loading. The usage of high-speed DIC was able to provide the damage onset location. This is valuable information for the numerical analysis development, which cannot focus on the obvious crack but will have to consider the specimen as an entity.

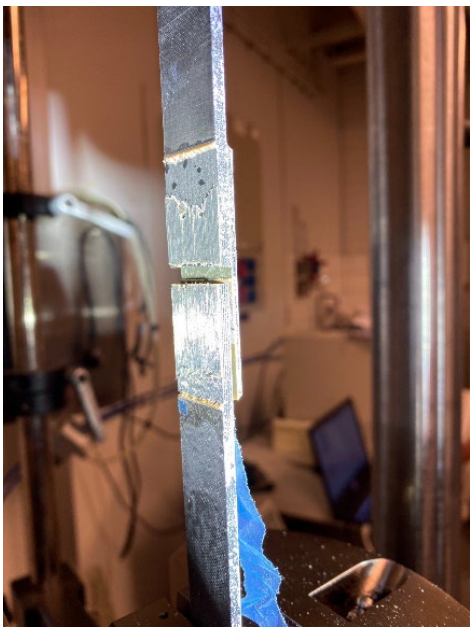

Figure 54: *The Double Strap Joint specimen with the precrack, after testing. A strap on one side detached during the test. Figure courtesy of Tampere University.*

All the specimens (types) will be modelled for FE analyses. For example, an analysis of an ENF specimen is shown in **Figure 55**. Methods for damage onset and propagation will be studied and evaluated in relation to the test data. At this point of the project, there are specimens that have shown the crack's likeliness to jump through the CFRP plies and adhesive film – the fracture path has progressed from adhesive to delamination and vice versa. The challenge in the analysis is to handle various damage mechanisms and combining different analysis methods. The development of progressive damage models for adhesive, as well as for the CFRP, are on-going in the project.

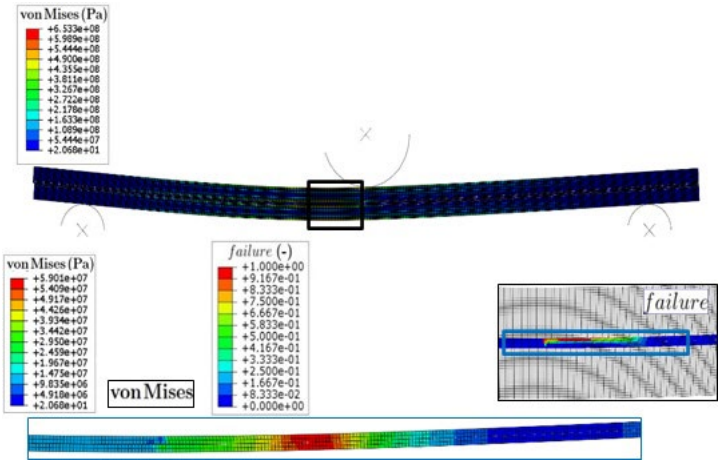

Figure 55: *An example of the progressive damage analysis of an ENF specimen related to the EDA Patchbond II project. Figure courtesy of Tampere University.*

Another strand of the EDA Patchbond II project involving the Finnish partners is the WP 500 regarding Structural Health Monitoring (SHM). In the WP 500, VTT is evaluating the performance of the Acoustic Emission (AE) based SHM system in the cyclic ENF and CLS coupon test program together with Tampere University and Eurofins Expert Services.

As the AE SHM system evaluation requires a stable enough defect growth, the main idea of cyclic loading is to provoke intentionally laminated artificial defect to grow in a controlled manner such that the growth (debonding) could be monitored with the AE SHM system. Real time ultrasonics are being used to validate the AE findings. Additionally installed strain sensors allow to control the test and help interpreting the results. Verasonics Vantage research ultrasound system utilizes Olympus 5 MHz linear array probe. As the ultrasound frequency inherently matches with the bandwidth of the AE sensors, measuring sequence was programmed with Matlab to trigger ultrasound scans once for each load cycle and having a minor temporal offset not to interfere with the AE measurements.

VTT carried out the 3-point bending ENF tests together with TUNI. Altogether, three coupons were tested. The initial debond (artificial flaw) was generated by applying a release film in between the two film adhesive layers, allowing a debond growth of 44 mm to the mid-point of the specimen. The ENF coupons were instrumented with a strain sensor, an Ultrasonic Testing (UT) probe, and a total of four AE sensors (**Figure 56**).

A critical aspect in the ENF test is the requirement of accurate crack (debond) length measurement during propagation, which is not a straightforward task. In case of testing a bonded joint, modern rubber-toughened adhesives usually present a significant ductile behaviour, thus Compliance Based Beam Method (CBBM) has been utilized as an effective data reduction scheme. During the test, only the specimen's measured compliance is required to estimate an equivalent crack length, and thus calculate the Strain Energy Release Rate (SERR) in mode II.

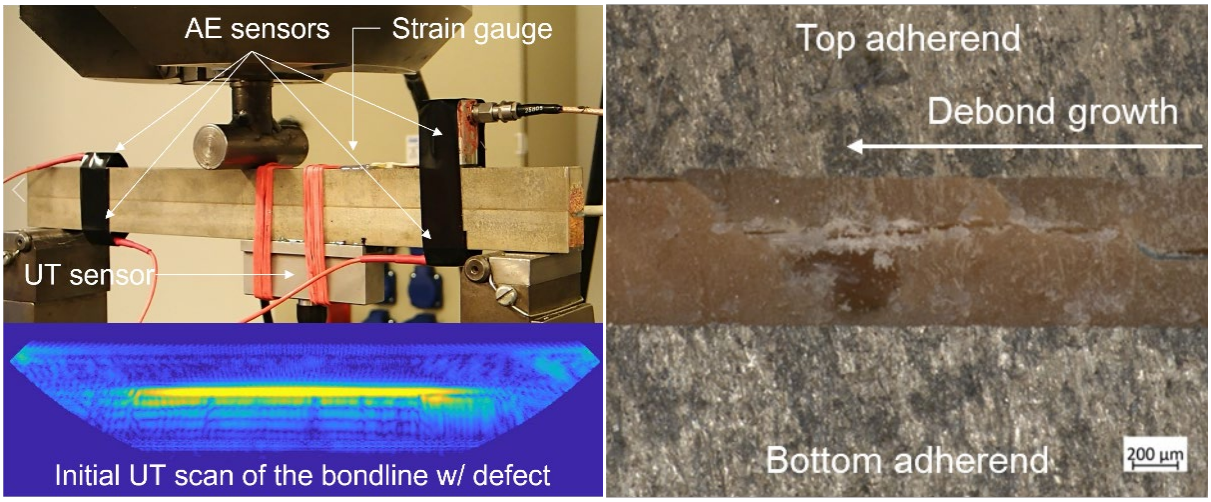

Figure 56: *Test set-up of the 3-point bending End Notched Flexure (ENF) test (left) and resulted bondline failure zoomed at the initial (and artificial) debond location (right). Figure courtesy of VTT.*

Evaluated debond growth based on ultrasound scans is presented in **Figure 57**, and SERR in mode II obtained by the CBBM is presented in **Figure 58**. Test period continues with the CLS tests, and the data analyses are currently on-going.

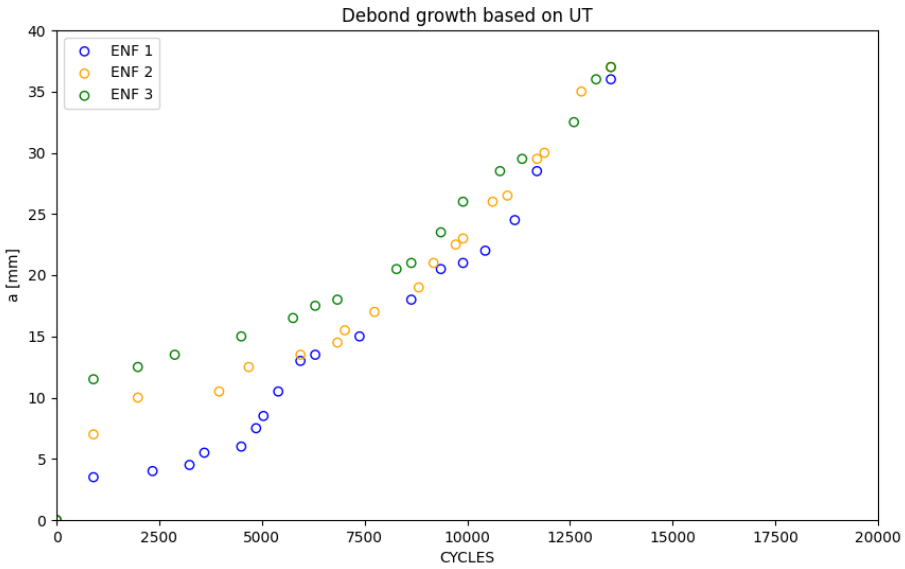

Figure 57: *Debond growth (a) in the ENF tests based on ultrasonic testing. Figure courtesy of VTT.*

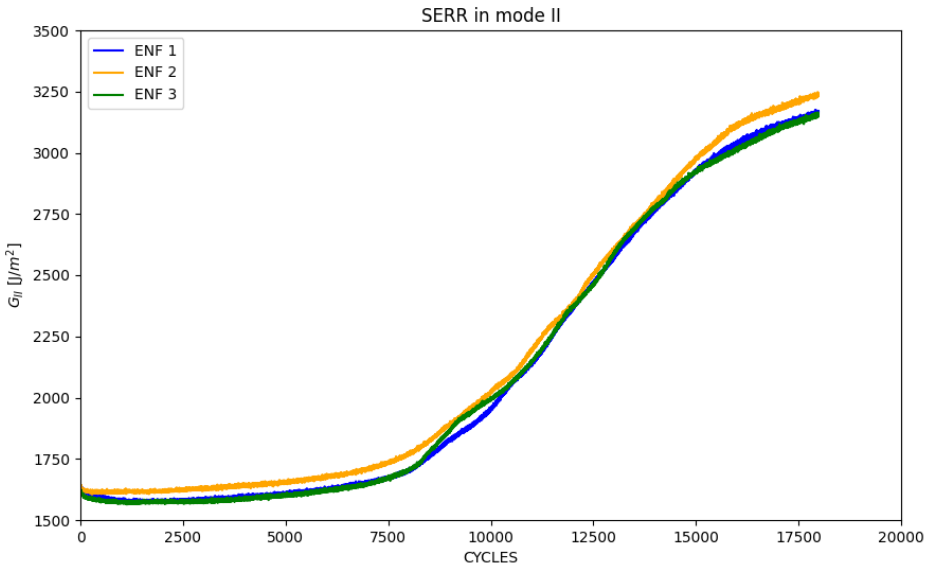

Figure 58: *Strain energy release rate in mode II (G_{II}) obtained by the CBBM in the ENF tests. Figure courtesy of VTT.*

2.5.2 Composite repair of the Wing Root Step Lap Joint

The inner wing root of F/A-18 fighter aircraft is a double-sided titanium-composite stepped lap bonded joint. A repair concept for a case where two innermost steps are damaged was developed and analyzed. The basic principle of the repair concept is to remove the damaged steps and bond a customized CRFP patch with a film adhesive as schematically illustrated in **Figure 59**. The validation of the repair concept follows a building block approach.

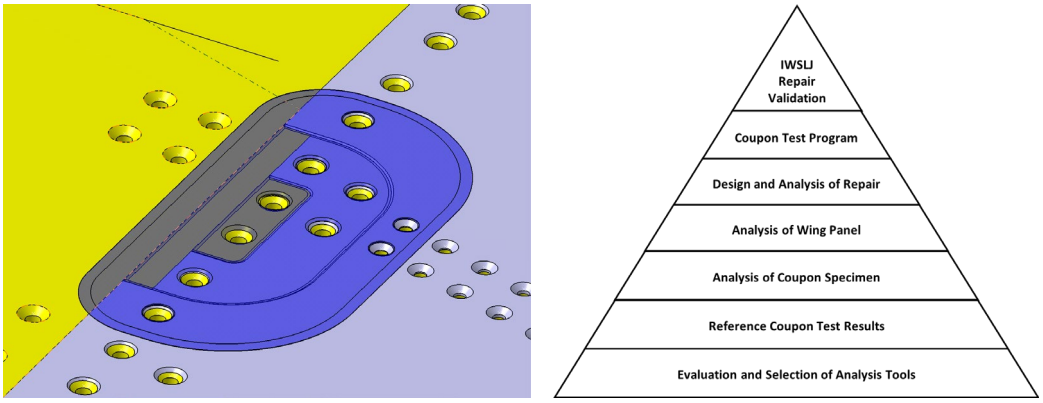

Figure 59: *The IWSLJ repair concept and building block approach for the repair validation. Figure courtesy of Patria Aviation.*

Since introduction of activities in Chapter 2.5.1 of Refs. [27], [28], the repair concept validation program entered the final phases where the coupon tests were performed in both static and fatigue loading and the results were evaluated. The test arrangements included both strain gage and DIC instrumentation of the test specimens together with low- and high-speed cameras. The DIC instrumentation consisted of two systems: low speed 3D DIC LaVision (2464×2065 pixels, 10 fps) and high-speed 3D DIC Photron FASTCAM NOVA S12 (1024×1024 pixels, 12800 fps). The high-speed camera used was Olympus i-Speed TR (1280×1024 pixels, 2000 fps). All tests and test arrangements shown in **Figure 60** were conducted by VTT and Eurofins Expert Services Ltd. More details about testing can be found in Refs. [107], [108], [42], [43], [103].

Figure 60: *Test arrangements for the IWSLJ coupon static tests [107]. HS = high-speed camera, LS = low-speed camera. Figure courtesy of VTT.*

The static tests included two reference specimens, two repaired specimens and two fail-safe specimens i.e., specimens like the repaired specimens but tested without the repair patch. In fatigue tests, two repaired coupons were tested up to 9000 SFH that represent two full lifetimes of the joint. After fatigue tests, a static RST was performed.

The specimens after the static tests are presented in **Figure 61** and test results in **Table 3**. The pass/fail criterion is based on ultimate load level of the joint including statistical and environmental effects. All specimens fulfilled the requirements for static certification. However, the initial failure of the specimens was different than expected. It was expected that the failure initiates at the composite end of the specimen, at the end tang of the titanium. In these tests, the failure initiated at the other end with delamination before the final failure of the whole specimen. The failure of the specimen was extremely sudden and even the high-speed camera with 2000 fps frame rate was not sufficient for detecting the initiation of the failure. The high-speed 3D DIC could have provided this information, but the cameras were focused to the expected failure location of the specimen, and failure always initiated outside the field of view (**Figure 62**). In addition, the titanium end of the specimen was outside visible area due to the universal test machine. An example of DIC analyses is presented in **Figure 63**.

Although, the failure loads were good and sufficient for the certification, they were also somewhat lower than expected. This is due to unexpected failure location. Further analysis of the specimens is required to get additional information. The RST results of the specimens after two full lifetime of fatigue testing are presented in **Table 4**. Both results are good for fatigue certification. The pass/fail criterion is set as 1.2×limit load level. Both specimens fulfilled this criterion although the first specimen had clearly lower strength. This specimen failed prematurely due to a fatigue crack at a fastener hole as shown in **Figure 64**.

Figure 61: *Failed specimen, static tests, IML side (upper), OML side (lower) [107]. Figure courtesy of VTT.*

Table 3: *Static test results. [107], [113], [114]*

Test Specimen	F_{ULT} [lbs]	Minimum Width [in]	Nx [lbs/in]	Required [lbs/in]	Pass/ Fail	Note
LS-ST-01-1	91965	1.919	47916	42595	PASS	Reference
LS-ST-01-2	89786	1.913	46945	42595	PASS	Reference
LS-ST-02-1	88381	1.920	46040	42595	PASS	Repaired
LS-ST-02-2	85810	1.921	44663	42595	PASS	Repaired
LS-ST-03-1	61604	1.919	32104	28397	PASS	Fail-safe
LS-ST-03-2	68025	1.916	35508	28397	PASS	Fail-safe

Table 4: *Static RST test results after fatigue. [107], [113], [114]*

Test Specimen	F_{ULT} [lbs]	Minimum Width [in]	Nx [lbs/in]	Required [lbs/in]	Pass/ Fail	Note
LS-FT-02-1	65685	1.921	34188	34076	PASS	Repaired RST
LS-FT-02-2	82997	1.922	43173	34076	PASS	Repaired RST

Figure 62: *High-speed camera image of the IWSLJ test specimen at the time of failure [107]. Initial failure location was outside the field of view. Figure courtesy of VTT.*

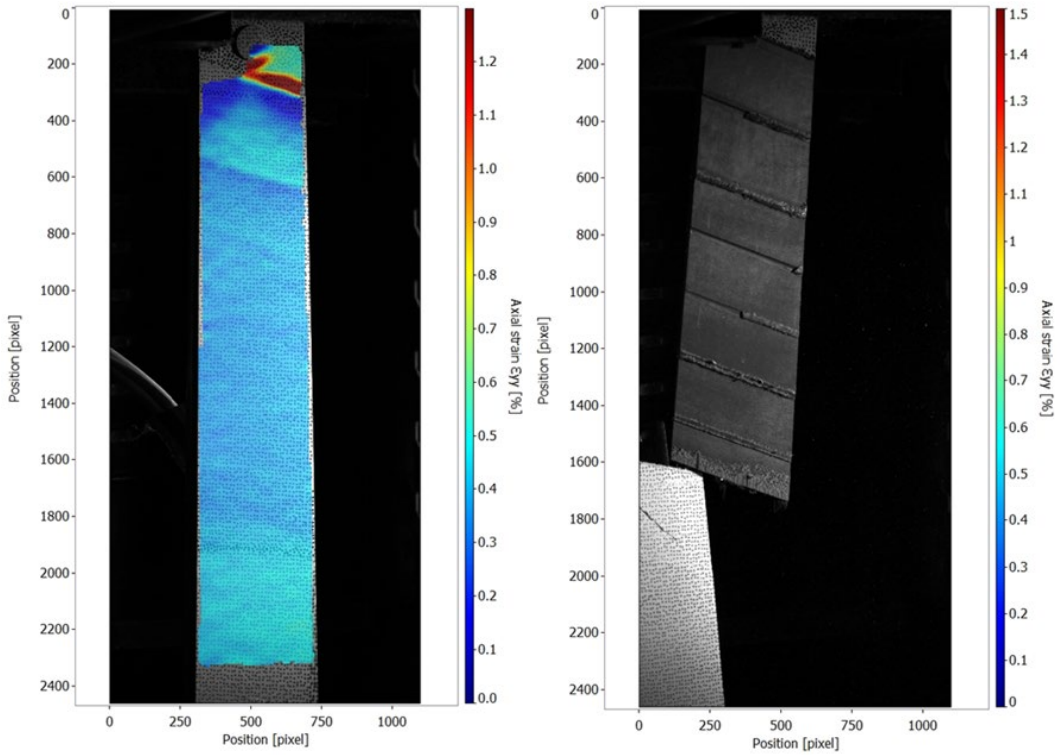

Figure 63: *Low-speed 3D-DIC axial strain field of the IWSLJ specimen just before failure (left), and after failure (right) [108]. A high strain concentration area is apparent at the edge of the laminate. Some diagonal joint steps are also visible. Figure courtesy of VTT.*

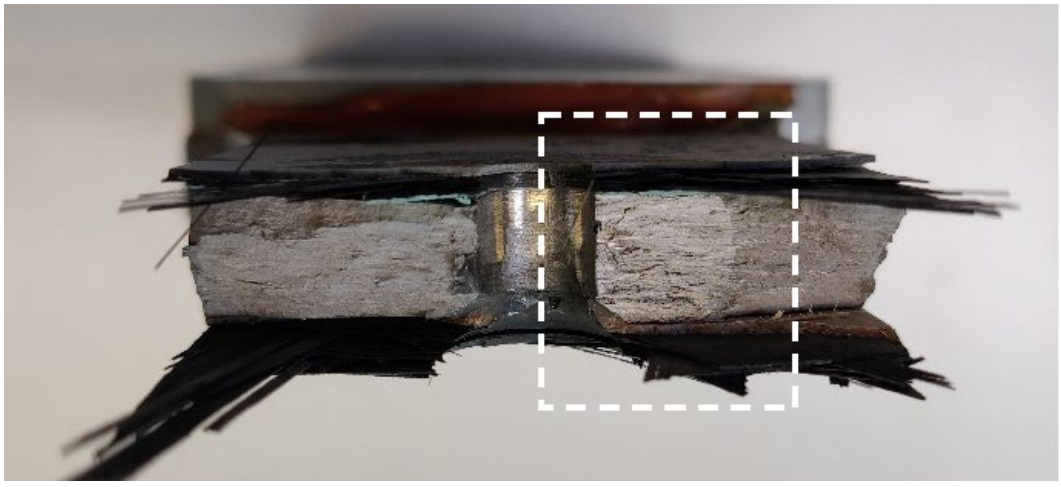

Figure 64: *Fatigue crack in the specimen LS-FT-01-01 [107]. Figure courtesy of VTT.*

Overall, based on the work performed in the coupon tests and in the whole repair concept validation program it can be concluded that the wing root joint is repairable, the repair concept is valid and certifiable for a two-step damage in steps closest to the wing root. The repair is able to restore the strength of the bondline and the total strength of the joint is not significantly affected by the weaker than expected bondline at the titanium root of the specimen. [113], [114]

3 Related activities

3.1 Design methods for a Mechanical Equipment and Subsystems Integrity Program (MECSIP)

The design of a Mechanical Equipment and Subsystems Integrity Program (MECSIP) is an essential step for identifying and monitoring the critical mechanical systems in current and future aircraft fleets. [71], [72]

The conducted design work related to the establishment of a MECSIP was divided into three different work elements. The first element focused on generating System Level Failure Modes and Effects Analysis (SFMEA) from three exemplary mechanical systems of the NH90 helicopter. The purpose of the work was to establish and utilize SFMEA capabilities according to MIL-STD-1629. According to FMEA logic, in a system-level failure-effect analyses, the cause of a failure is found at the subsystem level. The cause of a failure at the subsystem level is found at the individual component level, and the cause of a failure at the individual component level is defined by the conceivable different physical failure mechanisms. SFMEA can be utilized for example in the identification of Maintenance Significant Items (MSI's) with regard to the items potential failure effects related to flight safety, operational impact or failure mechanisms that are hidden to the user.

The second work element included creating a specification for the relevant data analytics functionalities for Proof of Concept (POC) software intended to aid in the implementation of a MECSIP. In the third work element, the feasible data analytics functionalities established earlier in the second work element were implemented with actual data into the POC software created by Combitech Ltd. The dashboard-style view of the constructed software tool intended to present system and subsystem reliability related statistics and facilitate the integrity management of i.a. maintenance significant items is shown in **Figure 65**.

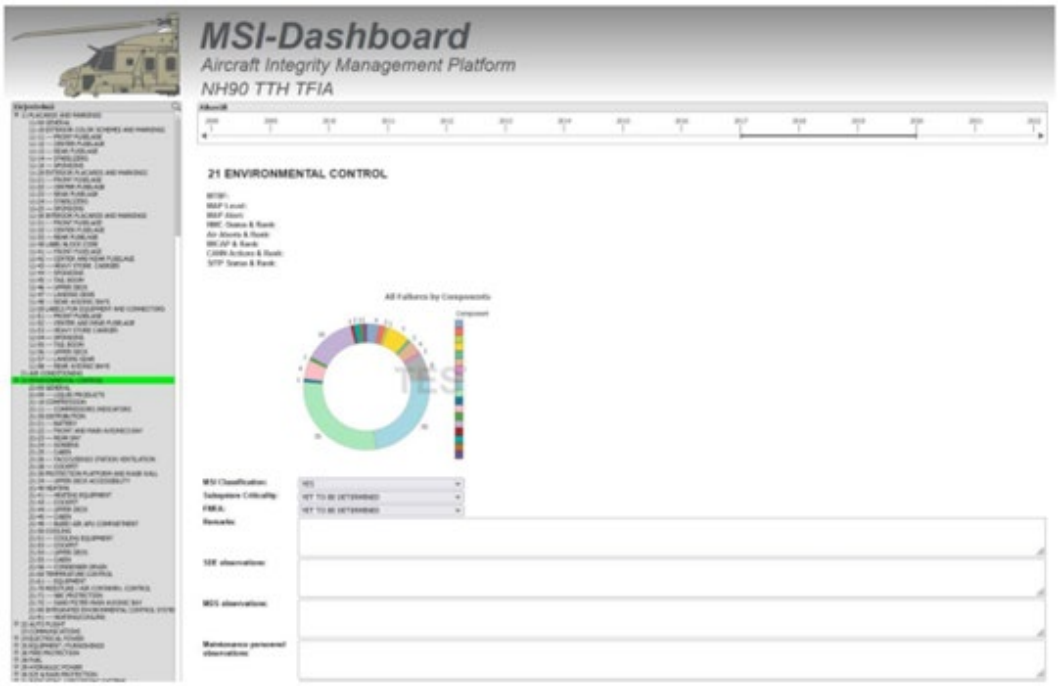

Figure 65: *POC level MSI-Dashboard (data not presented). Figure courtesy of Patria Aviation.*

The proof of concept level MSI-Dashboard included the following functionalities:

- ATA 100 based directory for system or subsystem MSI-Dashboard view selection.
- Time span selection functionality with immediate effect to the presented data in the MSI-Dashboard view
- Statistical gauges including:
    - the Mean Time Between Failure (MTBF) of the selected system, subsystem, and for the individual traceable components within them,
    - the number of system or subsystem caused air aborts, and rank score compared to the equivalent parameter from other systems or subsystems,
    - the number of cannibalizations (CANN), and rank score,
    - MAP & MAP level (Minimum Acceptable Performance), as defined by the user and compared to the actualized MTBF parameter,
    - MICAP (Mission Impaired Capability Awaiting Parts) -metric,
    - NMC (Not Mission Capable) -metric,
    - the total number of failure occurrences of the components included in the system or subsystem and the visualized mutual relationship between the number of failed components, as well as the rank score related to the total number of detected failure occurrences.
- Drop-down menus for selecting the system/subsystem MSI-status, system/subsystem criticality, and the status of system/subsystem conducted FMEA availability.
- Blank text fields, where the user may enter system/subsystem integrity related information, as seen necessary for succeeding in the task of mechanical equipment integrity management.

The conducted study also included brainstorming future MECSIP development work and the construction of an MSI-Dashboard integrity management software development roadmap. The next iteration of the current POC level tool shall facilitate other more advanced integrity management functionalities not yet present in the current stage of the constructed MECSIP tool.

3.2 Optical simulation of scratch repair in the F/A-18 transparencies

An on-aircraft system for assessing scratches and dents in F/A-18 aircraft transparencies (windshield and canopy, **Figure 66**) and applying optical simulation for optimizing their repair is presented. The motivation was to automatize the detection and quantification on transparency defects and to assist the manual repair process to minimize induced optical distortions by replacing visual inspection and subjective decision making with automatic, repeatable, and objective solution. The information can be applied to optimize the whole logistics chain of the repair process and to maximize aircraft availability. The system developed consist of three consecutive measurement tasks: First a machine vision-based scratch/dent detection and mapping is applied, enabling detecting, and classifying defects for further inspection. As a second step, the dimensions of the chosen defects are measured. Thirdly, based on the defect location and dimension, optical simulation is applied to estimate the effect of the repair process, and a most suitable one is chosen regarding optical distortion. The above on-aircraft machine vision system developed for defect detection automatically scans and subsequently maps all defects on the transparencies and provides estimates of their scattering from the pilot's visual perspective. The resulting map enables automatic classification of the scratches and dents found, based on user requirements. It also enables monitoring of the transparency defects' evolution through time, thus providing a modern tool for the transparencies' life cycle management. In addition to the above, an automized optical micrometre was developed for measuring the depth of the scratch or dent, based on 3D imaging. Finally, optical simulation models were developed for connecting the optical distortion induced by the material extraction in the repair process and vice versa. With the simulation, the effect of the repair can be mapped into standardized optical distortion measurement for evaluation. The performance of the defect mapping and depth estimation was assessed by real transparent samples and reference measurements. The simulation models were validated by comparing them with a real defect repair with before and after measurement of optical distortion. The developed system will be fielded to operational use within the Finnish Air Force. [77]

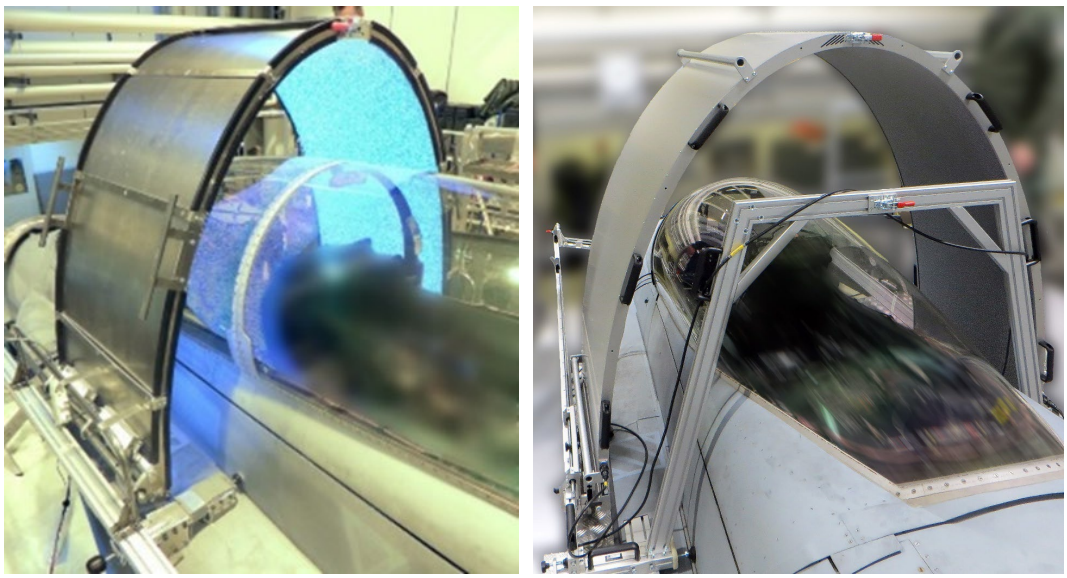

Figure 66: *An overview of the developed (left) and productized (right) on-aircraft scratch and dent detection system for the F/A-18C aircraft windshields and canopies. Figure courtesy of the FDF and Insta ILS Oy, respectively.*

References

[1] **From Observation Sorties to Multi-Role Fighters.** 2019. The Finnish Air Force web page. Retrieved from https://ilmavoimat.fi/en/history

[2] **The Lockheed Martin F-35A Lightning II is Finland's next multi-role fighter.** 2021. Ministry of Defence web page. Retrieved from https://www.defmin.fi/en/topical/press_releases_and_news/press_releases_archive/2021/the_lockheed_martin_f-35a_lightning_ii_is_finland_s_next_multi-role_fighter.12335.news#c5cce9fb

[3] **Vinka trainer aircraft to be retired after more than 40 years of service.** 2022. The Finnish Defence Forces web page. Retrieved from https://ilmavoimat.fi/-/vinkat-poistuvat-kaytosta-yli-40-vuoden-palveluksen-jalkeen?languageId=en_US

[4] **Grob G 115E.** 2023. The Finnish Defence Forces web page. Retrieved from https://puolustusvoimat.fi/en/equipment#/asset/view/id/205

[5] **BAE Systems Hawk.** 2023. The Finnish Defence Forces web page. Retrieved from https://puolustusvoimat.fi/en/equipment#/asset/view/id/202

[6] **Boeing F/A-18 Hornet.** 2023. The Finnish Defence Forces web page. Retrieved from https://puolustusvoimat.fi/en/equipment#/asset/view/id/201

[7] **All Finnish Air Force's Hornets Upgraded to MLU 2.** 2023. The Finnish Air Force web page. Retrieved from http://ilmavoimat.fi/en/article/-/asset_publisher/kaikki-ilmavoimien-hornetit-on-nyt-paivitetty-mlu-2-tasoon. Published in English on 5.1.2017 at 10.21.

[8] **Long-Term Development Key to Sustained Air Defence Capability.** 2023. The Finnish Air Force web page. Retrieved from https://ilmavoimat.fi/en/development_of_finlands_air_defense_capability.

[9] **Preliminary Assessment for Replacing the Capabilities of the Hornet Fleet, Final Report.** 2015. Helsinki: Ministry of Defence. ISBN 978-951-25-2680-2. Available at: https://www.defmin.fi/files/3178/Preliminary_Assessment_for_Replacing_the_Capabilities_of_the_Hornet_Fleet.pdf.

[10] **HX Program – new fighters for Finland by 2025.** 2021. Ministry of Defence web page. Retrieved from https://www.defmin.fi/en/frontpage/administrative_branch/strategic_capability_projects/hx_fighter_program/hx_fighter_program#6e21980d

[11] **Final Quotations for HX Fighter Programme Received.** 2021. Ministry of Defence web page. Retrieved from https://www.defmin.fi/en/topical/press_releases_and_news/final_quotations_for_hx_fighter_programme_received.11940.news#6e21980d

[12] Dümig, P. 2022. **Application of a statistically modeled load spectrum in the crack growth evaluation.** Technical Report № HN-L-0369 (in Finnish, classified). Halli: Patria Aviation Oy.

[13] ESDU Data Item 89046. **Fatigue of Aluminium Alloy Joints with Various Fastener Systems, Low Load Transfer.** ESDU International, Nov 1989, 42 p.

[14] ESDU Data Item 90009. **Fatigue of Aluminium Alloy Joints with Various Fastener Systems, Medium Load Transfer.** ESDU International, June 1990, 36 p.

[15] Hu, W., Tong, Y. C., Walker, K. F., Mongru, D., Amaratunga, R. and Jackson, P. 2006. **A Review and Assessment of Current Airframe Lifing Methodologies and Tools in Air Vehicles Division.** Research Report № DSTO-RR-0321. Fishermans Bend, Victoria, Australia: Defence Science and Technology Organisation (DSTO).

[16] Hukkanen, T. 2021. **GO-12 structural research: Flight test report.** Technical Report № GO-S-0025 (in Finnish, classified). Halli: Patria Aviation Oy.

[17] Hukkanen, T., Mattila, M. and Niva, J. 2022. **Preliminary design of a full-scale component fatigue test.** Report № HN-L-0357 (in Finnish, classified). Halli: Patria Aviation Oy.

[18] ICAF. 2001. **A Review of Recent Aeronautical Fatigue Investigations in Finland until March 2001.** (A. Siljander, Ed.). Research Report № BVAL33-011139. Espoo: VTT Technical Research Centre of Finland. Available at: http://www.vtt.fi/inf/julkaisut/muut/2001/icaf_2001_finland_review.pdf.

[19] ICAF. 2003. **A Review of Aeronautical Fatigue Investigations in Finland during the Period February 2001 - March 2003.** (A. Siljander, Ed.). Research Report № BTUO33-031123. Espoo: VTT Technical Research Centre of Finland. Available at: http://www.vtt.fi/inf/julkaisut/muut/2003/icaf_2003_finland_review.pdf.

[20] ICAF. 2005. **A Review of Aeronautical Fatigue Investigations in Finland during the Period April 2003 - April 2005.** (A. Siljander, Ed.). Research Report № BTUO33-051366. Espoo: VTT Technical Research Centre of Finland. Available at: http://www.vtt.fi/inf/julkaisut/muut/2005/icaf_2005_finland_review_issue1.pdf.

[21] ICAF. 2007. **A Review of Aeronautical Fatigue Investigations in Finland during the Period May 2005 - April 2007.** (A. Siljander, Ed.). ICAF Doc № 2410, Research Report № VTT-R-03406-07. Espoo: VTT Technical Research Centre of Finland. Available at: http://www.vtt.fi/inf/julkaisut/muut/2007/ICAF_FinlandReview_2007.pdf.

[22] ICAF. 2009. **A Review of Aeronautical Fatigue Investigations in Finland May 2007 - April 2009.** (A. Siljander, Ed.). ICAF Doc № 2418, Research Report № VTT-R-02540-09. Espoo: VTT Technical Research Centre of Finland. Available at: http://www.vtt.fi/inf/julkaisut/muut/2009/ICAF_Doc2418.pdf.

[23] ICAF. 2011. **A Review of Aeronautical Fatigue Investigations in Finland May 2009 - March 2011.** (E. Peltoniemi, A. Siljander, Eds.). ICAF Doc № 2427, Research Report № VTT-R-02827-11. Espoo: VTT Technical Research Centre of Finland. Available at: https://cris.vtt.fi/ws/portalfiles/portal/45002287/ICAF_Doc2427_FinlandReview_2011.pdf.

[24] ICAF. 2013. **A Review of Aeronautical Fatigue Investigations in Finland April 2011 - February 2013.** (A. Siljander, Ed.). ICAF Doc № 2428, Research Report № VTT-R-02105-13. Espoo: VTT Technical Research Centre of Finland. Available at: https://cris.vtt.fi/ws/portalfiles/portal/45002373/ICAF_FinlandReview_2013_issue1_3April13.pdf.

[25] ICAF. 2015. **A Review of Aeronautical Fatigue Investigations in Finland March 2013 - February 2015.** (A. Siljander, P. Varis, Eds.). ICAF Doc № 2432, Research Report № VTT-CR-01811-15. Espoo: VTT Technical Research Centre of Finland Ltd. Available at: http://www.vtt.fi/inf/julkaisut/muut/2015/ICAF_Doc_No_2432_FinlandReview_2015_issue_1_21May15.pdf.

[26] ICAF. 2017. **A Review of Aeronautical Fatigue Investigations in Finland March 2015 - March 2017.** (T. Viitanen, P. Varis, A. Siljander, Eds.). ICAF Doc № 2433, Research Report № VTT-CR-02002-17. Espoo: VTT Technical Research Centre of Finland Ltd. Available at: http://www.vtt.fi/inf/julkaisut/muut/2017/ICAF_Doc2433_Finland_Review_2017.pdf.

[27] ICAF. 2019. **A Review of Aeronautical Fatigue Investigations in Finland April 2017 - March 2019.** (T. Viitanen, A. Siljander, Eds.). Research Report № VTT-CR-00352-19. Espoo: VTT Technical Research Centre of Finland Ltd. Available at: https://cris.vtt.fi/ws/portalfiles/portal/24743703/ICAF_Finland_Review_2019.pdf.

[28] ICAF. 2021. **A Review of Aeronautical Fatigue Investigations in Finland April 2019 - April 2021.** (T. Viitanen, A. Siljander, Eds.). Research Report № VTT-CR-00448-21. Espoo: VTT Technical Research Centre of Finland Ltd. Available at: https://cris.vtt.fi/ws/portalfiles/portal/46540746/VTT_CR_00448_21.pdf.

[29] Jokinen, J. 2022. **Multidelamination analysis.** Project Report (in Finnish, classified). Tampere: Tampere University.

[30] Jokinen, J., Orell, O., Wallin, M. and Kanerva, M. 2020. **A concept for defining mixed-mode behaviour of tough epoxy film adhesives by single specimen design.** Journal of Adhesion Science and Technology, 34:18, 1982-1999, https://doi.org/10.1080/01694243.2020.1746606.

[31] Jokinen, J., Rodera Garcia, O., Hakala, P., Javanshour, F. and Kanerva, M. 2022. **Bearing strength prediction by CFRP and FFRP damage onset criteria for riveted joints**. Proceedings of the 20th European Conference on Composite Materials, ECCM20. 26-30 June 2022, Lausanne, Switzerland. Link: Proceedings of the 20th European Conference on Composite Materials - Composites Meet Sustainability (Vol 1-6) (epfl.ch)

[32] Juntunen, J. and Laakso, R. 2021. **Description of tare procedure.** Document № VTT-M-00873-21 (classified). Espoo: VTT Technical Research Centre of Finland Ltd.

[33] Juntunen, J. 2022. **Load Actuators.** Report № 21003109 (in Finnish, classified). Espoo: Eurofins Expert Services Ltd.

[34] Järvinen, H., Vaskelainen M., Niemi R.-P. and Mattila M. 2021. **Demands for design and qualification of airworthy parts produced by laser powder bed fusion (AM).** Report № HN-S-0100 (confidential). Halli: Patria Aviation Oy

[35] Järvinen, H., Vaskelainen M., Niemi R.-P., Mattila M. 2022. **Effect of as-built surface on tensile strength of additive manufactured titanium – test results and conclusions.** Report № HN-S-0102 (confidential). Halli: Patria Aviation Oy.

[36] Korteniemi, T. 2021. **Control surface lug attachment forces based on GO-12 flight test data.** Technical Report № GO-L-0007 (in Finnish, classified). Halli: Patria Aviation Oy.

[37] Korteniemi, T., Pirtola, J., Miettinen, A., Liukkonen, S., Siljander, A., Orell, O., Jokinen, J. and Kanerva, M. 2023. **The development of national MRO capability for a basic trainer aircraft: flight and ground tests**. Proceedings of the 31st Symposium of the International Committee on Aeronautical Fatigue and Structural Integrity (ICAF), Delft, The Netherlands, 26-29 June 2023.

[38] Koskela, J., Laakso, R., Koski, K., Vainionpää, A. and Forsström, A. 2023. [In preparation.] **Ability to Test and Analyse Small Cracks.** Customer Report № VTT-CR-00266-23 (in Finnish, classified). Espoo: VTT Technical Research Centre of Finland Ltd.

[39] Koski. K. 2022. **HW spectrum corresponding to planned average flying of the FINAF.** Research report № VTT-R-00943-22 (in Finnish, classified). Espoo: VTT Technical Research Centre of Finland Ltd.

[40] Koskinen, V.-V. 2021. **Water contact angle and related measurements to qualify surface treatments**. Master's thesis, Tampere: Tampere University, Faculty of Engineering and Natural Sciences, 2021.

[41] Koskinen, T. 2022. **Inspection report.** [NDI on table after 5.75 design lives.] Customer Report № VTT-CR-00459-22 (classified). Espoo: VTT Technical Research Centre of Finland Ltd.

[42] Koskinen, T. 2021. **Scanning Acoustic Microscope Inspection Report.** Customer Report № VTT-CR-00766-21 (classified). Espoo: VTT Technical Research Centre of Finland Ltd.

[43] Koskinen, T. 2021. **Scanning Acoustic Microscope Inspection Report.** Customer Report № VTT-CR-00765-21 (classified). Espoo: VTT Technical Research Centre of Finland Ltd.

[44] Laakso, R., et al. 2022. **Rudder Tests.** Customer Report № VTT-CR-00133-20 (classified). Espoo: VTT Technical Research Centre of Finland Ltd.

[45] Laakso, R. and Siljander, A. 2022. **Study of Marker Loads.** Customer Report № VTT-CR-01114-21 (in Finnish, classified). Espoo: VTT Technical Research Centre of Finland Ltd.

[46] Laakso, R., Koski, K., Vainionpää, A. and Siljander, A. 2023. **QF Marker Research.** Proceedings of the 31st symposium of ICAF - the International Committee on Aeronautical Fatigue and Structural Integrity, Delft, 26-29 June 2023.

[47] Laatikainen, Y., Hukkanen, T. and Vuori, M. 2020. **GO Mini-OLM flight preparations.** Technical Report № GO-S-0011 (in Finnish, classified). Halli: Patria Aviation Oy.

[48] **LifeWorks User's Manual**, Finland Air Force Version. 2004. The Boeing Company, July 26, 2004, Revision A.

[49] Liius, M. 2021. **Life estimation with crack initiation and crack growth analysis of Hornet Inner Wing Front Spar Fasteners 178, 184, 1438 and 1439**. Report № HN-L-0342 (in Finnish, classified). Tampere: Patria Aviation Oy.

[50] Liius, M. 2021. **Fail Safe Analysis Method for Hornet Vertical Tail Inner Structure**. Report № HN-L-0352 (in Finnish, classified). Tampere: Patria Aviation Oy.

[51] Lindbäck, J. E., Kapidžić, Z., Gustavsson, A. and Laakso, R. 2023. **Fatigue and damage tolerance testing of Gripen E/F rudder.** Proceedings of the 31h Symposium of the International Committee on Aeronautical Fatigue and Structural Integrity (ICAF), Delft, The Netherlands, 26–29 June 2023.

[52] Liukkonen, S. 2021. **Grob G115E Mini-OLM Flight Test Results.** Research Report № VTT-R-00440-19 (in Finnish, classified). Espoo: VTT Technical Research Centre of Finland Ltd.

[53] Liukkonen, S. 2020. **Grob Mini-OLM - GO-12 strain sensor installations.** Research Report № VTT-R-00829-20 (in Finnish, classified). Espoo: VTT Technical Research Centre of Finland Ltd.

[54] Liukkonen, S. 2022. **Grob Ground Tests – K1 – Main Landing Gear Leg Left.** Research Report № VTT-R-00513-22 (in Finnish, classified). Espoo: VTT Technical Research Centre of Finland Ltd.

[55] Liukkonen, S. 2022. **Grob Ground Tests – K2 – Engine Mount.** Research Report № VTT-R-00599-22 (in Finnish, classified). Espoo: VTT Technical Research Centre of Finland Ltd.

[56] Liukkonen, S. 2022. **Grob Ground Tests – K3 – Horizontal Stabilizer Left.** Research Report № VTT-R-00674-22 (in Finnish, classified). Espoo: VTT Technical Research Centre of Finland Ltd.

[57] Liukkonen, S. 2022. **Grob Ground Tests – K4 – Rudder.** Research Report № VTT-R-00700-22 (in Finnish, classified). Espoo: VTT Technical Research Centre of Finland Ltd.

[58] Liukkonen, S. 2022. **Grob Ground Tests – K5 – Aileron Left.** Research Report № VTT-R-00729-22 (in Finnish, classified). Espoo: VTT Technical Research Centre of Finland Ltd.

[59] Liukkonen, S. 2022. **Grob Ground Tests – K6 – Trailing Edge Flap Left.** Research Report № VTT-R-00740-22 (in Finnish, classified). Espoo: VTT Technical Research Centre of Finland Ltd.

[60] Liukkonen, S. 2022. **Grob Ground Tests – K7 – Elevator Right.** Research Report № VTT-R-00757-22 (in Finnish, classified). Espoo: VTT Technical Research Centre of Finland Ltd.

[61] Liukkonen, S. 2022. **Grob Ground Tests – K8 – Elevator Left.** Research Report № VTT-R-00770-22 (in Finnish, classified). Espoo: VTT Technical Research Centre of Finland Ltd.

[62] Liukkonen, S. 2022. **Grob Ground Tests – K9 – Wing Left.** Research Report № VTT-R-00797-22 (in Finnish, classified). Espoo: VTT Technical Research Centre of Finland Ltd.

[63] Liukkonen, S. 2022. **Grob Ground Tests – K10 – Fuselage.** Research Report № VTT-R-00798-22 (in Finnish, classified). Espoo: VTT Technical Research Centre of Finland Ltd.

[64] Miettinen, A. 2023. **GO Structural Components' Ground Tests.** Technical Report № GO-L-0014 (in Finnish, classified). Halli: Patria Aviation Oy.

[65] Malmi, S., Kettunen, J., Dümig, P. and Mattila, M. 2022. **The operational spectrum for the wing of the FINAF Hawk aircraft.** Report № HW-L-0152 (in Finnish, classified). Halli: Patria Aviation Oy.

[66] Malmi, S. 2023. **F/A-18 Hornet, SAFE Fatigue Tracking of Structures, Management Report, Period 3, 2022.** Report № HN-L-1076 (in Finnish, classified). Tampere: Patria Operations, AE&A.

[67] MathWorks® Documentation. **Kernel Distribution**. https://se.mathworks.com/help/stats/kernel-distribution.html. Accessed May 02, 2023.

[68] Miettinen, A. and Reivonen, T. 2021. **Fail Safe Analysis of Hornet FY233.7 Former.** Report № HN-L-0349 (in Finnish, classified). Tampere: Patria Aviation Oy.

[69] **MSC Nastran**, http://www.mscsoftware.com/product/msc-nastran, 2018. Accessed: March 2023.

[70] **MpCCI**, http://www.mpcci.de/, 2019. Accessed: March 2023.

[71] Mustonen, J. 2022. **Summary report of the system integrity management software development.** Report № NH-S-0091 (in Finnish, classified). Halli: Patria Aviation Oy.

[72] Mustonen, J. and Lehtinen, S. 2021. **System-level failure and impact analyzes of three mechanical systems.** Report № NH-S-0082 (in Finnish, classified). Halli: Patria Aviation Oy.

[73] **NASGRO®**, Fracture Mechanics & Fatigue Crack Growth Software, Southwest Research Institute® (SwRI), https://www.swri.org/consortia/nasgro. Accessed: May 02, 2023.

[74] Nieminen, V., Viitanen, T., Koski, K., Laakso, R. and Savolainen, M. 2023. **VIBFAT – Vibration-induced fatigue life estimation of the Vertical Tail of the F/A-18 aircraft using virtual sensing.** Proceedings of the 31st Symposium of the International Committee on Aeronautical Fatigue and Structural Integrity (ICAF), Delft, The Netherlands, 26-29 June 2023.

[75] Nieminen, V. 2023. **Modal Testing of Vertical Tail of F/A-18 Hornet.** Proceedings of the 31st symposium of the International Committee on Aeronautical Fatigue and Structural Integrity (ICAF), Delft, 26-29 June 2023.

[76] Niva, J. 2022. **Fatigue test plan for the LLT and MLT joint specimens.** Report № HN-L-0356 (in Finnish, classified). Halli: Patria Aviation Oy.

[77] Okkonen, M., Mäyrä, A., Siljander, A. and Siitonen, M. 2023. **Optical simulation of scratch repair in F/A-18 transparencies.** Proceedings of the 31st Symposium of the International Committee on Aeronautical Fatigue and Structural Integrity (ICAF), Delft, The Netherlands, 26-29 June 2023.

[78] Orell, O., Jokinen, J., Kallio, M. and Kanerva, M. 2021. **Revised notched coating adhesion test to account for plasticity and 3D behaviour**. Polymer Testing, 102 (2021), https://doi.org/10.1016/j.polymertesting.2021.107319

[79] Orell, O., Jokinen, J. and Kanerva, M. 2022. **Fatigue characterization of adhesive joints in aeroplanes – the development of a negative load ratio (R<0) testing method**, Proceedings of the 33rd Congress of the International Council of the Aeronautical Sciences (ICAS), Stockholm, Sweden, September 4-9, 2022.

[80] Orell, O., Jokinen, J. and Kanerva, M. 2023. **Use of DIC in characterization of mode II crack propagation in adhesive fatigue testing**. International Journal of Adhesion and Adhesives, Volume 122, February 2023, 103332, https://doi.org/10.1016/j.ijadhadh.2023.103332.

[81] Orell, O., Jokinen, J. and Kanerva, M. 2022. **Main Landing Gear Leg DIC Analyses.** (In Finnish, classified). Tampere: Tampere University.

[82] Orell, O., Jokinen, J. and Kanerva, M. 2022. **Engine Mount DIC Analyses.** (In Finnish, classified). Tampere: Tampere University.

[83] Orell, O., Jokinen, J. and Kanerva, M. 2022. **K3 DIC Analyses.** (In Finnish, classified). Tampere: Tampere University.

[84] Orell, O., Jokinen, J. and Kanerva, M. 2022. **K4 DIC Analyses.** (In Finnish, classified). Tampere: Tampere University.

[85] Orell, O., Jokinen, J. and Kanerva, M. 2022. **K5 DIC Analyses.** (In Finnish, classified). Tampere: Tampere University.

[86] Orell, O., Jokinen, J. and Kanerva, M. 2022. **K6 DIC Analyses.** (In Finnish, classified). Tampere: Tampere University.

[87] Orell, O., Jokinen, J. and Kanerva, M. 2022. **K7 DIC Analyses.** (In Finnish, classified). Tampere: Tampere University.

[88] Orell, O., Jokinen, J. and Kanerva, M. 2022. **K8 DIC Analyses.** (In Finnish, classified). Tampere: Tampere University.

[89] Orell, O., Jokinen, J. and Kanerva, M. 2022. **K9 DIC Analyses.** (In Finnish, classified). Tampere: Tampere University.

[90] Orell, O., Jokinen, J. and Kanerva, M. 2022. **K10 DIC Analyses.** (In Finnish, classified). Tampere: Tampere University.

[91] Pournoori, N., Rodera Garcia, O., Jokinen, J., Hokka, M. and Kanerva, M. 2021. **Failure prediction for high-strain rate and out-of-plane compression of fibrous composites**. Composites Science and Technology, 218 (2021), https://doi.org/10.1016/j.compscitech.2021.109141

[92] Pournoori, N., Hokka, M. and Kanerva, M. 2022. **In situ damage characterization of CFRP using ultra-fast synchrotron X-ray phase-contrast imaging**. Synchrotron Light Finland 2022, 13th FSRUO annual meeting, 1.12.–2.12.2022.

[93] Raza, H., Rodera, O., Carpenter, K., Pärnänen, T., Jokinen, J., Kanerva, M. and Bayandor, J. **Predictive methods for initiation of delamination and intra-laminar damage in carbon fibre reinforced polymer laminates subject to impact**. The Aeronautical Journal, *Submitted for acceptance*.

[94] Raza, H., Rodera Garcia, O., Carpenter, K., Pärnänen, T., Jokinen, J., Kanerva, M. and Bayandor, J. 2021. **Review of predictive methods for capturing onset of damage and initial delamination in carbon fibre reinforced polymer laminates subject to impact**. Proceedings of the 32nd Congress of the International Council of the Aeronautical Sciences (ICAS), Shanghai, China, September 6-10, 2021. https://www.icas.org/ICAS_ARCHIVE/ICAS2020/data/preview/ICAS2020_1014.htm

[95] Reijonen, J., Vaajoki, A. and Puukko, P. 2021. **Process qualification methodology for laser powder bed fusion of Ti-6Al-4V for military aviation.** Research Report № VTT-CR-00811-21 (confidential). Espoo: VTT Technical Research Centre of Finland Ltd.

[96] Reijonen, J., Vaajoki, A., Alhainen, J., Solin, J. and Puukko, P. 2023. **Process qualification methodology for laser powder bed fusion of Ti-6Al-4V for military aviation – part 3 process repeatability.** Research Report № VTT-CR-00142-23 (confidential). Espoo: VTT Technical Research Centre of Finland Ltd.

[97] Rodera Garcia, O., Corrêa Soares, G., Javanshour, F., Pournoori, N., Jokinen, J., Hokka, M. and Kanerva, M. 2022. **High-speed thermal mapping and impact damage onset in CFRP and FFRP**. Proceedings of the 20th European Conference on Composite Materials, ECCM20. 26-30 June 2022, Lausanne, Switzerland. Proceedings of the 20th European Conference on Composite Materials - Composites Meet Sustainability (Vol 1-6) (epfl.ch).

[98] Romppainen, H. 2022. **Life estimation Analysis of Hornet Outer Wing Aileron Hinge**. Report № HN-L-0363 (in Finnish, classified). Tampere: Patria Aviation Oy.

[99] Salmi, M., Partanen, J., Tuomi, J., Chekurov, S., Björkstrand, R., Huotilainen, E., Kukko, K., Kretzschmar, N., Akmal, J., Jalava, K., Koivisto, S., Vartiainen, M., Metsä-Kortelainen, S., Puukko, P., Jussila, A., Riipinen, T., Reijonen, J., Tanner, H. and Mikkola, M. 2018. **Digital Spare Parts**. Espoo: Aalto University & VTT Technical Research Centre of Finland Ltd. Available at: https://publications.vtt.fi/julkaisut/muut/2018/DIVA_final_report.pdf

[100] Suresh, S. and Ritchie, R. O. 1984. **Propagation of short fatigue cracks.** International Metals Reviews, Vol.29, No.6, pp. 445–476.

[101] Tikka, J. and Salonen, T. 2007. **Parameter Based Fatigue Life Analysis of F18 Aircraft.** In: Lazzeri, L. and Salvetti, A. (Eds.) Durability and Damage Tolerance of Aircraft Structures: Metals vs. Composites, Volume I, Proceedings of the 24th Symposium of the International Committee on Aeronautical Fatigue, Naples, Italy. 16-18 May 2007. Pisa, Italy: Pacini Editore, 2007, pp. 412-426. ICAF-Doc. 2417.

[102] Tikka, J. and Salonen, T. 2015. **Practical Experience of Neural Network Based Fatigue Life Monitoring.** In: Siljander, A. (Ed.) Embracing the future – respecting the past; supporting aging fleets with new technologies, Proceedings of the 34th Conference and the 28th Symposium of the International Committee on Aeronautical Fatigue and Structural Integrity, Helsinki, Finland. 1-5 June 2015, pp. 879-888. ISBN 978-951-38-7442-1.

[103] Tuhti, A. 2021. **Radiographic Inspection Report.** Customer Report № VTT-CR-00583-21 (classified). Espoo: VTT Technical Research Centre of Finland Ltd.

[104] Vaajoki, A., Solin, J., Alhainen, J. and Reijonen, J. 2022. **Process qualification methodology for laser powder bed fusion of Ti-6Al-4V for military aviation – part 2 process stability.** Research Report № VTT-CR-00277-22 (confidential). Espoo: VTT Technical Research Centre of Finland Ltd.

[105] Viitanen, T. 2022. **HN-416 Onboard HOLM System's Electrical Calibration 2022.** Research Report № VTT-R-00419-22 (in Finnish, classified). Espoo: VTT Technical Research Centre of Finland Ltd.

[106] Viitanen, T. 2022. **HN-432 Onboard HOLM System's Electrical Calibration 2022.** Research Report № VTT-R-00830-22 (in Finnish, classified). Espoo: VTT Technical Research Centre of Finland Ltd.

[107] Viitanen, T., Forsström, A., Koskinen, T. and Tuhti, A. 2022. **Inner Wing Step Lap Joint Repair Validation – Coupon Tests.** Research Report № VTT-R-00929-22 (classified). Espoo: VTT Technical Research Centre of Finland Ltd.

[108] Viitanen, T. and Forsström, A. 2022. **Inner Wing Step Lap Joint Repair Validation Coupon Tests – Additional Low-Speed 3D DIC Analyses.** Memorandum № VTT-M-01021-22 (classified). Espoo: VTT Technical Research Centre of Finland Ltd.

[109] Vos, J. B., Charbonnier, D., Siikonen, T., Salminen, E., Hoffren, J., Gehri, A. and Stefani, P. 2018. **Swiss/Finnish Collaboration on Aero-elastic simulations for the F/A-18 fighter**. In *2018 Applied Aerodynamics Conference* (p. 3642).

[110] Wallin, M. 2022. **Specification for analyzing the interaction effects for multiple delaminations.** Report № HN-K-0042 (in Finnish, classified). Halli: Patria Aviation Oy.

[111] Wallin, M. 2022. **Specification for fatigue tests on aluminium alloy joints with various fastener systems.** Report № HN-L-0360 (in Finnish, classified). Halli: Patria Aviation Oy.

[112] Wallin, M. 2022. **Simulation of variable amplitude loading by statistical means.** Technical Report № HN-L-0367 (in Finnish, classified). Halli: Patria Aviation Oy.

[113] Wallin, M. 2021. **Validation of Prototype Repair for IWSLJ Bondline Damages.** Report № HN-K-0041 (classified). 46 p. Halli: Patria Aviation Engineering.

[114] Wallin, M. 2022. **Validation and Certification of Bonded Repair on F-18 Wing Root Step Lap Joint** (NATO UNCLASSIFIED)**.** Certification of Bonded Repair on Composite Aircraft Structures, Presentation at NATO AVT-361 Research Workshop, Amsterdam, 18-20 October 2022, 19 p.

[115] Yle News. 2023. **Finnish Air Force training jet crashes in Central Finland.** Available at: https://yle.fi/a/74-20031919.

Report's title	
A REVIEW OF AERONAUTICAL FATIGUE INVESTIGATIONS IN FINLAND MAY 2021 – APRIL 2023	
Customer, contact person, address Finnish Defence Forces Logistics Command, Joint System Centre, Air Systems Division Mr. Ari Kivistö P. O. Box 69; FI-33541 Tampere; Finland	
Project name PIIKKI_2023 – Toimeksianto_2	Project number 136487-1.2
Editors Tomi Viitanen, Aslak Siljander	Pages 73
Keywords ICAF, aeronautical fatigue, structural integrity, military aircraft, fixed wing, FDF, FINAF, Finland	Report identification code VTT-CR-00252-23/ 21.06.2023

Summary

This document was prepared for the delivery to the 38th Conference of the International Committee on Aeronautical Fatigue and Structural Integrity (ICAF) scheduled to be held in Delft, The Netherlands, 26-29 June 2023.

A review is given of the aircraft structural fatigue research and associated activities which form part of the programs within the Air Force Command Finland (AFCOMFIN), the Finnish Defence Force Logistics Command, Joint Systems Centre (FDFLOGCOM JSC), Air Systems Division; Army Command Finland (ARCOMFIN); Aalto University; Arecap Ltd; Elomatic Ltd; Emmecon Ltd; Eurofins Expert Services Oy; Insta ILS Oy; Patria Aviation Oy; Tampere University; Trano Oy; Trueflaw Ltd; and VTT Technical Research Centre of Finland Ltd (VTT).

The review summarizes fatigue related research programs and investigations on specific military aircraft since the previous Finnish National Review compiled for the International Committee on Aeronautical Fatigue and Structural Integrity (ICAF) webinar, 30 June 2021.

Confidentiality	Public

Espoo 21 June 2023

Tomi Viitanen
Senior Scientist (VTT),
ICAF National Delegate Finland

Aslak Siljander
Principal Scientist (VTT)

Editors' contact address
VTT, P. O. Box 1000, FI-02044 VTT, Finland (Street: Kivimiehentie 3, Espoo, Finland)